

Holographic Wilson Loops, Dielectric Interfaces, and Topological Insulators

John Estes^{1,2,a}, Andy O'Bannon^{3,b}, Efstratios Tsatis^{4,c} and Timm Wrase^{5,d}

¹ *Blackett Laboratory, Imperial College, London, SW7 2AZ, United Kingdom*

² *Institute of Theoretical Physics, KULeuven, Celestijnenlaan 200D B-3001 Leuven, Belgium*

³ *Department of Applied Mathematics and Theoretical Physics, University of Cambridge, Cambridge CB3 0WA, United Kingdom*

⁴ *Department of Engineering Sciences, University of Patras, 26110 Patras, Greece*

⁵ *Stanford Institute for Theoretical Physics, Stanford University, Stanford, CA 94305, United States*

^ajohnaldonestes@gmail.com, ^bA.OBannon@damtp.cam.ac.uk,
^cetsatis@upatras.gr, ^dtimm.wrase@stanford.edu

Abstract

We use holography to study (3+1)-dimensional $\mathcal{N} = 4$ supersymmetric $SU(N_c)$ Yang-Mills theory (SYM) in the large- N_c and large coupling limits, with a (2+1)-dimensional interface where the Yang-Mills coupling or θ -angle changes value, or “jumps.” We consider interfaces that either break all supersymmetry or that preserve half of the $\mathcal{N} = 4$ supersymmetry thanks to certain operators localized to the interface. Specifically, we compute the expectation values of a straight timelike Wilson line and of a rectangular Wilson loop in the fundamental representation of $SU(N_c)$. The former gives us the self-energy of a heavy test charge while the latter gives us the potential between heavy test charges. A jumping coupling or θ -angle acts much like a dielectric interface in electromagnetism: the self-energy or potential includes the effects of image charges. $\mathcal{N} = 4$ SYM with a jumping θ -angle may also be interpreted as the low-energy effective description of a fractional topological insulator. For non-supersymmetric interfaces, we find that the self-energy and potential are qualitatively similar to those in electromagnetism, despite the differences between $\mathcal{N} = 4$ SYM and electromagnetism. For supersymmetric interfaces, we find dramatic differences from electromagnetism which depend sensitively on the coupling of the test charge to the adjoint scalars of $\mathcal{N} = 4$ SYM. In particular, we find one special case where a test charge has vanishing image charge.

Contents

1	Introduction and Summary	2
1.1	Motivation	7
1.2	Summary and Outlook	8
2	Holographic Conformal Interfaces	10
2.1	Non-Supersymmetric Janus	11
2.2	Supersymmetric Janus	15
2.3	Janus and Topological Insulators	17
3	Wilson Loops: Field Theory Calculation	25
3.1	Electromagnetism	25
3.2	$SU(N_c)$ $\mathcal{N} = 4$ SYM at large N_c	31
4	Wilson Loops: Holographic Calculation	36
4.1	String Equations of Motion and Solutions	38
4.2	Holographic Renormalization of the String Action	41
4.3	Straight Wilson Lines	48
4.4	Perpendicular Wilson Loops	54
4.5	Parallel Wilson Loops	58
4.6	Wilson Loops on the Interface	59
	Appendix: On Holographic Renormalization in Janus Spacetimes	62

1 Introduction and Summary

$\mathcal{N} = 4$ supersymmetric $SU(N_c)$ Yang-Mills (SYM) theory in (3+1)-dimensions is a conformal field theory (CFT), meaning the theory is invariant under the (3+1)-dimensional conformal group, $SO(4,2)$. The 't Hooft large- N_c limit consists of taking $N_c \rightarrow \infty$ while sending the Yang-Mills coupling $g \rightarrow 0$, keeping the 't Hooft coupling $\lambda \equiv g^2 N_c$ fixed. That limit provides various simplifications, for example, in any small- λ perturbative expansion of a correlation function, non-planar diagrams are suppressed by powers of $1/N_c$.

In string theory, $\mathcal{N} = 4$ SYM can be realized as the low-energy theory describing a stack of N_c coincident D3-branes, where the Yang-Mills coupling is fixed by the string coupling, $g^2 = 2\pi g_s$. The Anti-de Sitter/Conformal Field Theory (AdS/CFT) correspondence is the conjectured equivalence between $\mathcal{N} = 4$ SYM and type IIB string theory formulated on the near-horizon geometry of the D3-branes, $AdS_5 \times S^5$ [1–3]. Here AdS_5 is five-dimensional AdS space and S^5 is a five-sphere,

whose $SO(4,2)$ and $SO(6)$ isometries are dual to the $SO(4,2)$ spacetime symmetry and $SO(6)$ R-symmetry of $\mathcal{N} = 4$ SYM, respectively. Taking large N_c , small g_s , and fixed but large $g_s N_c$, the low-energy dynamics of the string theory is well-approximated by type IIB supergravity. In the SYM theory these correspond to the 't Hooft limit with large 't Hooft coupling. AdS/CFT is a holographic duality because the field theory in some sense “lives” at the boundary of AdS_5 .

In the space of deformations of $\mathcal{N} = 4$ SYM, a special subset preserve (2+1)-dimensional conformal symmetry, *i.e.* an $SO(3,2)$ subgroup of $SO(4,2)$. For example, consider $\mathcal{N} = 4$ SYM on a half-space, that is, half of $\mathbb{R}^{3,1}$ with a boundary that is $\mathbb{R}^{2,1}$. Suppose we take two copies of this theory, with different values of g , and glue them together along their boundaries. We thus obtain a (3+1)-dimensional theory with a coupling that jumps in one spatial direction, say the x_3 direction. We will call the location of the jump, which we may set to $x_3 = 0$, an interface. Clearly for such a system translational symmetry in x_3 is broken, nevertheless, the theory preserves translational symmetry along the interface and, with appropriate boundary conditions, an entire $SO(3,2)$ subgroup of $SO(4,2)$, namely the subgroup that leaves the (2+1)-dimensional interface invariant. We thus obtain a *conformal* interface, or, following standard parlance, an “Interface CFT” [4–8].¹

Examples of interface CFTs include $\mathcal{N} = 4$ SYM theory with a jumping coupling, as well as related theories obtained by S-duality, or more generally by $SL(2, \mathbb{R})$ transformations, including for example $\mathcal{N} = 4$ SYM with a constant coupling but a jumping θ -angle. A jumping coupling breaks all supersymmetry (SUSY) [5], and hence its $SL(2, \mathbb{R})$ -duals also do. Various amounts of SUSY may be restored by adding operators of the $\mathcal{N} = 4$ SYM theory localized entirely at the interface [5, 6, 8, 13, 14]. Notice that adding interface-localized operators does not introduce any new propagating degrees of freedom at the interface.

What physical effects does a jumping coupling have? To gain some intuition, consider (3+1)-dimensional Maxwell theory. Let us consider the Maxwell action first in non-relativistic form, with electric and magnetic fields E^i and B^i , with $i = 1, 2, 3$, and electric permittivity ϵ and magnetic permeability μ . In general, ϵ and μ may each jump independently, but if we impose relativistic invariance, so that the speed of light $c = 1/\sqrt{\epsilon\mu} \equiv 1$ is constant, and convert to relativistic notation, introducing the field strength $F^{\mu\nu}$ with $F^{i0} \equiv E^i$ and $F^{ij} \equiv -\epsilon^{ijk} B^k$, then we find

$$\frac{\epsilon}{8\pi} E^i E^i - \frac{1}{8\pi\mu} B^i B^i = \frac{\epsilon}{8\pi} [E^i E^i - B^i B^i] = -\frac{1}{4g^2} F^{\mu\nu} F_{\mu\nu}, \quad (1.1)$$

where $1/g^2 = \epsilon/4\pi$. A jumping coupling g in the relativistic theory thus represents an ϵ and μ that jump simultaneously in such a way that c remains constant. A jumping ϵ occurs at the interface between two materials with different dielectric constants. The main physical effect of a dielectric interface is to induce image charges: a test charge on one side of the interface will experience a

¹A CFT in which a defect preserves some conformal symmetry is called a “defect CFT” [7]. Generically some degrees of freedom may be localized to the defect. An example of such a defect CFT in string theory is the low-energy theory describing the (2+1)-dimensional intersection of D3-branes with D5- and/or NS5-branes, $\mathcal{N} = 4$ SYM with constant (non-jumping) coupling coupled to (2+1)-dimensional hypermultiplets that preserve an $SO(3,2)$ subgroup of $SO(4,2)$ [9–12]. Interface CFTs are special cases of defect CFTs in which a coupling constant jumps at an interface, and no degrees of freedom are localized to that interface.

potential equivalent to that produced by a fictitious image charge on the opposite side.

Remarkably, the holographic duals for many conformal interfaces in large- N_c , strongly-coupled $\mathcal{N} = 4$ SYM have been found [4, 12, 15–21], and generically are deformations of the $AdS_5 \times S^5$ solution of type IIB supergravity that have only an $SO(3, 2)$ isometry in the non-compact directions, *i.e.* an AdS_4 factor. For example, $\mathcal{N} = 4$ SYM with a jumping coupling is dual to type IIB supergravity formulated on the so-called “Janus” spacetime [4].² The Janus solution breaks all SUSY but preserves an AdS_4 factor as well as the entire S^5 , and includes a non-trivial dilaton whose value jumps at the AdS boundary, which is the holographic representation of the jumping coupling. $SL(2, \mathbb{R})$ transformations produce solutions with an axion that jumps at the boundary, dual to $\mathcal{N} = 4$ SYM with a jumping θ -angle. All half-BPS conformal defect solutions of type IIB supergravity were found in refs. [12, 17–20], including a SUSY version of Janus.³

Our goal in this paper is to compute the self-energy of a single heavy test charge, as well as the potential between heavy test charges, in four interface CFTs: $\mathcal{N} = 4$ SYM with a jumping coupling or a jumping θ -angle (but never both), with and without SUSY.

To be more precise, we will compute the expectation values of Wilson loops in the fundamental representation of $SU(N_c)$, which represent the phase acquired by an infinitely heavy test quark traversing the loop. We will consider two kinds of loops. The first is the straight time-like Wilson line (technically a loop only if we include the “point at infinity”), which in the infinite-time limit gives the self-energy of a single heavy test quark. The second is the rectangular Wilson loop, representing a heavy quark and anti-quark, which in the infinite-time limit gives the potential between the quark and anti-quark. To be still more precise, we will actually compute Maldacena loops [22, 23], which involve not only the $\mathcal{N} = 4$ SYM gauge fields but also the adjoint scalars. We will refer to the Maldacena loop as a Wilson loop, unless stated otherwise. In all cases, we expect the interface to modify the result of the undeformed $\mathcal{N} = 4$ SYM theory. For example, we expect a jump in the coupling to act much like a dielectric interface in ordinary classical electrodynamics, in the sense that a self-energy or potential will include effects from image charges.

In $\mathcal{N} = 4$ SYM without an interface, the (renormalized) expectation value of the straight Wilson line is trivial, indicating that a single heavy test quark has vanishing self-energy. This very special property of $\mathcal{N} = 4$ SYM follows from SUSY, specifically the fact that the straight Wilson line is half-BPS, which prevents radiative corrections to its expectation value [24, 25].

As for the rectangular Wilson loop in $\mathcal{N} = 4$ SYM without an interface, the distance L between the quark and anti-quark is the only scale in the problem, hence dimensional analysis dictates that the potential be Coulombic, $V(\lambda, L) = f(\lambda)/L$, and the non-trivial information is the dependence on λ , *i.e.* the function $f(\lambda)$.⁴ At large λ , the Wilson loop is described holographically by a string

²To be more precise, $\mathcal{N} = 4$ SYM with a jumping coupling and a particular interface-localized operator is dual to the Janus solution, as we discuss in detail in section 2.

³Recall that here a half-BPS solution preserves eight Poincaré supercharges and eight superconformal generators. 1/8-BPS Janus solutions are also known [15, 16, 21]. In what follows “SUSY Janus” always refers to the half-BPS Janus solution.

⁴At leading order in the large- N_c expansion the potential will not depend on N_c .

hanging down into AdS_5 with both endpoints at the boundary. The on-shell action of that string gives the Wilson loop expectation value [22, 23], and hence the potential:

$$V(\lambda, L) = -\frac{4\pi^2}{\Gamma(1/4)^4} \frac{\sqrt{2\lambda}}{L}, \quad \lambda \gg 1 \text{ holographic result.} \quad (1.2)$$

At small λ , the Wilson loop expectation value may be computed straightforwardly in perturbation theory. In fact, the sum of all planar diagrams without internal vertices, the ladder diagrams, gives [25, 26] (in each case, only the leading term is shown)

$$V(\lambda, L) = \begin{cases} -\frac{1}{4\pi} \frac{2\lambda}{L}, & \lambda \ll 1 \\ -\frac{1}{\pi} \frac{\sqrt{2\lambda}}{L}, & \lambda \gg 1. \end{cases} \quad \text{sum of ladder diagrams.} \quad (1.3)$$

When $\lambda \gg 1$, the dependence on λ is the same as the holographic result, although the numerical coefficient is different.⁵ In other words, the sum of ladder diagrams contain some, but not all, contributions to the potential at strong coupling. The leading behavior in λ changes from the weak-coupling factor of λ to the strong-coupling factor of $\sqrt{\lambda}$ due to screening effects [22, 23].

For $\mathcal{N} = 4$ SYM with a conformal interface, we can use the $SO(3, 2)$ symmetry to constrain the forms of the self-energy and potential. The $SO(3, 2)$ is a *subgroup* of $SO(4, 2)$, so in particular the $SO(3, 2)$ dilatation generator is that of the original $SO(4, 2)$, and as such acts on all of x_1 , x_2 , and x_3 . The interface spans the x_1 and x_2 directions, and sits at $x_3 = 0$.

In the presence of the interface, the expectation value of a single straight Wilson line will depend only on its position in the x_3 direction, $x_3 = L_3$. We expect a single test charge to induce an image charge on the opposite side of the interface, a distance $|L_3|$ from the interface. We can then express the self-energy of the test charge as a potential V between the test charge and its image. Due to scale invariance, $V \propto 1/(2|L_3|)$, with a coefficient that depends on the strength of the image charge, and that in our case must go to zero if the jump in the coupling or θ -angle goes to zero.

For the rectangular Wilson loop in the presence of the interface, L is no longer the only scale in the problem. The quark and anti-quark provide two points that define a line. That line may be parallel to the interface, perpendicular, or some linear combination of the two. For simplicity we will consider only the perpendicular and parallel cases, as depicted in figure 1. Moreover, in the perpendicular case we will only consider test charges on opposite sides of the interface, rather than both test charges on the same side. In each case the potential V can depend on two scales. For the perpendicular case, depicted in fig. 1 (a), we parameterize the two scales as the x_3 positions of the two test charges, denoted x_3^L and x_3^R , where the superscripts L and R denote “left” ($x_3 < 0$) and “right” ($x_3 > 0$). The distance between the test charges is $L = x_3^R - x_3^L$. If we define an “average distance” $L_{av} \equiv \frac{1}{2}(x_3^R + x_3^L)$, then dimensional analysis and scale invariance constrain

⁵As emphasized in refs. [25, 26], in the ladder summation at leading order in the $\lambda \gg 1$ limit, the existence of a $\sqrt{\lambda}$ factor is gauge-independent, however the coefficient of this factor is gauge-dependent. The result in eq. (1.3) is quoted in Feynman gauge.

the potential to take the form $V(\lambda, L, L_{\text{av}}) = \frac{1}{L} f(\lambda, L_{\text{av}}/L)$. For the parallel case, depicted in fig. 1 (b), we parameterize the two scales as the distance between the quark and anti-quark, L , and their position in the x_3 direction, $x_3 = L_3$. Dimensional analysis and scale invariance constrain the potential to take the form $V(\lambda, L, L_3) = \frac{1}{L} f(\lambda, L_3/L)$. In each case, our objective is to extract the non-trivial information contained in the function $VL = f$.

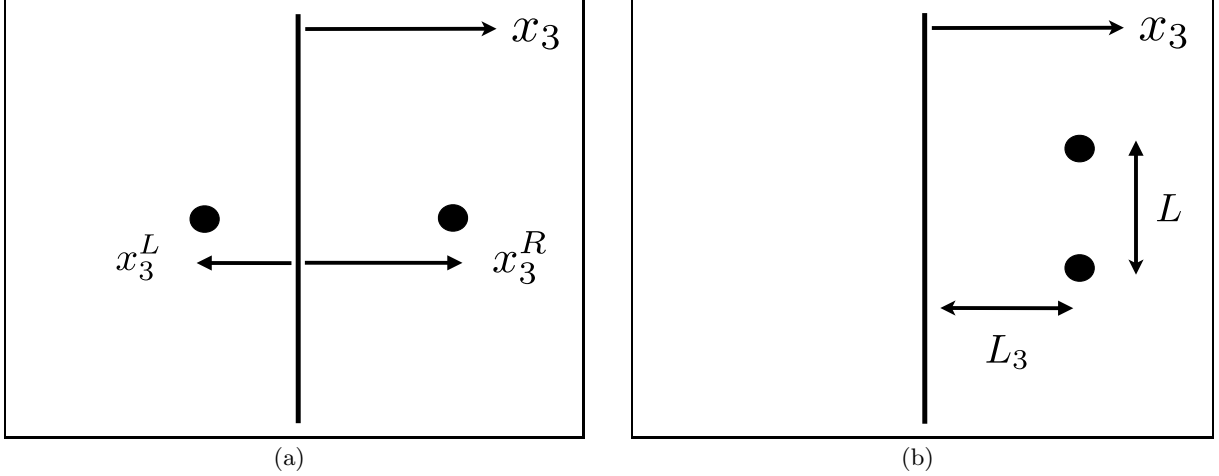


Figure 1: Depictions of the orientations of the rectangular Wilson loops in the two cases we consider. The vertical axis is one of the directions x_1 or x_2 , the horizontal axis is x_3 . The solid black vertical line represents the interface where the coupling or θ -angle jumps, which is at $x_3 = 0$. The quark and anti-quark, represented by the solid black dots, define a line that is either parallel or perpendicular to the defect. (a) The perpendicular case, where the quark and anti-quark sit at positions x_3^L and x_3^R from the interface. We consider only $x_3^L < 0$ and $x_3^R > 0$. (b) The parallel case, where L is the distance between the quark and anti-quark, which are located at $x_3 = L_3$.

Wilson lines or loops located precisely on the interface, at $x_3 = 0$, are special cases, and raise several questions. First is a question about interface CFTs in general (regardless of any test charges): what are the values of g and the θ exactly at the interface? Do we use the values from $x_3 < 0$, from $x_3 > 0$, some kind of average values, or some more complicated functions? Second, for a single test charge at finite x_3 , we have $V \propto 1/(2|L_3|)$, but if we send $L_3 \rightarrow 0$ does V diverge? In physical terms, at $x_3 = 0$, doesn't the test charge sit exactly on top of its own image charge? Can we sensibly define V in such circumstances? To address questions such as these, we will include in our analysis Wilson lines and loops sitting precisely at $x_3 = 0$.

For all four interface CFTs that we consider we obtain results in the large- N_c , large coupling limits using holography, where the Wilson loop is described by a string in Janus spacetime [4, 22, 23]. Previous holographic calculations of Wilson loop expectation values in $\mathcal{N} = 4$ SYM with conformal defects appear in refs. [4, 27, 28]. For the non-SUSY interface with a jumping coupling, we also consider finite N_c and small coupling, and obtain results using perturbation theory.

1.1 Motivation

Why bother computing Wilson loop expectation values in $\mathcal{N} = 4$ SYM theory with conformal interfaces? Many reasons come to mind, but we will emphasize only two.

First, Wilson loops provide a valuable check of the AdS/CFT correspondence. In $\mathcal{N} = 4$ SYM with a constant coupling, the expectation value of a circular Wilson loop may be computed exactly, for all values of N_c and λ , from a Gaussian matrix model [25, 29, 30]. In the large- N_c and large- λ limits, the exact result for the circular Wilson loop expectation value agrees precisely with the holographic result, providing one of the many direct tests of the AdS/CFT correspondence.

The existence of a matrix model for the circular Wilson loop expectation value can be deduced in various ways. One way begins with the expectation value of the straight Wilson line, which is trivial, as mentioned above. A conformal transformation maps the straight line to a circle, upon including one additional point, the point at infinity [31]. The circular Wilson loop has a non-trivial expectation value, suggesting that the only contribution to the expectation value must come from a single point, the point at infinity, which in turn suggests the existence of a matrix model. Notice that the main ingredients here were 1) the triviality of the straight Wilson line expectation value and 2) conformal symmetry. Another way to detect the matrix model is to compute the circular Wilson loop expectation value using perturbation theory in λ . Remarkably, here the sum of ladder diagrams gives the *exact* answer [25, 29]. The net contribution from all non-ladder diagrams is zero. The matrix model can then be constructed from the combinatorics of the ladder diagrams [25, 29].

Wilson loops may also provide direct tests for $\mathcal{N} = 4$ SYM with various conformal interfaces and their holographic duals. Our work is one step in that direction.

As a second motivation, analysis of $\mathcal{N} = 4$ SYM with a jumping θ angle may shed light on certain (3+1)-dimensional topological insulators (TIs). One definition of a TI is an insulator with topologically-protected gapless edge modes that give rise to quantized, dissipationless transport. Since 1980, the canonical example of a TI has been the integer quantum Hall state (QHS), a (2+1)-dimensional insulating state where the gapless modes are (1+1)-dimensional chiral fermions giving rise to an integer-quantized Hall conductivity. The integer QHS breaks time reversal symmetry, T . Since 2005 a number of (3+1)-dimensional TIs have been discovered that preserve T , including Bi_2Se_3 , Bi_2Te_3 , and Sb_2Te_3 , where the edge modes are (2+1)-dimensional Dirac fermions, giving rise to \mathbb{Z}_2 -quantized magneto-electric response. To date, the edge modes of some (3+1)-dimensional T -invariant TIs have been observed directly, however the \mathbb{Z}_2 -quantized magneto-electric response has not yet been observed. For reviews of TIs, see for example refs. [32–35].

In the Landau-Ginzburg paradigm, states of matter are classified by the symmetries they break, as detected by local order parameters. TIs clearly fall outside the Landau-Ginzburg paradigm: classifying TI states requires knowing not only the symmetries they break but also their topological quantum numbers. For that reason alone they are worth studying, although they deserve attention also for potential applications, such as quantum computing [32, 33].

All of the above TIs admit low-energy effective descriptions in terms of free fields: for the integer

QHS the effective description is Chern-Simons theory [36], while for the (3+1)-dimensional T-invariant TIs the effective description is Maxwell electrodynamics with a θ -angle that takes one of the two values allowed by T-invariance, zero or $\pi \pmod{2\pi}$ [37, 38]. These topological terms reproduce the dissipationless, quantized transport properties. The boundary between a (3+1)-dimensional T-invariant TI and the vacuum appears in the effective description as, for example, a θ -angle that jumps from π to zero.

In contrast to the integer QHS, the fractional QHS cannot be described in terms of free fields. An open question is whether (3+1)-dimensional T-invariant *fractional* TIs exist, whose signature would be fractionally-quantized magneto-electric response, and if so, what low-energy (interacting) theory describes their transport properties? One proposal for such an effective theory exploits non-Abelian gauge fields [39–41]. We emphasize, however that to date no T-invariant fractional TI has been observed experimentally.

As proposed in ref. [42], and as we will explain in detail in section 2.3, we can think of $\mathcal{N} = 4$ SYM with a θ -angle that jumps from zero to $\pi \pmod{2\pi}$ as the low-energy effective description of a very special (3+1)-dimensional T-invariant fractional TI. $\mathcal{N} = 4$ SYM is unlikely to be realized experimentally, but does have the advantage that strong-coupling calculations are tractable via AdS/CFT. A natural question is whether any unexpected or exotic effects occur in $\mathcal{N} = 4$ SYM with a jumping θ -angle, especially at large coupling. Our work is a first step towards answering that and other related questions.

1.2 Summary and Outlook

In sections 2.1 and 2.2 we review non-SUSY and SUSY Janus, respectively, and in section 2.3 we explain in detail how $\mathcal{N} = 4$ SYM with a jumping θ -angle describes a fractional TI. We turn to the calculation of Wilson loop expectation values, and the self-energy or potential V , in section 3. In section 3.1 we compute V in ordinary electromagnetism with a jumping coupling and θ -angle. In section 3.2 we compute the expectation value for a rectangular Wilson loop parallel to a non-SUSY interface where the coupling jumps in $\mathcal{N} = 4$ SYM with arbitrary N_c , using perturbation theory. With one special choice of boundary conditions on the scalars of $\mathcal{N} = 4$ SYM, for which the self-energy of a single test charge vanishes, and in the large- N_c and large coupling limits, we also calculate the contribution to this Wilson loop expectation value from the sum of ladder diagrams. In section 4 we turn to the holographic calculation of V . Sections 4.1 and 4.2 describe in detail how we solve the equations of motion for strings in Janus spacetimes and compute the on-shell string action. In sections 4.3 through 4.6 we present our results for V , which are mostly numerical, but include some exact results for a single test charge in $\mathcal{N} = 4$ with a SUSY interface with a small jump in the coupling or θ -angle. We collect some useful technical results in an appendix.

For all non-SUSY interfaces that we consider in large- N_c , strongly-coupled $\mathcal{N} = 4$ SYM, we find that our holographic results for V are qualitatively similar to the analogous results in electromagnetism. For example, consider a single test charge. In electromagnetism with a jumping coupling,

a test charge is always attracted to the side of the interface with smaller coupling, as we review in section 3.1. With a jumping θ -angle, the test charge is always attracted towards the interface. Electromagnetism is a linear theory, so the interaction potential V between two test charges follows simply by linear superposition. Our holographic results for large- N_c , strongly-coupled $\mathcal{N} = 4$ SYM with a non-SUSY interface indicate that with a jumping coupling or θ -angle the test charge is attracted to the side with smaller coupling or to the interface, respectively. In other words, the induced image charge has the same sign as in electromagnetism. This similarity is striking, given the many differences between the two theories: electromagnetism is a free theory of gauge fields alone, while $\mathcal{N} = 4$ SYM is an interacting theory of gauge fields, fermions, and scalars, and moreover we study the large-coupling limit and we study test charges that couple not only to the gauge fields but also to the scalars. Additionally, we find that our results for the interaction potential between two test charges are qualitatively similar to those of electromagnetism: compare for example our holographic result for the potential between two test charges along a line perpendicular to a non-SUSY interface shown in fig. 10 with the analogous results in electromagnetism shown in fig. 5. This similarity is striking because $\mathcal{N} = 4$ SYM is not a linear theory.

For large- N_c , strongly-coupled $\mathcal{N} = 4$ SYM with a SUSY interface, the results for the self-energy of a test charge depend sensitively on the coupling of the charge to the adjoint scalars. For example, for a SUSY interface where the coupling jumps we find one case where the induced image charge vanishes! For a SUSY interface where the θ -angle jumps, we find cases where the image charge has the “wrong” sign, as compared to our intuition from electromagnetism, and cases where the image charge either diverges or goes to zero as the jump in the θ -angle goes to infinity, in dramatic contrast to electromagnetism. The interface-localized terms that are the main difference between the non-SUSY and SUSY interfaces play a decisive role in determining image charges.

For two test charges located precisely on an interface in large- N_c , strongly-coupled SYM, we find a (holographic) renormalization scheme that subtracts the infinite self-energy of the test charges, allowing us to define a finite interaction potential between them. Within that renormalization scheme, we can thus define an effective ’t Hooft coupling precisely on the interface. For an interface where the coupling jumps, either non-SUSY or SUSY, we find surprising similarity between our numerical results for the effective ’t Hooft coupling and an effective coupling for the analogous system in electromagnetism, defined by simply deleting any self-interaction terms from the potential.

Our results raise a number of questions for future research. For example, as mentioned above, with a SUSY interface where the coupling jumps, we find one kind of test charge with vanishing image charge *i.e.* we find a trivial timelike Wilson line. Our system has conformal symmetry, so we may map that line to a circle. Does that circular Wilson loop have non-zero expectation value? If so, can we reproduce that expectation value from a matrix model? Indeed, in ref. [27] a matrix model was derived for a circular Wilson loop sitting exactly on the interface. Our results suggest that something similar may be possible for a circular Wilson loop away from the interface.

What about dyonic test charges in $\mathcal{N} = 4$ SYM, holographically dual to (p, q) -strings? What kinds of image charges do they have in the presence of non-SUSY and SUSY interfaces? What

about defects in $\mathcal{N} = 4$ SYM that support localized degrees of freedom, as arise for example in the (2+1)-dimensional intersection of D3-branes with D5- and/or NS5-branes [9–12]? How do those affect the self-energy of a test charge? What can $\mathcal{N} = 4$ SYM with a jumping θ -angle teach us about fractional TIs? Do any novel effects appear at strong coupling? What are the edge modes in $\mathcal{N} = 4$ SYM with a jumping θ -angle? Can we study them holographically?

As a caution to the reader: we use a Lorentzian-signature metric in sections 2 and 3.1 and a Euclidean-signature metric in sections 3.2 and 4, and in the appendix. Throughout the paper we work exclusively in the Einstein frame of type IIB supergravity.

2 Holographic Conformal Interfaces

We will study $\mathcal{N} = 4$ SYM with conformal interfaces, which preserve an $SO(3, 2)$ subgroup of the $SO(4, 2)$ conformal group. The holographic duals will therefore include an AdS_4 subspace, so let us recall the AdS_4 foliation, or AdS_4 “slicing,” of AdS_5 . We begin with the metric of Lorentzian-signature AdS_5 , in Poincaré slicing,

$$ds_{AdS_5}^2 = R^2 \frac{dr^2}{r^2} + \frac{r^2}{R^2} (-dt^2 + dx_1^2 + dx_2^2 + dx_3^2), \quad (2.1)$$

where R is the AdS_5 radius of curvature, which is related to the string length squared α' as (in Einstein frame) $R^4 = 4\pi N_c \alpha'^2$, and r is the AdS_5 radial coordinate. The Poincaré horizon, which represents the point at infinity in the field theory, is at $r = 0$, while the boundary is at $r \rightarrow \infty$. The radial coordinate r is dual to the field theory’s energy scale, with $r = 0$ corresponding to the infrared (IR) and $r \rightarrow \infty$ corresponding to the ultraviolet (UV) [43, 44]. A cartoon of AdS_5 in Poincaré slicing appears in fig. 2 (a). Introducing new coordinates u and x via

$$r = R^2 u \cosh x, \quad x_3 = \frac{\tanh x}{u}, \quad (2.2)$$

puts the metric into AdS_4 slicing,

$$ds_{AdS_5}^2 = R^2 (dx^2 + \cosh^2 x ds_{AdS_4}^2), \quad (2.3)$$

where the unit-radius AdS_4 metric is

$$ds_{AdS_4}^2 = \frac{du^2}{u^2} + u^2 (-dt^2 + dx_1^2 + dx_2^2). \quad (2.4)$$

In AdS_4 slicing, we can approach the Poincaré horizon by fixing x and taking $u \rightarrow 0$, which in eq. (2.2) sends $r \rightarrow 0$ and $x_3 \rightarrow \infty$. We can approach the boundary in three ways. If we take $x \rightarrow +\infty$ with u fixed, then from eq. (2.2) we see that $r \rightarrow \infty$ with $x_3 > 0$, so this route can take us to half of the boundary. If we take $x \rightarrow -\infty$ with u fixed, we reach a boundary point with $x_3 < 0$, so this route can take us to the other half of the boundary. If we fix x and take $u \rightarrow \infty$, which is the boundary of the AdS_4 subspace, then we find $r \rightarrow \infty$ and $x_3 = 0$, so this route takes us to boundary points directly on the interface. We depict AdS_5 in AdS_4 slicing in fig. 2 (b).

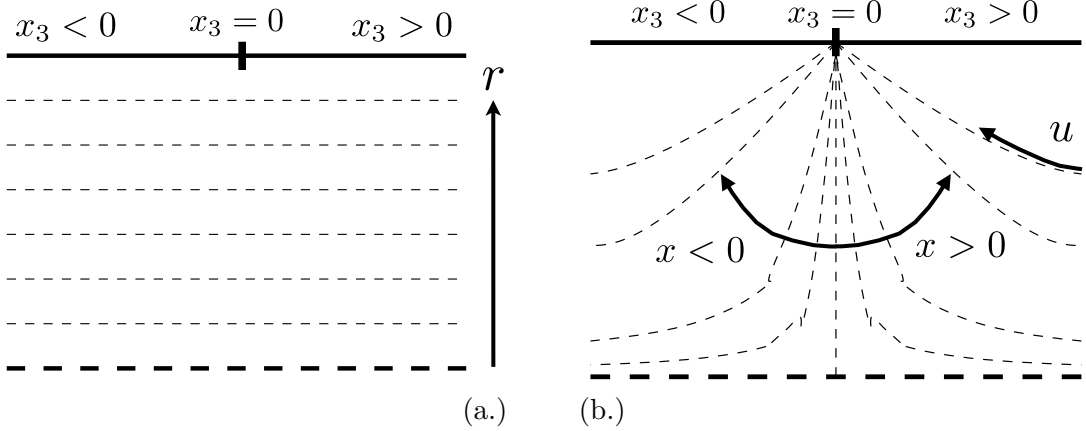


Figure 2: Cartoons depicting two different “slicings” of AdS_5 , the Poincaré and the AdS_4 slicings, adapted from fig. 1 of ref. [45]. (a.) Poincaré slicing, with the metric written in eq. (2.1). The horizontal axis is the x_3 direction and the vertical axis is the r direction. We have suppressed all other directions. The heavy dashed horizontal line is the Poincaré horizon $r = 0$. The thin dashed lines are surfaces of fixed r , the Poincaré slices. The solid horizontal line is the boundary $r \rightarrow \infty$. (b.) AdS_4 slicing, with the metric written in eq. (2.3). The AdS_5 Poincaré horizon and boundary are again depicted by the heavy dashed and solid horizontal lines, respectively. The u and x directions are depicted with arrows. The thin dashed lines are surfaces of constant x , the AdS_4 slices. For details of how to reach the AdS_5 Poincaré horizon and boundary in these coordinates, see the accompanying text.

2.1 Non-Supersymmetric Janus

The non-SUSY Janus solution of type IIB supergravity is a one-parameter dilatonic deformation of the $AdS_5 \times S^5$ solution in which only the metric, dilaton, and Ramond-Ramond (RR) five-form are non-trivial [4, 16]. We begin by writing the $AdS_5 \times S^5$ solution in AdS_4 slicing, as in eq. (2.3), but changing to a new x coordinate,

$$x \rightarrow -\tanh^{-1} x, \quad (2.5)$$

so that eq. (2.2) becomes

$$r = \frac{R^2 u}{\sqrt{1-x^2}}, \quad x_3 = -\frac{x}{u}, \quad (2.6)$$

and the boundary regions formerly at $x \rightarrow \pm\infty$ now correspond to $x \rightarrow \mp 1$. The $AdS_5 \times S^5$ metric then takes the form

$$ds^2 = R^2 \left(\frac{1}{(1-x^2)^2} dx^2 + \frac{1}{1-x^2} ds_{AdS_4}^2 \right) + R^2 ds_{S^5}^2, \quad (2.7)$$

with $ds_{S^5}^2$ the metric of a unit-radius S^5 . The dilaton, ϕ , is constant: $\phi = \phi_0$.

To write the metric and dilaton of the non-SUSY Janus solution, we need some special functions. First, we need the Weierstrass elliptic function $\wp(x)$, defined by the equation

$$(\partial_x \wp)^2 = 4\wp^3 - g_2\wp - g_3, \quad (2.8)$$

with periods g_2 and g_3 . Next, we need the Weierstrass sigma- and zeta-functions, $\sigma(x)$ and $\zeta(x)$ respectively, which are related to $\wp(x)$ via

$$\wp(x) = -\zeta'(x), \quad \zeta(x) = \frac{\sigma'(x)}{\sigma(x)}. \quad (2.9)$$

The metric of the non-SUSY Janus solution is [4, 16]

$$ds^2 = R^2 (\gamma^{-1} h(x)^2 dx^2 + h(x) ds_{AdS_4}^2) + R^2 ds_{S^5}^2, \quad (2.10)$$

with warp factor

$$h(x) = \gamma \left(1 + \frac{4\gamma - 3}{\wp(x) + 1 - 2\gamma} \right), \quad (2.11)$$

where $\wp(x)$ has periods

$$g_2 = 16\gamma(1 - \gamma), \quad g_3 = 4(\gamma - 1). \quad (2.12)$$

The dilaton, $\phi(x)$, is fixed by the warp factor via

$$\frac{\partial \phi}{\partial x} = \frac{\gamma \sqrt{6(1 - \gamma)}}{h(x)}. \quad (2.13)$$

Upon integrating in x , we find

$$\phi(x) = \phi_0 + \sqrt{6(1 - \gamma)} \left(x + \frac{4\gamma - 3}{\wp'(\chi)} \left(\ln \frac{\sigma(x + \chi)}{\sigma(x - \chi)} - 2\zeta(\chi)x \right) \right), \quad (2.14)$$

where the constant χ is defined by $\wp(\chi) = 2(1 - \gamma)$.

The non-SUSY Janus solution also has a non-trivial Ramond-Ramond (RR) five-form, with N_c units of flux on the S^5 [4, 16]. To compute Wilson loops we will introduce strings into the non-SUSY Janus spacetime. In Einstein frame the string action involves the dilaton and the pull-backs of the metric and Neveu-Schwarz (NS) two-form, therefore we will not need the RR five-form, so we will omit it from our review of the non-SUSY Janus solution.

The non-SUSY Janus solution is completely specified by the four real constants R , ϕ_0 , N_c , and γ . We can constrain the value of γ as follows. When $\gamma = 3/4$ the warp factor $h(x) = 1$, and the solution is a product geometry $AdS_4 \times \mathbb{R} \times S^5$ with a linear dilaton. Solutions with $\gamma < 3/4$ are generally singular, so we will impose $\gamma > 3/4$. On the other hand, to maintain reality of the dilaton we must impose $\gamma \leq 1$. When $\gamma = 1$, the warp factor becomes $h(x) = \frac{1}{1-x^2}$, so the metric becomes that of eq. (2.7), for $AdS_5 \times S^5$ with radius of curvature R . Additionally, when $\gamma = 1$ the dilaton becomes constant, $\phi(x) = \phi_0$. In summary, we take $\gamma \in (3/4, 1]$. Notice that the internal space is an S^5 for any γ .

The boundary is defined as the location in x where the metric diverges. Clearly that will occur where $h(x)$ has a pole, which occurs at points with $x = x_0$ obeying $\wp(x_0) = 2\gamma - 1$. When $\gamma = 1$, we find $x_0 = \pm 1$, as expected for $AdS_5 \times S^5$. More generally, since $h(x)$ is an even function the geometry will have two asymptotic boundaries at $x = \pm x_0$. To make the asymptotic boundaries explicit, let us change variables. In the $x \rightarrow \pm x_0$ limits, we take

$$x \equiv \pm x_0 \mp 2\sqrt{\gamma} e^{\mp 2\hat{x}}, \quad (2.15)$$

so that for large \hat{x} the Janus metric approaches

$$ds^2 = R^2 \left(d\hat{x}^2 + \frac{e^{2\hat{x}}}{4} ds_{AdS_4}^2 + ds_{S^5}^2 \right), \quad (2.16)$$

which we recognize as the asymptotic form of the AdS_4 -sliced $AdS_5 \times S^5$ metric in eq. (2.3). Taking $x \rightarrow +x_0$ brings us to points on the boundary with $x_3 < 0$ while taking $x \rightarrow -x_0$ brings us to points on the boundary with $x_3 > 0$. In other words, the geometry has two asymptotic $AdS_5 \times S^5$ regions at $x = \pm x_0$, corresponding to the two halves of space in the dual CFT. Crucially, however, when $\gamma \neq 1$, the value of the dilaton will not be the same in the two regions. Let

$$\phi_{\pm} \equiv \lim_{x \rightarrow \mp x_0} \phi(x), \quad \delta\phi \equiv \phi_+ - \phi_-, \quad (2.17)$$

so that the dilaton approaches ϕ_+ at boundary points to the “right” of the interface, $x_3 > 0$, and approaches ϕ_- for boundary points to the “left” of the interface, $x_3 < 0$. A formula for the jump in the dilaton $\delta\phi$ as a function of γ is straightforward to obtain but unilluminating, so we will omit it. We will note however that $\delta\phi = 0$ when $\gamma = 1$ (the $AdS_5 \times S^5$ solution) and $\delta\phi$ increases as γ decreases, with $\delta\phi \rightarrow \infty$ as $\gamma \rightarrow 3/4$ (where the dilaton is linear in x). We can thus obtain a $\delta\phi$ of any size within the region $\gamma \in (3/4, 1]$. In short, the non-SUSY Janus solution has one free parameter beyond that of the pure $AdS_5 \times S^5$ solution, namely γ , which controls the size of the jump in the dilaton at the boundary.

Clearly the field theory dual to the Janus solution is a deformation of $\mathcal{N} = 4$ SYM with a g , and hence a $\lambda = g^2 N_c$, whose value jumps at $x_3 = 0$. To make a more precise statement, we need the dictionary between ϕ and g . We can fix the dictionary using the $SL(2, \mathbb{R})$ transformation properties of type IIB supergravity and large- N_c $\mathcal{N} = 4$ SYM, as follows. On the supergravity side, the complex axio-dilaton τ , which we define as

$$\tau \equiv C_{(0)} + i e^{-2\phi}, \quad (2.18)$$

where $C_{(0)}$ is the axion, transforms covariantly under $SL(2, \mathbb{R})$, that is, under an $SL(2, \mathbb{R})$ transformation τ changes as

$$\tau \rightarrow \frac{a\tau + b}{c\tau + d}, \quad (2.19)$$

where $a, b, c, d \in \mathbb{R}$ and $ad - bc = 1$. Notice that our ϕ gives the open string coupling, and hence is related to the closed string coupling, g_s , via $e^{2\phi} = g_s$.

To find the corresponding $SL(2, \mathbb{R})$ -covariant object in $\mathcal{N} = 4$ SYM, we need to fix the normalization of the fields in the classical Lagrangian. The field content of $\mathcal{N} = 4$ $SU(N_c)$ SYM consists of a gauge field, \hat{A}_μ , six real scalars $\hat{\Phi}^I$ with $I = 1, 2, \dots, 6$, and four Weyl fermions, all in the adjoint representation of $SU(N_c)$. The hats on \hat{A}_μ and $\hat{\Phi}^I$ are meant to indicate that these objects are matrices valued in the Lie algebra of $SU(N_c)$. The scalars are in the **6** and the fermions are in the **4** of the $SO(6)$ R-symmetry. In what follows we will ignore the fermions. In the $\mathcal{N} = 4$ SYM Lagrangian, $\mathcal{L}_{\mathcal{N}=4}$, the terms involving only the gauge fields and scalars are,⁶

$$\mathcal{L}_{\mathcal{N}=4} \supset -\frac{1}{4g^2} \text{tr} \hat{F}_{\mu\nu} \hat{F}^{\mu\nu} + \frac{\theta}{32\pi^2} \epsilon^{\mu\nu\rho\sigma} \text{tr} \hat{F}_{\mu\nu} \hat{F}_{\rho\sigma} - \frac{1}{2g^2} \text{tr} (D^\mu \hat{\Phi}^I D_\mu \hat{\Phi}^I) + \frac{1}{4g^2} \text{tr} ([\hat{\Phi}^I, \hat{\Phi}^J][\hat{\Phi}^I, \hat{\Phi}^J]), \quad (2.20)$$

where D_μ is the gauge-covariant derivative and the traces are over color indices. We have normalized the fields so that all terms (not involving θ) have an overall $1/g^2$. With that choice of normalization, the $SL(2, \mathbb{R})$ -covariant coupling of $\mathcal{N} = 4$ SYM is

$$\tau \equiv \frac{\theta}{2\pi} + i \frac{2\pi}{g^2}, \quad (2.21)$$

hence we obtain the dictionary: in each asymptotic $AdS_5 \times S^5$ region, we have

$$C_{(0)} = \frac{\theta}{2\pi}, \quad e^{2\phi} = \frac{g^2}{2\pi}, \quad (2.22)$$

and by extension $\lambda = g^2 N_c = 2\pi N_c e^{2\phi}$. Given the asymptotic values ϕ_\pm we can thus determine the values of the coupling on the two sides of the interface, g_\pm or λ_\pm . Recalling that in the 't Hooft limit g^2 is $\mathcal{O}(1/N_c)$, the natural scaling for θ in the 't Hooft limit is $\mathcal{O}(N_c)$, so that both $\text{Re } \tau$ and $\text{Im } \tau$ have the same $\mathcal{O}(N_c)$ scaling. Notice that with those scalings, $g^2 \theta$ is $\mathcal{O}(N_c^0)$.

For the moment let us set $\theta = 0$, and ask the following question: what is the classical Lagrangian of the field theory dual to the non-SUSY Janus solution [5, 6]? To construct the most general classical Lagrangian that includes a jumping coupling and that is consistent with the $SO(3, 2) \times SO(6)$ symmetry of the non-SUSY Janus solution, the first step is to promote g to a smooth function of x_3 in eq. (2.20). Generically, such a function will introduce at least one dimensionful scale, so to recover scale invariance we will ultimately take a limit in which g becomes a step function. With g a smooth function of x_3 , we next write the classical action as a sum of all possible operators consistent with the $SO(3, 2) \times SO(6)$ symmetry, including operators involving powers of $\partial_3 g$. Via field redefinitions and integration by parts, the action can be reduced to the sum of two terms, namely the $\mathcal{N} = 4$ SYM Lagrangian plus an additional non-trivial term involving the scalars and fermions, which we call \mathcal{L}_{int} , to which the scalars' contribution is

$$\mathcal{L}_{\text{int}} \supset \kappa \frac{\partial_3 g}{g^3} \hat{\Phi}^I D_3 \hat{\Phi}^I, \quad (2.23)$$

with some real constant κ [5, 6]. The fermions' contribution to \mathcal{L}_{int} introduces no other constants beyond κ . \mathcal{L}_{int} becomes localized to the interface when g becomes a step function. One ambiguity

⁶Our choice of orientation is $\epsilon^{0123} = +1$.

remains: the symmetries do not fix the value of κ . No corresponding free parameter appears in the Janus solution, so presumably the field theory dual to Janus has a specific value of κ . What that value is remains an open question.

The value $\kappa = 1$ is special. When $\kappa = 1$, integrating the scalars' bulk kinetic terms by parts produces an interface term that exactly cancels the term in eq. (2.23). Moreover, as argued in ref. [5], $\kappa = 1$ might be the only value of κ for which $SO(3, 2)$ conformal symmetry will be preserved at the quantum level.

What is the physical meaning of κ ? Put briefly, for test charges that couple to the scalars, κ controls the size of image charges. In the presence of a jumping coupling, a test charge that couples to the scalars will interact with an image charge via scalar exchange. \mathcal{L}_{int} is quadratic in the scalars and so modifies the scalar propagator, hence κ will influence the size of the image charge. We will see in detail how κ enters the scalar propagators in section 3.2. In particular, we will see that when $\kappa = 0$, the gauge and scalar propagators are of the same form, and as a result their contributions to the image charges cancel, so that effectively a test charge has no image charge.

A direct way to determine κ would be to calculate in the field theory the interaction potential between a test charge and its image for large N_c , large λ , and arbitrary κ , and then compare to a holographic calculation of the same quantity. We will not attempt such a direct comparison here. Nevertheless, our holographic calculation of the interaction potential will show that test charges have nonzero image charges. That in turn suggests that the field theory dual to the non-SUSY Janus solution must have non-zero κ . In other words, our holographic calculation will provide suggestive evidence *excluding* a single value, $\kappa = 0$.

If we begin with a jumping coupling that breaks all SUSY, then $SL(2, \mathbb{R})$ transformations can generate a jumping θ -angle. For the theory with a jumping θ -angle all possible interface-localized operators consistent with $SO(3, 2)$ symmetry and an $SO(3) \times SO(3)$ subgroup of the $SO(6)$ symmetry were written in ref. [8]. These operators will then appear in the action with coefficients that, in the absence of SUSY, are undetermined *a priori*. Here again, a comparison of interaction potentials computed from field theory and from holography could in principle provide information about these coefficients.

2.2 Supersymmetric Janus

The SUSY Janus solution of type IIB supergravity is a deformation of the $AdS_5 \times S^5$ solution in which the metric, dilaton, RR five-form, and RR and NS three-forms are non-trivial [18]. We begin with the AdS_4 foliation of AdS_5 with radial coordinate x in eq. (2.3) (not the x coordinate in eq. (2.7)). Next we rewrite the S^5 as a pair of S^2 's fibered over a line segment with coordinate y , so that the S^5 metric takes the form

$$ds_{S^5}^2 = dy^2 + \cos^2 y ds_{S^2}^2 + \sin^2 y ds_{S^2}^2, \quad (2.24)$$

with $ds_{S^2}^2$ the metric of a unit-radius S^2 and $y \in [0, \pi/2]$, where at each endpoint, $y = 0$ or $y = \pi/2$, one or the other S^2 collapses to zero size. The coordinates x and y together describe a Riemann

surface, which may equivalently be parameterized by a complex coordinate $v \equiv x + iy$. The SUSY Janus geometry is a fibration of the AdS_4 and the two S^2 's over the Riemann surface. Notice that the Riemann surface has the topology of a strip:

$$\text{Re}(v) = x \in (-\infty, \infty), \quad \text{Im}(v) = y \in [0, \pi/2]. \quad (2.25)$$

The metric and dilaton of the SUSY Janus solution are given by [18]

$$ds^2 = f_4^2 ds_{AdS_4}^2 + f_1^2 ds_{S^2}^2 + f_2^2 ds_{S^2}^2 + \rho^2 dv d\bar{v}, \quad (2.26a)$$

$$e^{4\phi} = N_2/N_1, \quad (2.26b)$$

where $ds_{AdS_4}^2$ is the metric of unit-radius AdS_4 in eq. (2.4). The warp factors f_4^2 , f_1^2 , f_2^2 , and ρ^2 all depend on v and \bar{v} , as do the functions N_1 and N_2 appearing in the equation for ϕ . To write these functions, let us introduce $h_1(v, \bar{v})$ and $h_2(v, \bar{v})$, two real, harmonic functions on the Riemann surface parameterized by z , which obey the boundary conditions

$$h_1|_{y=0} = \partial_y h_2|_{y=0} = 0, \quad h_2|_{y=\pi/2} = \partial_y h_1|_{y=\pi/2} = 0. \quad (2.27)$$

For SUSY Janus these harmonic functions are [18]

$$h_1(v, \bar{v}) = -i\alpha_1 \sinh\left(v - \frac{\delta\phi}{2}\right) + c.c., \quad h_2(v, \bar{v}) = \alpha_2 \cosh\left(v + \frac{\delta\phi}{2}\right) + c.c., \quad (2.28)$$

which are completely specified by the three constants α_1 , α_2 and $\delta\phi$, whose physical meaning we discuss below. The functions appearing in the SUSY Janus metric and dilaton are completely determined by $h_1(v, \bar{v})$ and $h_2(v, \bar{v})$ as follows [18]:

$$w \equiv \partial_v h_1 \partial_{\bar{v}} h_2 + \partial_{\bar{v}} h_1 \partial_v h_2, \quad (2.29a)$$

$$N_1 = 2h_1 h_2 |\partial_v h_1|^2 - h_1^2 w, \quad N_2 = 2h_1 h_2 |\partial_v h_2|^2 - h_2^2 w, \quad (2.29b)$$

$$f_4^8 = 16 \frac{N_1 N_2}{w^2}, \quad \rho^8 = \frac{2^8 N_1 N_2 w^2}{h_1^4 h_2^4}, \quad (2.29c)$$

$$f_1^8 = 16 h_1^8 \frac{N_2 w^2}{N_1^3}, \quad f_2^8 = 16 h_2^8 \frac{N_1 w^2}{N_2^3}. \quad (2.29d)$$

The geometry has two asymptotically $AdS_5 \times S^5$ regions, where $\text{Re}(v) = x \rightarrow \pm\infty$. To be explicit, a change of coordinates as $x \rightarrow \pm\infty$,

$$x = \hat{x} \pm \frac{1}{2} \ln \cosh(\delta\phi), \quad (2.30)$$

puts the asymptotic SUSY Janus metric in the same form as the asymptotic AdS_4 -sliced $AdS_5 \times S^5$ metric in eq. (2.3). The values of the AdS_5 radius and the dilaton in the two asymptotic regions are

$$R^4 = 16 |\alpha_1 \alpha_2| \cosh(\delta\phi), \quad e^{2\phi_{\pm}} = \left| \frac{\alpha_2}{\alpha_1} \right| e^{\pm\delta\phi}, \quad (2.31)$$

which clarify the meaning of the constants α_1 , α_2 , and $\delta\phi$. The bulk metric and dilaton depend on three parameters, α_1 , α_2 , and $\delta\phi$, which map to three physical parameters, the asymptotic AdS_5 radius, the overall background value of the dilaton, and the size of the jump in the dilaton at the boundary, $\delta\phi = \phi_+ - \phi_-$. To recover $AdS_5 \times S^5$, we simply take $\delta\phi = 0$ in all of the above.

The SUSY Janus solution also includes a non-trivial RR five-form with N_c units of flux on the internal space as well as a non-trivial RR two-form with flux on one S^2 and a non-trivial NS two-form with flux on the other S^2 [18]. To compute Wilson loops we will introduce strings into the SUSY Janus spacetime. In Einstein frame the string action involves the dilaton and the pull-backs of the metric and NS two-form. We will thus not need the RR five-form or two-form, so we will omit them from our review of SUSY Janus. Furthermore, for the strings we will study in section 4 the pull-back of the NS two-form will vanish, hence we will omit the NS two-form also.

What is the classical Lagrangian of the field theory dual to SUSY, jumping-coupling Janus? As shown in ref. [6] the classical Lagrangian is $\mathcal{L}_{\mathcal{N}=4}$, with $\theta = 0$ and with g promoted to a function of x_3 , plus a term \mathcal{L}_{int} , to which the scalars' contribution is

$$\mathcal{L}_{\text{int}} \supset \frac{\partial_3 g}{g^3} \text{tr} \left(-\frac{2}{3} i \epsilon^{IJK} \hat{\Phi}^I [\hat{\Phi}^J, \hat{\Phi}^K] + D_3(\hat{\Phi}^I \hat{\Phi}^I) \right) - \frac{(\partial_3 g)^2}{g^4} 2 \text{tr} \hat{\Phi}^I \hat{\Phi}^I, \quad I, J, K = 1, 2, 3, \quad (2.32)$$

in the limit where g approaches a step function, in which case \mathcal{L}_{int} becomes localized to the interface. Here I, J, K run over 1, 2, 3, so that \mathcal{L}_{int} involves only three of the six scalars, and thus breaks the $SO(6)$ R-symmetry down to $SO(3) \times SO(3)$, which matches the isometry of the two S^2 's in the internal space of the SUSY Janus solution. Notice that SUSY fixes the coefficients of the terms in \mathcal{L}_{int} . Performing an $SL(2, \mathbb{R})$ transformation will generate a jumping θ -angle, as well as new interface-localized terms whose coefficients are again fixed by SUSY, as argued in ref. [8].

2.3 Janus and Topological Insulators

For both non-SUSY and SUSY Janus, we can generate new solutions with non-vanishing axion using $SL(2, \mathbb{R})$ transformations. An $SL(2, \mathbb{R})$ transformation of the Janus solution leaves the Einstein metric unchanged, but produces a new dilaton, ϕ' , and a non-trivial axion, $C_{(0)}$:

$$C_{(0)} = \frac{b d + a c e^{-4\phi}}{d^2 + c^2 e^{-4\phi}}, \quad e^{2\phi'} = d^2 e^{2\phi} + c^2 e^{-2\phi}, \quad (2.33)$$

where $a, b, c, d \in \mathbb{R}$ and $ad - bc = 1$. The transformation appears to introduce three new parameters (four real numbers with a constraint), but by an appropriate constant shift of ϕ , which was a symmetry of the $C_{(0)} = 0$ solution, we can always set either c or d to one. The $SL(2, \mathbb{R})$ transformation thus introduces only two new parameters, the two asymptotic values of $C_{(0)}$. We can easily construct solutions with the dilaton constant at the boundary but with a jumping axion by demanding $e^{2\phi'_+} = e^{2\phi'_-}$, or equivalently

$$d^2 e^{2\phi_+} + c^2 e^{-2\phi_+} = d^2 e^{2\phi_-} + c^2 e^{-2\phi_-} \quad \Rightarrow \quad \frac{c^2}{d^2} = \frac{e^{2\phi_+} - e^{2\phi_-}}{e^{-2\phi_-} - e^{-2\phi_+}}. \quad (2.34)$$

For the $C_{(0)}$ in eq. (2.33) to be finite and for a solution to eq. (2.34) to exist, c and d must both be non-zero, which implies that $e^{2\phi'}$ satisfies a bound, $e^{2\phi'} \geq 2|cd|$. Recall that the string coupling is $g_s = e^{2\phi'}$. If we work with $SL(2, \mathbb{Z})$, so that c and d are integers, then because of this bound the string coupling will be order one or larger. To remain in the weakly-coupled regime, we thus move outside of $SL(2, \mathbb{Z})$, to $SL(2, \mathbb{R})$, so that we can adjust c and d to keep g_s sufficiently small. Although we are then not guaranteed quantized charges in the full quantum theory, type IIB string theory, at the classical level $SL(2, \mathbb{R})$ transformations give us perfectly valid solutions of supergravity. We can achieve a $\delta C_{(0)}$ of any size by suitable adjustments of a , b , c , and d .

As mentioned in the introduction, we can think of $\mathcal{N} = 4$ SYM with a constant coupling and a θ -angle jumping from zero to π (mod 2π) as the low-energy effective description of a (3+1)-dimensional T-invariant fractional TI, as we will now explain in detail.

A TI is a physical system with

1. a $U(1)$ symmetry for which we will study transport, for example the $U(1)$ gauge invariance of electromagnetism,
2. a mass gap in the sector charged under the $U(1)$ (hence an insulator), and
3. a topological quantum number distinct from the vacuum, which appears at low energies as a quantized, dissipationless transport coefficient. Here “topological” means invariant under any continuous deformation that preserves all symmetries and does not close the mass gap.

Since 1980, the canonical example of a TI has been the integer QHS, which breaks time reversal symmetry, T, and where the topological quantum number is the Hall conductivity. Since 2005 a number of TIs have been discovered that preserve T. One example is HgTe, for which electronic transport is effectively (2+1)-dimensional. In (3+1) dimensions, examples include Bi_2Se_3 , Bi_2Te_3 , and Sb_2Te_3 . For reviews of TIs, see for example refs. [32–35].

The physics of all the TIs mentioned above is simplest to understand via two levels of effective field theory. We start at the shortest length scales, or highest energies, with a lattice Hamiltonian and associated band structure, which by assumption is that of an insulator, with a valence band separated from a conduction band by a band gap. Here the topological quantum number appears as a topological invariant associated with a Berry’s connection defined over momentum space (the Brillouin zone) using the electronic Bloch wave-functions. In the integer QHS the topological quantum number is the first Chern number of this (Abelian) Berry’s connection, summed over all occupied bands [46] (the TKNN invariant), which is \mathbb{Z} -valued. For the (3+1)-dimensional T-invariant TIs, the topological quantum number is the \mathbb{Z}_2 -valued integral of the (non-Abelian) Chern-Simons form built from the Berry’s connection [37, 38, 47–49].

Integrating out all bands except the top-most band, we reach the first level of effective field theory: a free Dirac Hamiltonian whose mass matrix, which may involve non-trivial Dirac matrices, encodes the information about the symmetries of the state. For the integer QHS, the effective theory is some number of Dirac fermions with real masses, which break T. Here the \mathbb{Z} -valued topological invariant

appears simply as the number of Dirac fermions. For the (3+1)-dimensional T-invariant TIs, the effective theory is a single Dirac fermion with a complex mass. Here the \mathbb{Z}_2 -valued topological invariant appears as the phase of that mass, which can be either of two values allowed by T-invariance, zero or $\pi \pmod{2\pi}$. In other words, the mass is real but can be positive or negative.

Integrating out the massive Dirac fermion(s), we obtain the second, and lowest, level of effective field theory, a topological term for external $U(1)$ electric and magnetic fields.⁷ Here the topological invariant appears as the coefficient of this term, and thus determines a dissipationless, quantized transport coefficient associated with the $U(1)$ charge. In the integer QHS, the ultimate low-energy physics is described by Chern-Simons theory [36, 50, 51], whose coefficient determines the Hall conductivity, which is thus \mathbb{Z} -quantized. For the (3+1)-dimensional T-invariant TIs, the low-energy physics is a θ -angle term, where T-invariance demands that the value of θ be either zero or $\pi \pmod{2\pi}$ [37, 38] (the phase of the mass in the previous level of effective description). The θ -angle term determines the magneto-electric response [37, 38]: an applied magnetic field generates an electric polarization and an applied electric field generates a magnetization. In a (3+1)-dimensional T-invariant TI, the magneto-electric response is thus \mathbb{Z}_2 -quantized.

An analysis of quantum anomalies in TI states reveals that gapless fermionic modes must necessarily exist at the boundary between a TI and the vacuum, which we will call “edge modes” [52].⁸ Given that the bulk of the material is insulating, these edge modes are what give rise to quantized $U(1)$ response. Indeed, topology and symmetry forbid the edge modes from becoming localized, hence they produce dissipationless $U(1)$ response even in the presence of arbitrarily strong disorder, so long as that disorder does not alter the symmetries [53]. In the integer QHS the edge modes are (1+1)-dimensional chiral fermions [54, 55]. In (3+1)-dimensional T-invariant TI states, the edge modes are (2+1)-dimensional Dirac fermions [49, 56].

The edge modes appear in the first level of effective description when the Dirac mass varies in space with a zero at the location of the boundary, indicating the presence of boundary-localized zero modes [37, 56]. Reaching the lowest level of effective description requires giving the edge modes a mass, for example by breaking some or all of the symmetry “locally”, at the boundary only, *i.e.* somehow suppressing the transmission of symmetry-breaking effects to the bulk [37, 56]. Integrating out the now-massive edge modes, we reach the lowest level of effective description, a topological term whose coefficient jumps at the boundary. For example, for (3+1)-dimensional T-invariant TIs, the ultimate low-energy description of the boundary is a θ -angle term where θ jumps from zero to $\pi \pmod{2\pi}$ at the boundary [37].

Remarkably, a complete classification exists for all TI states that can be described by Hamiltonians in the same universality classes as the free Dirac Hamiltonians (*i.e.* connected by adiabatic

⁷If the $U(1)$ is gauged, and the associated dynamical gauge field is gapless, then the effective description at any scale must include gauge field kinetic terms, *i.e.* a Maxwell action. For simplicity, we will neglect the Maxwell contribution to the low-energy effective action, so that all electric and magnetic fields are external and non-dynamical.

⁸More generally, such edge modes exist at the boundary between two TIs with different topological quantum numbers. Notice that the anomaly analysis proves that the two definitions of TIs, the one we gave in the introduction, in terms of gapless edge modes, and the one in this section, are equivalent.

continuity) [52, 57–61]. What TI states are possible for Hamiltonians in other universality classes remains an open question. To date, the only examples realized experimentally are fractional QHSs, in which the Hall conductivity is quantized to be a rational number times the electron’s charge (in units of Planck’s constant). Fractional QHSs are states that cannot be adiabatically deformed into a state of free electrons. A natural question is whether fractional T-invariant TIs exist to which analogous statements would apply.

To our knowledge, no precise definition of fractionalization exists.⁹ The concept of fractionalization is simple, however: in an interacting many-electron system, the low-energy emergent degrees of freedom can carry a fraction of the electron’s charge. Indeed, that is what happens in (1+1)-dimensional interacting many-electron systems, Luttinger liquids [63], where charge and spin propagate independently, and is also what happens in fractional QHSs [64].

In one approach to fractionalization, which goes by various names, the “partonic,” “projective,” or “slave particle” approach [36, 65–71], we begin by writing the electron creation operator as a product of some number of other operators, *i.e.* some constituent “partons.” The statistics and $U(1)$ charges of these partons must be arranged such that their product is fermionic and has a net $U(1)$ charge equal to the electron’s. We must also enlarge the Hilbert space to account for these new degrees of freedom, with a constraint that only electrons appear in physical states. Of course, such a description, which introduces additional, redundant degrees of freedom, is always possible, but usually is an unnecessary complication. A fractionalized phase, however, corresponds to a “deconfined” phase for the partons, *i.e.* a phase in which the partons are eigenstates (or at least long-lived approximate eigenstates) of the Hamiltonian, rather than the electrons, in which case the partons are the more appropriate variables to use.

Suppose for example we want the electron to fractionalize into n constituent partons. We can achieve that by extending the symmetry group from $U(1)$ to $U(1) \times SU(n)$, with the partons in the fundamental representation of $SU(n)$. An electron is then a singlet of $SU(n)$ but charged under the $U(1)$. At the first level of effective field theory we obtain not a free Dirac Hamiltonian for the electron but a theory of partons interacting via emergent $SU(n)$ gauge fields, which in this context are called “statistical gauge fields” [36, 41]. A fractionalized state then is a deconfined, or at least non-confined, state of this non-Abelian gauge theory.¹⁰ To describe a partonically fractionalized T-invariant TI [39–41], the partons must have complex masses whose phases are either zero or π (mod 2π). Integrating out the partons, at the lowest level of effective theory we obtain $SU(n)$ gauge fields with a θ -angle equal to zero or π with periodicity 2π , and a $U(1)$ θ -angle equal to zero or π/n with a periodicity $2\pi/n$, which guarantees T-invariance [39]. The fractional $U(1)$ θ -angle will clearly produce fractional magneto-electric response. Besides deconfined non-Abelian statistical

⁹For a recent attempt to define an order parameter for fractionalization, see ref. [62].

¹⁰The partonic description of fractionalization obviously has many similarities to Quantum Chromodynamics (QCD), but also has one major difference: the energy scales are “reversed.” In partonic fractionalization, the electron is the appropriate *high-energy* degree of freedom, while the partons and non-Abelian gauge fields appear as *low-energy*, emergent degrees of freedom. In QCD, the partons and gauge fields (quarks and gluons) are the appropriate *high-energy* degrees of freedom, and the analogue of the electron, namely the baryon (charged under $U(1)$ baryon number but a singlet of $SU(3)$ color), is an emergent, *low-energy* degree of freedom.

gauge fields (with gauge group $SU(n)$ or otherwise), (3+1)-dimensional partonically fractionalized T-invariant TIs can be described by non-Abelian statistical gauge fields with the gauge group Higgsed to a discrete subgroup or by Abelian statistical gauge fields [41].

What are the edge modes in a (3+1)-dimensional partonically fractionalized T-invariant TI? They are (2+1)-dimensional fermions in “half” of a fractional QHS, *i.e.* the Hall conductivity is quantized to be $1/2$ times a rational number times the electron’s charge [39]. Gapping these edge modes and integrating out both the partons and the edge modes, we reach a description of the edge at the lowest level of effective field theory, with an $SU(n)$ θ -angle that jumps from zero to π (mod 2π) and a $U(1)$ θ -angle that jumps from zero to π/n (mod $2\pi/n$). In other words, on one side is the vacuum, a state that is non-fractionalized and topologically trivial, while on the other side is the TI, which is fractionalized and topologically non-trivial.

We can now state our main proposal: we can think of $\mathcal{N} = 4$ SYM with a θ -angle that jumps from zero to π as the low-energy effective description of a (3+1)-dimensional fractional T-invariant TI, where the statistical gauge fields are the $SU(N_c)$ gauge fields. Clearly such a fractional TI is very special, being in some sense the maximally SUSY fractional TI. Moreover, notice that $\mathcal{N} = 4$ SYM with a jumping θ -angle actually describes an interface between a state that is fractionalized and topologically non-trivial and a state that is fractionalized and topologically trivial, *i.e.* *both* states are fractionalized. Said another way, in our interpretation, our topologically-trivial vacuum state is the conformally-invariant vacuum of $\mathcal{N} = 4$ SYM, which, being non-confining, we interpret as fractionalized.

The statement that $\mathcal{N} = 4$ SYM with a jumping θ -angle is the low-energy effective description of a fractional TI raises several important questions. Where is the $U(1)$ symmetry that will have fractional θ -angle, *i.e.* the $U(1)$ mentioned in part 1 of our definition of TIs above?¹¹ What kind of edge modes did the system have, before we gapped them and integrated them out to obtain $\mathcal{N} = 4$ SYM with a jumping θ -angle? We will not be able to answer these questions completely, but we will take some first steps.

In previous constructions of holographic duals to (3+1)-dimensional fractional TI states [72, 73] the $U(1)$ was a global flavor symmetry. In particular, consider $\mathcal{N} = 4$ SYM coupled to a number N_f of $\mathcal{N} = 2$ SUSY hypermultiplets in the fundamental representation of $SU(N_c)$, *i.e.* flavor fields. The $\mathcal{N} = 2$ hypermultiplet includes a Dirac fermion and two complex scalars. Borrowing from QCD parlance, we will call the Dirac fermion a quark and the scalars squarks.

$\mathcal{N} = 2$ SUSY admits a constant complex hypermultiplet mass. We will assume that the mass matrix in flavor space is proportional to the identity, so that the theory has a global $U(N_f)$ symmetry which we may decompose as $U(1) \times SU(N_f)$. Again borrowing from QCD parlance, we will

¹¹We are not the first to propose that $\mathcal{N} = 4$ SYM with a jumping θ -angle can be interpreted as the low-energy effective description of a fractional TI. A similar proposal was made in ref. [42], however there the $SU(N_c)$ was identified as the generalization of the $U(1)$ of electromagnetism, rather than as the gauge group of the statistical gauge fields. Clearly that cannot be the case. In a TI the $U(1)$ of electromagnetism has gauge-invariant currents from which we can measure transport coefficients. The $SU(N_c)$ gauge currents are not gauge-invariant, hence we have no obvious way to define gauge-invariant transport coefficients from them.

call the $U(1)$ factor baryon number, and henceforth ignore the $SU(N_f)$ factor. Notice that both the quarks and the squarks are charged under baryon number.

If $N_f \ll N_c$ then we can take the so-called probe limit, where we expand all observables in the small parameter N_f/N_c and retain terms only up to order $N_f N_c$. Physically, the probe limit corresponds to discarding quantum effects due to the flavor fields. In diagrammatic perturbation theory in λ , the probe limit consists of discarding diagrams with quark or squark loops.

The holographic dual of large- N_c , strongly-coupled $\mathcal{N} = 4$ SYM coupled to N_f hypermultiplets, in the probe limit, is type IIB supergravity in $AdS_5 \times S^5$ with N_f probe D7-branes extended along $AdS_5 \times S^3$ [74]. Roughly speaking, the magnitude and phase of the complex hypermultiplet mass are dual to the two worldvolume scalars on the D7-branes that describe the position of the D7-branes in the two transverse directions on the S^5 . The conserved baryon number current is dual to the D7-brane $U(1)$ worldvolume gauge field [75, 76]. In the probe limit the action that describes the dynamics of the worldvolume scalars and gauge field is a Dirac-Born-Infeld action plus a Wess-Zumino term describing the coupling to the background RR five-form.

A nonzero, real $\mathcal{N} = 2$ SUSY-preserving mass M appears in the bulk, in the probe limit, as a D7-brane that “ends” at some radial position [74]. More precisely, at the AdS_5 boundary the D7-branes wrap an equatorial $S^3 \subset S^5$, but as they extend into the bulk the S^3 shrinks and eventually collapses to a point at some radial position. The effective tension of the D7-branes goes to zero at that point, hence the D7-branes “end” there. Recalling that the radial direction corresponds to the energy scale in the field theory [43, 44], we expect the position where the D7-branes ends to correspond to the mass scale M . In fact that position corresponds to the scale $M/\sqrt{\lambda}$ [77].

In the language of partonic fractionalization, we can think of the hypermultiplet fields as the partons and the $SU(N_c)$ gauge fields as the statistical gauge fields. Giving the hypermultiplets a mass whose phase varies in one spatial direction as a step function, jumping from zero to π at some position, will produce an edge between fractionalized T-invariant TI states, as described above. Integrating out the partons, and also gapping and integrating out the edge modes, we reach the lowest level of effective theory, in which the baryon number $U(1)$ acquires a θ -angle that jumps from zero to π/N_c , and hence the baryon number response will exhibit a fractional magneto-electric effect, while the $SU(N_c)$ gauge fields will acquire a θ -angle that jumps from zero to π . In the probe limit, however, the jump in the $SU(N_c)$ θ -angle is a sub-leading effect, and will not be apparent.

Remarkably, holographic duals of such an edge between fractional TI states have been found, using probe D7-branes [72, 73]. Clearly these D7-branes will have a more complicated embedding than the simple “D7-brane that ends,” so we will not attempt to describe the solutions for the worldvolume fields in detail, rather we just will highlight a few salient points. Two solutions have been found so far, one solution that breaks all SUSY, and in which only the worldvolume scalars, and not the worldvolume gauge field, are active [72], and another solution that preserves four real supercharges of the $AdS_5 \times S^5$ background, and in which both the worldvolume scalars and the gauge field are active [73]. The baryon number $U(1)$ ’s fractional θ -angle can be extracted from the probe D7-brane Wess-Zumino term [72]. The probe D7-brane does not affect any of the background

supergravity fields, including the axion, which indicates that in the field theory the $SU(N_c)$ θ -angle does not jump, as expected in the probe limit.

Most importantly, the edge modes are apparent in the bulk: near the interface, the D7-branes bend and become extended along $AdS_4 \times S^4$ [72]. Such D7-branes along $AdS_4 \times S^4$ (in the absence of worldvolume gauge field flux) break all SUSY, and are dual to (2+1)-dimensional fermions alone, with no scalar superpartners, and with couplings only to the $\mathcal{N} = 4$ SYM gauge field and one of the six real $\mathcal{N} = 4$ SYM scalars, both restricted to the (2+1)-dimensional interface [78–83]. These (2+1)-dimensional fermions are the edge modes of the holographic fractional TI states described above. A combination of perturbation theory in λ and holographic calculations reveals that these fermions exhibit a phase transition as a function of coupling [83]: at small λ , the vacuum preserves parity and T , but above some critical λ the fermions pair, such that the Dirac mass operator acquires a nonzero expectation value, spontaneously breaking parity and T . Very similar D7-branes, extended along $AdS_4 \times S^2 \times S^2$ with worldvolume fluxes on the S^2 's, also describe (2+1)-dimensional defect fermions coupled to $\mathcal{N} = 4$ SYM, with different couplings to the adjoint scalars than those of the fermions described by the D7-brane along $AdS_4 \times S^4$, and presumably would describe the edge modes in some fractional TI. Indeed, D7-branes extended along $AdS_4 \times S^2 \times S^2$ have been used to describe quantum Hall states [84–86] and to model graphene [87], among other things [88–90]. Here again the fermions exhibit an instability at large λ , where a net baryon number charge density of these fermions is unstable to forming a striped phase similar to a charge density wave [91].

The crucial observation for us is that the non-SUSY jumping-axion Janus solution carries D7-brane charge. Indeed, the D7-brane charge is localized at the boundary, at the point where the axion jumps, and can be detected by the monodromy of the axion about that point. The Janus geometry actually has a conical singularity there, associated with an angular excess [4], as expected for D7-branes. In fact, the jumping-axion Janus solution is closely related to the solution of refs. [92–95], which describes a continuous distribution of D7-branes in $AdS_5 \times S^5$, and is dual to $\mathcal{N} = 4$ SYM with a θ -angle that varies linearly in x_3 . In some sense, the solution of refs. [92–95] represents a continuum of jumping-axion Janus solutions “smeared” in the x_3 direction.

The fact that the non-SUSY jumping-axion Janus solution carries both D3-brane and D7-brane charge (nonzero RR five-form flux and axion monodromy, respectively) suggests that such a solution could be constructed from an intersection of D3-branes and D7-branes. Indeed, since non-SUSY jumping-axion Janus carries *only* D3-brane and D7-brane charge, the relevant intersection may be precisely the non-SUSY intersection of ref. [72]. To go from the probe D7-brane solutions of ref. [72] to the non-SUSY jumping-axion Janus solution, we would need to leave the probe limit, allowing the D7-branes to back-react on the fields of supergravity, and require the D7-branes to end at (or near) the boundary, so that in the field theory both the partons and the edge modes are, in effect, infinitely heavy, and can be integrated out. If we performed those steps then, recalling that the radial coordinate is dual to the field theory energy scale, we would expect the resulting solution to look like non-SUSY jumping-axion Janus deep in the bulk (far in the IR).

Many things about such a construction are unclear and confusing to us, on both sides of the

correspondence, however. For example, on the supergravity side, the back-reaction of the D7-branes will break the $SO(6)$ isometry of the S^5 to a subgroup, since as probes the D7-branes wrap only a submanifold of the S^5 . How can the full $SO(6)$ isometry be restored deep in the bulk? On the field theory side, all SUSY and part of the R-symmetry are broken, so if we integrate out the hypermultiplets on both sides of the interface, and gap the edge modes and integrate them out, we have little reason to expect that the resulting effective Lagrangian would be precisely that of $\mathcal{N} = 4$ SYM with a jumping θ -angle. According to the rules of effective field theory, with all SUSY and part of the R-symmetry broken, many terms besides those of the $\mathcal{N} = 4$ Lagrangian are allowed. Such issues may be clearer if SUSY is restored: a D-brane construction of SUSY jumping-axion Janus may be more straightforward, especially on the field theory side, where the SUSY should provide greater control over allowed terms in a low-energy effective action.¹²

If we could determine an intersection of D3-branes and D7-branes that gives rise to non-SUSY jumping-axion Janus, then we could determine the edge modes in the dual fractional TI. If we assume that such a D-brane construction exists, then we can identify the “missing” $U(1)$: the $U(1)$ with fractional θ -angle is the baryon number $U(1)$. When the D7-branes are in a probe limit, that $U(1)$ appears in the open string sector in the bulk, as the $U(1)$ worldvolume D7-brane gauge field. Including the back-reaction of the D7-branes, and requiring that the D7-branes end at the boundary, we expect to find a description in terms of closed strings alone, with the bulk degrees of freedom that are dual to the $U(1)$ localized at the boundary, at the point where the axion jumps. Such modes would be very much like singletons, in that they would be non-dynamical, boundary-localized modes. Indeed, such modes would be similar to a familiar singleton: recall that the worldvolume theory on a stack of N_c D3-branes is actually $U(N_c)$, not just $SU(N_c)$, where the “extra” $\mathcal{N} = 4$ $U(1)$ vector multiplet appears in holography as a non-dynamical, boundary-localized singleton mode (for a review, see section 3.1 of ref. [96]). In our case, since the baryon number $U(1)$ is global (unlike the $U(1) \in U(N_c)$), any effective low-energy description will include only the jumping fractional θ -angle, and not a Maxwell term.

To summarize, our proposal is the following. Non-SUSY Janus with an axion that jumps from zero to $1/2$ (mod one) is the holographic dual of an interface CFT that we can interpret as the low-energy effective description of an interface between two fractionalized states, a topologically trivial vacuum and a T-invariant TI. More precisely, the interface CFT is $\mathcal{N} = 4$ SYM with a θ -angle that jumps from zero to π (mod 2π). We interpret the $SU(N_c)$ gauge fields as statistical gauge fields. The $U(1)$ with fractional θ -angle is a global symmetry, namely a baryon number $U(1)$ associated with the partons and edge modes that we integrated out to obtain the interface CFT. We leave several open questions for future research, chief among them being: what were the edge modes that were integrated out?

¹²Notice that the SUSY probe D7-brane solution of ref. [73] cannot give rise to the SUSY jumping-axion Janus solution reviewed in section 2.2, since the former preserves only four real supercharges while the latter preserves sixteen real supercharges of the $AdS_5 \times S^5$ solution.

3 Wilson Loops: Field Theory Calculation

Our goal is to calculate the potential V representing the self-energy of a single test charge or the potential between heavy test charges in $\mathcal{N} = 4$ SYM with a conformal interface, with gauge group $SU(N_c)$ and in the large- N_c limit. In subsection 3.1 we review the analogous calculation in ordinary electromagnetism, where many of the physical effects associated with an interface already appear. In section 3.2 we turn to the calculation of V in $\mathcal{N} = 4$ SYM using perturbation theory in the 't Hooft coupling. Later we will compare our results for V in electromagnetism and in $\mathcal{N} = 4$ SYM to our holographic results in section 4.

3.1 Electromagnetism

The Lagrangian of (3+1)-dimensional electromagnetism, in the absence of sources, is

$$\mathcal{L}_{EM} = -\frac{1}{4g^2} F_{\mu\nu} F^{\mu\nu} - \frac{\theta}{32\pi^2} \epsilon^{\mu\nu\rho\sigma} F_{\mu\nu} F_{\rho\sigma}, \quad (3.1)$$

where $F_{\mu\nu}$ is the $U(1)$ field strength. In order to study an interface, we will allow g and θ to be functions of position. Let us define the canonical momentum $G^{\mu\nu}$ as

$$G_{\mu\nu} \equiv -2 \frac{\delta \mathcal{L}_{EM}}{\delta F^{\mu\nu}} = \frac{1}{g^2} F_{\mu\nu} + \frac{\theta}{8\pi^2} \epsilon_{\mu\nu\rho\sigma} F^{\rho\sigma}, \quad (3.2)$$

which is also known as a “constitutive relation.” Next we introduce electric and magnetic source currents,

$$J_e^\mu = 2\pi(\rho_e, j_e^i), \quad J_m^\mu = (\rho_m, j_m^i), \quad (3.3)$$

respectively, where the time components of the currents, ρ_e and ρ_m , are the electric and magnetic charge densities, while j_e^i and j_m^i are the spatial electric and magnetic currents, with $i = 1, 2, 3$. The factor of 2π in our definition of J_e^μ is for later convenience. Including the sources, the equation of motion and Bianchi identity may be written as

$$\partial_\mu G^{\mu\nu} = J_e^\nu, \quad \frac{1}{2} \epsilon^{\mu\nu\rho\sigma} \partial_\mu F_{\rho\sigma} = J_m^\nu. \quad (3.4)$$

Next, let us introduce the electric field E^i , magnetic field B^i , electric displacement D^i , and magnetic displacement H^i :

$$F^{i0} \equiv E^i, \quad F^{ij} \equiv -\epsilon^{ijk} B^k, \quad G^{i0} \equiv D^i, \quad G^{ij} \equiv -\epsilon^{ijk} H^k. \quad (3.5)$$

The explicit expressions for the fields \vec{D} and \vec{H} in terms of \vec{E} and \vec{B} are

$$\vec{D} = \frac{1}{g^2} \vec{E} + \frac{\theta}{4\pi^2} \vec{B}, \quad \vec{H} = \frac{1}{g^2} \vec{B} - \frac{\theta}{4\pi^2} \vec{E}. \quad (3.6)$$

For later use, let us also define a matrix \mathcal{M} by rewriting the constitutive relation:

$$\begin{pmatrix} 2\pi\vec{D} \\ \vec{B} \end{pmatrix} = \mathcal{M} \begin{pmatrix} \vec{E} \\ 2\pi\vec{H} \end{pmatrix}, \quad \mathcal{M} \equiv \begin{pmatrix} \frac{2\pi}{g^2} + \frac{g^2\theta^2}{8\pi^3} & \frac{g^2\theta}{4\pi^2} \\ \frac{g^2\theta}{4\pi^2} & \frac{g^2}{2\pi} \end{pmatrix}. \quad (3.7)$$

Using \vec{E} , \vec{B} , \vec{D} , and \vec{H} , the equation of motion and Bianchi identity take familiar forms,

$$\begin{aligned}\vec{\nabla} \cdot \vec{D} &= \rho_e, & \vec{\nabla} \cdot \vec{B} &= \rho_m, \\ \vec{\nabla} \times \vec{H} &= \frac{\partial \vec{D}}{\partial t} + \vec{j}_e, & -\vec{\nabla} \times \vec{E} &= \frac{\partial \vec{B}}{\partial t} + \vec{j}_m.\end{aligned}\quad (3.8)$$

The net electric and magnetic charges are defined from the above equations as

$$Q^e = \int d^3x \vec{\nabla} \cdot \vec{D}, \quad Q^m = \int d^3x \vec{\nabla} \cdot \vec{B}. \quad (3.9)$$

We will consider an interface at $x_3 = 0$, allowing both g and θ to jump there, with values g_- and θ_- in the $x_3 < 0$ region and values g_+ and θ_+ in the $x_3 > 0$ region. We will calculate the potential V in the two regions $x_3 > 0$ and $x_3 < 0$ using the method of *image charges*.

We begin by introducing a single test charge and determining the fields \vec{E} , \vec{B} , \vec{D} , and \vec{H} it produces in the presence of the interface. From the equations of motion in eq. (3.8), we can show that at the interface, the perpendicular components of $(2\pi\vec{D}, \vec{B})$ and the parallel components of $(\vec{E}, 2\pi\vec{H})$ must be continuous. Explicitly, these matching conditions are

$$\begin{aligned}D_3|_{x_3 \rightarrow 0^-} &= D_3|_{x_3 \rightarrow 0^+}, & B_3|_{x_3 \rightarrow 0^-} &= B_3|_{x_3 \rightarrow 0^+}, \\ E_i|_{x_3 \rightarrow 0^-} &= E_i|_{x_3 \rightarrow 0^+}, & H_i|_{x_3 \rightarrow 0^-} &= H_i|_{x_3 \rightarrow 0^+},\end{aligned}\quad i = 1, 2. \quad (3.10)$$

We can reproduce these conditions by introducing image charges. To be concrete, consider a dyonic test charge with electric charge Q^e and magnetic charge Q^m . We will arrange these into a column vector $Q = (2\pi Q^e, Q^m)^T$. We will place our test dyon at position $\vec{x}' = (x'_1, x'_2, x'_3)$, with $x'_3 = L_3 > 0$, which is the side with coupling and θ -angle g_+ and θ_+ , as depicted in fig. 3. Next we introduce electric and magnetic potentials Φ_e and Φ_m , defined by

$$\vec{D} = -\vec{\nabla}\Phi_e, \quad \vec{B} = -\vec{\nabla}\Phi_m, \quad (3.11)$$

and arrange these into a column vector also, $\Phi = (2\pi\Phi_e, \Phi_m)^T$. We can then introduce the image charges Q^+ and Q^- by writing

$$\Phi(\vec{x}) = \begin{cases} \frac{Q}{4\pi} \frac{1}{r} + \frac{Q^+}{4\pi} \frac{1}{\tilde{r}} & x_3 > 0, \quad (\text{same side as } Q) \\ \frac{Q}{4\pi} \frac{1}{r} + \frac{Q^-}{4\pi} \frac{1}{r} & x_3 < 0, \quad (\text{side opposite to } Q) \end{cases} \quad (3.12)$$

where

$$r = |\vec{x} - \vec{x}'|, \quad \tilde{r} = |\vec{x} - \vec{x}' + 2L_3\hat{x}_3|, \quad (3.13)$$

where \hat{x}_3 is the unit vector in the x_3 direction. In the $x_3 > 0$ region, the image charge appears to be in the $x_3 < 0$ region, as depicted in fig. 3 (a), hence the distance to Q is r while the distance to Q^+ is \tilde{r} , which is larger than r . In the $x_3 < 0$ region the test charge Q and its image Q^- are coincident, hence only r appears in $\Phi(\vec{x})$ in that region. In other words, in the $x_3 < 0$ region, the effect of the

interface is to shift the charge $Q \rightarrow Q + Q^-$, as depicted in fig. 3 (b). A straightforward exercise shows that the continuity/matching conditions on \vec{E} , \vec{B} , \vec{D} , and \vec{H} are satisfied if we choose [42]

$$Q^+ = (\mathcal{M}_+ \mathcal{M}_-^{-1} + 1)^{-1} (\mathcal{M}_+ \mathcal{M}_-^{-1} - 1) Q, \quad Q^- = -Q^+, \quad (3.14)$$

where \mathcal{M}_\pm are the values of \mathcal{M} on the two sides of the interface. The image charges are completely determined by Q and by the values of g and θ on each side of the interface. Notice that if g and θ are the same on both sides of the interface, then $\mathcal{M}_+ \mathcal{M}_-^{-1} = 1$ and hence $Q^+ = 0$ and $Q^- = 0$.

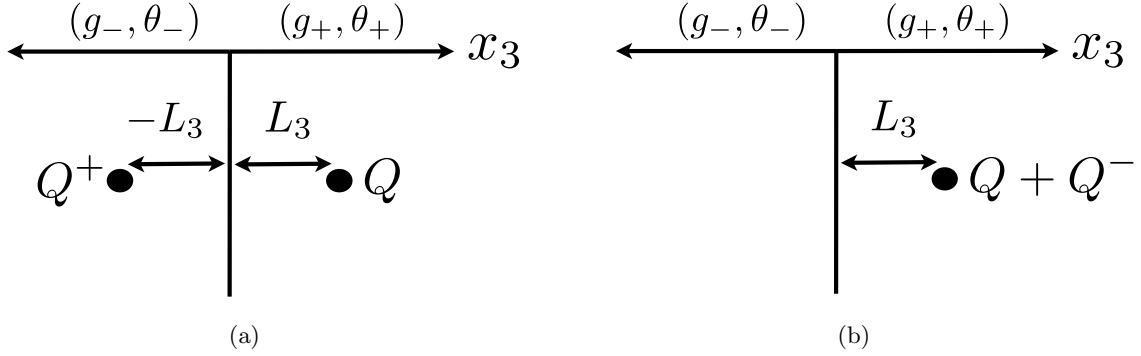


Figure 3: Depiction of the image charges associated with a test charge Q in electromagnetism with a jumping coupling and/or θ -angle. The horizontal axis is the x_3 direction, with the interface at $x_3 = 0$: the coupling and θ -angle have values (g_-, θ_-) for $x_3 < 0$ and (g_+, θ_+) for $x_3 > 0$. We place the test charge Q (the black dot) in the $x_3 > 0$ region, at a position $x_3 = L_3$. (a) Observers in the $x_3 > 0$ region will detect an image charge Q^+ in the $x_3 < 0$ region, a distance L_3 from the interface. (b) Observers in the $x_3 < 0$ region will detect an image charge Q^- coincident with Q . Equivalently, in the $x_3 < 0$ region the interface effectively shifts the charge Q as $Q \rightarrow Q + Q^-$.

Using the image charges Q^+ and Q^- in eq. (3.14), we can compute the potential energy between test charges in the presence of an interface. The magnetic contribution to the potential energy comes from Φ_m , while the electric contribution comes not from Φ_e but from the potential V defined in terms of the electrostatic force, $Q^e \vec{E} \equiv -\vec{\nabla} V$. From eqs. (3.6) and (3.11) we have

$$\vec{E} = g^2 \vec{D} - \frac{g^2 \theta}{4\pi^2} \vec{B} = -g^2 \vec{\nabla} \Phi_e + \frac{g^2 \theta}{4\pi^2} \vec{\nabla} \Phi_m. \quad (3.15)$$

Away from the interface, where g and θ are constant and hence commute with the gradient $\vec{\nabla}$, we thus find

$$V = Q^e \left(g^2 \Phi_e - \frac{g^2 \theta}{2\pi} \Phi_m \right). \quad (3.16)$$

V is the appropriate potential to compare to our Wilson loop results.

Let us compute V first for the simplest case, with a single test charge Q that is purely electric, $Q = (2\pi Q^e, 0)^T$. We want to compute V in the $x_3 > 0$ region, that is, we want to know the

interaction energy of Q^e with its own image charge. Using eq. (3.14), we can easily compute the values of the image charges,

$$Q^{e+} = Q^e \frac{16\pi^4(g_-^2 - g_+^2) + g_+^4 g_-^4 (\theta_+^2 - \theta_-^2)}{16\pi^4(g_+^2 + g_-^2)^2 + g_+^4 g_-^4 (\theta_+ - \theta_-)^2}, \quad (3.17a)$$

$$Q^{m+} = Q^e \frac{8\pi^2 g_+^4 g_-^4 (\theta_+ - \theta_-)}{4\pi^2(g_+^2 + g_-^2)^2 + g_+^4 g_-^4 (\theta_+ - \theta_-)^2}. \quad (3.17b)$$

Notice that when $\theta_+ \neq \theta_-$ the image charge is dyonic (both Q^{e+} and Q^{m+} are nonzero). The electric and magnetic fields in the $x_3 > 0$ region are then

$$\vec{E}(\vec{x}) = \frac{g_+^2 Q^e}{4\pi} \frac{\vec{x} - \vec{x}'}{|\vec{x} - \vec{x}'|^3} + \frac{g_+^2 \tilde{Q}^e}{4\pi} \frac{\vec{x} - \vec{x}' + 2L_3 \hat{x}_3}{|\vec{x} - \vec{x}' + 2L_3 \hat{x}_3|^3}, \quad (3.18a)$$

$$\vec{B}(\vec{x}) = \frac{Q^{m+}}{4\pi} \frac{\vec{x} - \vec{x}' + 2L_3 \hat{x}_3}{|\vec{x} - \vec{x}' + 2L_3 \hat{x}_3|^3}. \quad (3.18b)$$

On the right-hand side in eq. (3.18a), the first term is the field produced by Q^e itself while the second term is the field produced by the image charges, which includes contributions from both the electric and magnetic image charges Q^{e+} and Q^{m+} , via eq. (3.15). We have labeled the net contribution \tilde{Q}^e . Explicitly, \tilde{Q}^e is given by

$$\tilde{Q}^e = Q^{e+} - \frac{\theta_+}{2\pi} Q^{m+} = Q^e \left[\frac{g_-^2 - g_+^2}{g_-^2 + g_+^2} - \frac{2g_+^4 g_-^6 (\theta_+ - \theta_-)^2}{16\pi^4(g_-^2 + g_+^2)^3 + g_+^4 g_-^4 (g_-^2 + g_+^2)(\theta_+ - \theta_-)^2} \right]. \quad (3.19)$$

The potential energy V between Q^e and its image is thus simply

$$V(L_3) = \frac{g_+^2}{4\pi} \frac{Q^e \tilde{Q}^e}{2L_3}. \quad (3.20)$$

Essentially all the physical effects of the interface can be deduced from eq. (3.20): since Maxwell electrodynamics is a linear theory, the potential produced by a distribution of charges will ultimately be some linear superposition of the potential for a single charge.

Consider two special cases. First consider a constant θ -angle, $\theta_+ = \theta_-$, with a jumping coupling. If $g_+ > g_-$, that is, if we place Q^e on the side with larger coupling, then from eq. (3.19) we see that \tilde{Q}^e will have the *opposite* sign to Q^e , hence Q^e will be attracted to the interface. Alternatively, if $g_+ < g_-$, then \tilde{Q}^e will have the *same* sign as Q^e , hence Q^e will be repelled from the interface. The general lesson is that Q^e is always attracted to the side with smaller coupling. The second special case is a constant coupling, $g_+ = g_-$, with a jumping θ -angle. In this case, the \tilde{Q}^e in eq. (3.19) always has opposite sign to Q^e : the last term in eq. (3.19) is Q^e times a strictly negative number. Whether $\theta_+ > \theta_-$ or vice-versa doesn't matter. We thus conclude that with constant coupling and jumping θ -angle, Q^e is always attracted towards the interface.

We can also consider the analogues in electromagnetism of the rectangular Wilson loops depicted in fig. 1. The analogue of fig. 1 (a) is two purely electric test charges Q_1^e and Q_2^e along a line

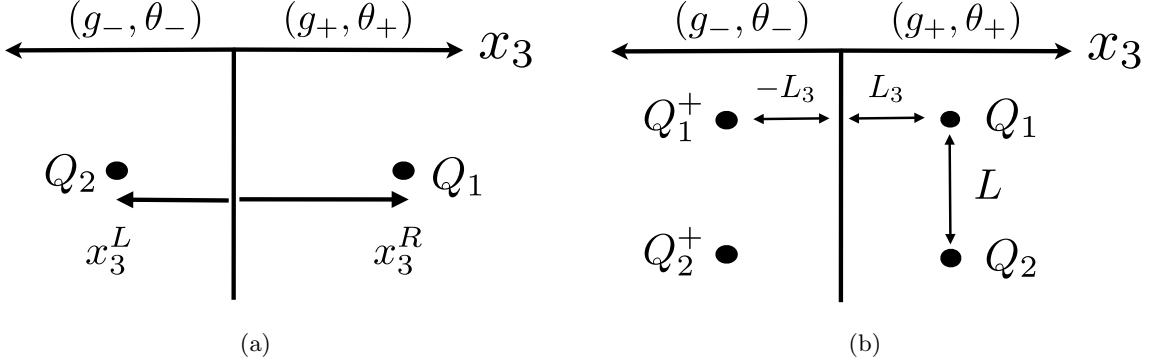


Figure 4: Depictions of the analogues in electromagnetism of the rectangular Wilson loops of $\mathcal{N} = 4$ SYM shown in fig. 1. Our conventions are the same as in fig. 3. (a) The analogue of the perpendicular rectangular Wilson loop of fig. 1 (a): two test charges Q_1 and Q_2 along a line perpendicular to the interface, on opposite sides of the interface. Q_1^e has $x_3^R > 0$ and Q_2^e has $x_3^L < 0$. For clarity, in this case we have not depicted the image charges. (b) The analogue of the parallel rectangular Wilson loop of fig. 1 (b): two test charges Q_1 and Q_2 along a line parallel to the interface, in the $x_3 > 0$ region, separated from each other by a distance L and from the interface by a distance L_3 . Also depicted are the corresponding image charges Q_1^+ and Q_2^+ .

perpendicular to the interface, on opposite sides of the interface, with $Q_2^e = -Q_1^e$, as depicted in fig. 4 (a). We take Q_1^e to be at position $x_3^R > 0$ and Q_2^e to be at $x_3^L < 0$, so that $L = x_3^R - x_3^L > 0$ is the distance between the charges. We will also define $L_{av} = \frac{1}{2}(x_3^R + x_3^L)$, such that

$$\frac{L_{av}}{L} = \frac{1}{2} \frac{x_3^R + x_3^L}{x_3^R - x_3^L} \in \left[-\frac{1}{2}, +\frac{1}{2} \right], \quad (3.21)$$

where $L_{av}/L \in [-1/2, 0)$ means $x_3^R < -x_3^L$, so that the charge on the right is closer to the interface than the charge on the left, and $L_{av}/L \in (0, +1/2]$ means $x_3^R > -x_3^L$, so that the charge on the left is closer. $L_{av}/L = 0$ means $x_3^R = -x_3^L$, so that the two test charges sit perfectly symmetrically about the interface. The potential in this case is

$$V_{\perp}(L, L_{av}) = \frac{g_+^2}{4\pi} \frac{Q_1^e Q_2^e}{L} + \frac{g_+^2}{4\pi} \frac{Q_1^e \tilde{Q}_2^e}{L} + \frac{g_+^2}{4\pi} \frac{Q_1^e \tilde{Q}_1^e}{L + 2L_{av}} + \frac{g_-^2}{4\pi} \frac{Q_2^e \hat{Q}_2^e}{L - 2L_{av}}, \quad (3.22)$$

where \hat{Q}^e is simply \tilde{Q}^e after swapping g_+ and g_- . On the right-hand-side of eq. (3.22), the first term comes from the interaction of Q_1^e with Q_2^e , which has nothing to do with the interface, the second term is the interaction of Q_1^e with Q_2^e 's image charge, which is in fact coincident with Q_2^e , the third term comes from the interaction of Q_1^e with its own image, and the fourth term comes from the interaction of Q_2^e with its own image. If $L_{av}/L \rightarrow -1/2$, then $x_3^R/x_3^L \rightarrow 0$, so that Q_1^e approaches the interface. From eq. (3.22) we can see that the dominant interaction (the smallest denominator) will be the third term. Conversely, if $L_{av}/L \rightarrow +1/2$ then Q_2^e approaches the interface, and the dominant interaction is the fourth term. Physically, in each limit the potential diverges because

a test charge sits exactly on top of its image. In each case we can invoke the lessons we learned for the single test charge to determine whether the potential diverges to $+\infty$ or $-\infty$ (repulsion or attraction, respectively). For example, if θ is constant and $g_+ > g_-$ then we expect Q_1^e to be attracted to its image and Q_2^e to be repelled, hence we expect $V_\perp \rightarrow \pm\infty$ as $L_{av}/L \rightarrow \pm 1/2$. With a constant g and jumping θ , we expect $V_\perp \rightarrow -\infty$ in both limits. In fig. 5 we plot $V_\perp(L, L_{av})$ and observe the expected behavior in each case.

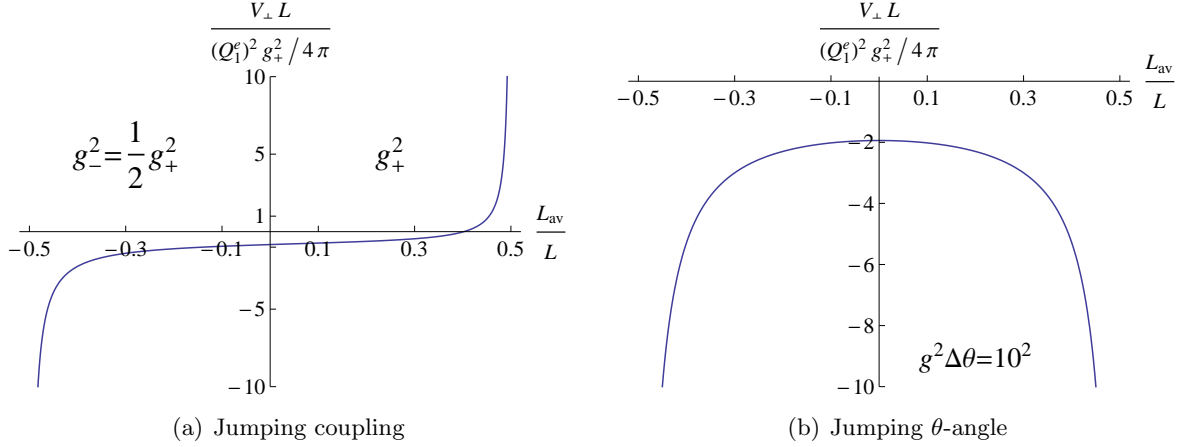


Figure 5: The potential $V_\perp(L, L_{av})$ of eq. (3.22) between two test electric charges along a line perpendicular to the interface, as depicted in fig.4 (a), multiplied by $L/(Q_1^e)^2 g_+^2 / 4\pi$, as a function of L_{av}/L , for two cases: (a) constant θ and jumping g , with $g_-^2 = \frac{1}{2}g_+^2$, (b) constant g and jumping θ , with $g^2|\theta_- - \theta_+| \equiv g^2\Delta\theta = 10^2$. In each case we see the potential diverging as a test charge approaches its own image, as explained in detail in the accompanying text.

The analogue of fig. 1 (b) is two purely electric test charges, Q_1^e and Q_2^e , separated by a distance L from each other and defining a line parallel to the interface at some position $x'_3 = L_3 > 0$, as depicted in fig. 4 (b). Additionally, we take these charges to be equal and opposite, $Q_2^e = -Q_1^e$, and will thus treat them together as a dipole of length L . Each of Q_1^e and Q_2^e will induce an image charge, \tilde{Q}_1^e and \tilde{Q}_2^e respectively, with values given by eq. (3.19). The potential V is then

$$V_\parallel(L, L_3) = \frac{g_+^2}{4\pi} \left[\frac{Q_1^e Q_2^e}{L} + \frac{Q_1^e \tilde{Q}_1^e}{2L_3} + \frac{Q_2^e \tilde{Q}_2^e}{2L_3} + \frac{Q_1^e \tilde{Q}_2^e}{\sqrt{L^2 + 4L_3^2}} \right]. \quad (3.23)$$

On the right-hand side in eq. (3.23), the first term comes from the interaction of Q_1^e with Q_2^e , the second and third terms come from the interactions of Q_1^e and Q_2^e with their own image charges, respectively, and the fourth term comes from the interaction of Q_1^e and Q_2^e with each other's image charges. The fourth term on the right-hand-side is actually invariant under $Q_1^e \leftrightarrow Q_2^e$ because $\tilde{Q}_2^e \propto Q_2^e$ (recall eq. (3.19)). For a dipole parallel to the interface, each charge is closer to its own image than to the other charge's image: $\sqrt{L^2 + 4L_3^2} \geq 2L_3$ (the hypotenuse of a right triangle is longer than either side). We thus expect the interaction of each charge with its own image to

be larger than the interaction with the other charge's image. The net result is that the general rules we learned for the single test charge apply also for the dipole in this case, for example if the θ -angle is constant but the coupling jumps, then the dipole will be attracted to the side with smaller coupling. In fig. 6 we plot $V_{\parallel}(L, L_3)$ in two cases, constant θ with jumping g , and constant g with jumping θ , and observe the expected behavior in each case.

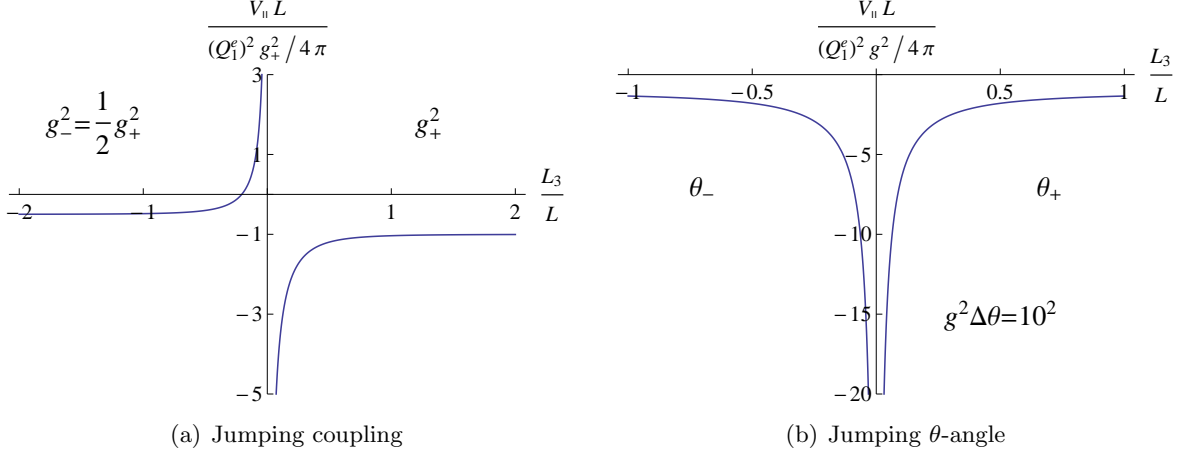


Figure 6: The potential $V_{\parallel}(L, L_3)$ of eq. (3.23) of an electric dipole parallel to the interface at $x_3 = L_3$, as depicted in fig.4 (b), multiplied by $L/(Q_1^e)^2 g_+^2 / 4\pi$, as a function of L_3/L , for two cases. (a) Constant θ and jumping g , with $g_-^2 = \frac{1}{2}g_+^2$, where we see that the potential produces a force towards the left, *i.e.* the dipole is attracted to the side with smaller coupling. As $L_3/L \rightarrow +\infty$, the curve approaches -1 and as $L_3/L \rightarrow -\infty$ the curve approaches $-1/2$: when the dipole is infinitely far from the interface, all that remains is the Coulomb interaction between Q_e^1 and Q_e^2 , with a strength determined by the value of g on that side of the interface. When $L_3/L \rightarrow 0$, the potential diverges because the test charges sit exactly on top of their images. (b.) Constant g and jumping θ , with $g^2 \Delta\theta = 10^2$, where we see that the potential produces a force towards the interface, *i.e.* the dipole is attracted to the interface. As $L_3/L \rightarrow \pm\infty$ the curve approaches -1 , and as $L_3/L \rightarrow 0$ the curve diverges to $-\infty$, for the same physical reasons as in the first case.

3.2 $SU(N_c)$ $\mathcal{N} = 4$ SYM at large N_c

In this subsection we compute the potential V between two heavy test charges in $\mathcal{N} = 4$ SYM with a conformal interface using perturbation theory in the 't Hooft coupling. We present explicit results for V in perturbation theory only in the case of a non-SUSY interface where the coupling jumps, and only for test charges along a line parallel to the interface. In that case we show that for a special value of the interface parameter κ defined in eq. (2.23), $\kappa = 0$, the self-energy of a single test charge vanishes. Our results for V in perturbation theory are valid for any N_c . In the large- N_c limit and large-coupling limits, and for $\kappa = 0$ only, we also compute the contribution to V from the sum of ladder diagrams.

Following refs. [23, 24], we define the Wilson loop operator for $\mathcal{N} = 4$ SYM with a conformal interface, in Euclidean signature,¹³ as

$$W_{\mathcal{R}}[C] \equiv \frac{1}{N_c} \text{tr}_{\mathcal{R}} \mathcal{P} \exp \oint_C ds \left(i \hat{A}_{\mu}(x(s)) \dot{x}^{\mu}(s) + \hat{\Phi}_I(x(s)) \sqrt{\dot{x}^2(s)} \theta^I(s) \right), \quad (3.24)$$

where on the right-hand side the factor of $1/N_c$ is our choice of normalization, the trace is taken in representation \mathcal{R} of $SU(N_c)$, the \mathcal{P} denotes path-ordering, C denotes a closed path parameterized by s (where dots denote $\frac{\partial}{\partial s}$), and the θ^I are the components of a unit-norm vector in \mathbb{R}^6 . Physically, if we introduce an infinitely heavy test charge in representation \mathcal{R} moving along C , the interaction of the test charge with the gauge fields and scalars will produce an insertion of $W_{\mathcal{R}}[C]$ into the path integral of $\mathcal{N} = 4$ SYM. The expectation value $\langle W_{\mathcal{R}}[C] \rangle$ is completely determined by the choices of \mathcal{R} , C , and the θ^I .

We will choose the θ^I to be s -independent constants. We will choose \mathcal{R} to be the fundamental representation of $SU(N_c)$, so that the test charge is a quark. We will choose C to be a rectangle, representing a source quark and anti-quark separated by a distance L propagating for some (Euclidean) time T . Henceforth we will suppress the \mathcal{R} and C notation, so $W_{\mathcal{R}}[C] \rightarrow W$. The expectation value of the rectangular Wilson loop is related to the potential between the heavy test charges, V , as

$$V = - \lim_{T \rightarrow \infty} \frac{1}{T} \log \langle W \rangle. \quad (3.25)$$

When the 't Hooft coupling is small, $\lambda \ll 1$, we can compute $\langle W \rangle$ in perturbation theory. Expanding the Wilson loop expectation value, we find

$$\begin{aligned} \langle W \rangle = 1 & - \frac{N_c}{2} \oint_C ds \oint_C d\tilde{s} \dot{x}^{\mu}(s) \dot{x}^{\nu}(\tilde{s}) \langle A_{\mu}(x(s)) A_{\nu}(x(\tilde{s})) \rangle \\ & + \frac{N_c}{2} \oint_C ds \oint_C d\tilde{s} |\dot{x}(s)| |\dot{x}(\tilde{s})| \theta^I \theta^J \langle \Phi^I(x(s)) \Phi^J(x(\tilde{s})) \rangle + \dots, \end{aligned} \quad (3.26)$$

where we have stripped away the color factors by first writing $\hat{A}_{\mu}(x) = A_{\mu}^a(x) T^a$ with $SU(N_c)$ generators T^a , and similarly for $\hat{\Phi}^I$, then performing the trace using $\text{tr} T^a T^b = \delta^{ab} N_c$, and then defining A_{μ} via

$$\langle A_{\mu}^a(x) A_{\nu}^b(\tilde{x}) \rangle \equiv \delta^{ab} \langle A_{\mu}(x) A_{\nu}(\tilde{x}) \rangle, \quad (3.27)$$

and similarly for the scalars. The \dots in eq. (3.26) represents all terms of higher order in perturbation theory. To compute $\langle W \rangle$ at leading order, we need the gauge and scalar propagators.

We will compute the gauge and scalar propagators of $\mathcal{N} = 4$ SYM only for an interface with a jumping coupling. We take the θ -angle to vanish on both sides of the interface. Our calculation will follow that of refs. [5, 25, 26] very closely.

First let us recall the form of the gauge and scalar propagators for constant g . The standard canonically-normalized scalar propagator, $\Delta(x, \tilde{x})$, which satisfies $-\partial_{\mu} \partial^{\mu} \Delta(x, 0) = \delta^{(4)}(x)$, is

$$\Delta(x, \tilde{x}) = \frac{1}{4\pi^2} \frac{1}{(x - \tilde{x})^2}. \quad (3.28)$$

¹³We use Euclidean signature in the remainder of the paper, including the appendix.

Following refs. [25, 26], we choose the covariant gauge condition $\partial^\mu A_\mu = 0$ and Feynman gauge, in which case the scalar and gauge propagators are almost identical:

$$\langle \Phi^I(x) \Phi^J(\tilde{x}) \rangle = \delta^{IJ} g^2 \Delta(x, \tilde{x}), \quad \langle A_\mu(x) A_\nu(\tilde{x}) \rangle = g^2 \delta_{\mu\nu} \Delta(x, \tilde{x}). \quad (3.29)$$

Now let us introduce a jumping coupling,

$$g(x_3) = g_- \Theta(-x_3) + g_+ \Theta(x_3), \quad (3.30)$$

where $\Theta(x_3)$ is the Heaviside step function,

$$\Theta(x_3) = \begin{cases} 0 & x_3 < 0, \\ +1 & x_3 \geq 0. \end{cases} \quad (3.31)$$

Anticipating the presence of image charges, let us introduce the matrix $R_{\mu\nu}$,

$$R_{\mu\nu} = \text{diag}(1, 1, 1, -1)_{\mu\nu}, \quad (3.32)$$

which implements a reflection in the x_3 direction.

To obtain the gauge propagator we follow the calculation of ref. [5]. We know that $\langle A_\mu(x) A_\nu(\tilde{x}) \rangle$ must be a linear combination of the following terms:

$$\delta_{\mu\nu} \Delta(x, \tilde{x}) \Theta(\pm x_3) \Theta(\pm \tilde{x}_3), \quad R_{\mu\nu} \Delta(x, R\tilde{x}) \Theta(\pm x_3) \Theta(\pm \tilde{x}_3), \quad \delta_{\mu\nu} \Delta(x, \tilde{x}) \Theta(\pm x_3) \Theta(\mp \tilde{x}_3). \quad (3.33)$$

We can fix the coefficients of that linear combination as follows. In the presence of the jumping coupling, we can again define fields \vec{E} , \vec{B} , \vec{D} , and \vec{H} as in eq. (3.5). Since we work to leading order in the coupling, where we ignore the non-Abelian interactions, \vec{E} , \vec{B} , \vec{D} , and \vec{H} will satisfy the equations of motion and Bianchi identity written in eq. (3.8), without sources. We can thus again derive the matching conditions in eq. (3.10), which we can easily translate into conditions on A_μ and hence on the A_μ propagator. Employing also the gauge constraint, we can write the final result for the gauge propagator as

$$\begin{aligned} \langle A_\mu(x) A_\nu(\tilde{x}) \rangle &= g_+^2 (\delta_{\mu\nu} \Delta(x, \tilde{x}) + Q^+ R_{\mu\nu} \Delta(x, R\tilde{x})) \Theta(x_3) \Theta(\tilde{x}_3) \\ &+ \frac{2g_+^2 g_-^2}{g_+^2 + g_-^2} \delta_{\mu\nu} \Delta(x, \tilde{x}) (\Theta(x_3) \Theta(-\tilde{x}_3) + \Theta(-x_3) \Theta(\tilde{x}_3)) \\ &+ g_-^2 (\delta_{\mu\nu} \Delta(x, \tilde{x}) + Q^- R_{\mu\nu} \Delta(x, R\tilde{x})) \Theta(-x_3) \Theta(-\tilde{x}_3), \end{aligned} \quad (3.34)$$

where the image charges are given by

$$Q^+ = \frac{g_-^2 - g_+^2}{g_+^2 + g_-^2}, \quad Q^- = \frac{g_+^2 - g_-^2}{g_+^2 + g_-^2}. \quad (3.35)$$

The formula for Q^+ is simply eq. (3.19) with $\theta_+ = \theta_-$ and $Q^e = 1$. Our result for the gauge propagator agrees with that of ref. [5], and reduces to the result in eq. (3.29) when $g_+ = g_-$.

For the scalar propagator, we start by writing the most general form consistent with the symmetries, using arguments similar to those given above for the gauge field propagator,

$$\begin{aligned} \langle \Phi^I(x) \Phi^J(\tilde{x}) \rangle &= \delta^{IJ} \left(g_+^2 \Delta(x, \tilde{x}) \Theta(x_3) + g_-^2 \Delta(x, \tilde{x}) \Theta(-x_3) \right. \\ &\quad + g_+^2 Q^{++} \Delta(x, R\tilde{x}) \Theta(x_3) \Theta(\tilde{x}_3) + g_-^2 Q^{--} \Delta(x, R\tilde{x}) \Theta(-x_3) \Theta(-\tilde{x}_3) \\ &\quad \left. + Q^{-+} \Delta(x, \tilde{x}) \Theta(-x_3) \Theta(\tilde{x}_3) + Q^{+-} \Delta(x, \tilde{x}) \Theta(x_3) \Theta(-\tilde{x}_3) \right), \end{aligned} \quad (3.36)$$

where $Q^{\pm\pm}$ and $Q^{\pm\mp}$ are image charges whose values are determined by the interface-localized terms quadratic in the scalars, eqs. (2.23) and (2.32).

For the non-SUSY interface, $Q^{\pm\pm}$ and $Q^{\pm\mp}$ are determined by the value of κ , the coefficient of the interface-localized term in eq. (2.23). For example, consider $\kappa = 0$. In that case, the gauge field and the scalars obey the same equation of motion, and thus must obey the same matching conditions. With our choice of gauge, they must thus have the same propagator, up to factors of $\delta_{\mu\nu}$, $R_{\mu\nu}$, and δ^{IJ} , so when $\kappa = 0$ we have $Q^{++} = Q^{+-} = Q^+$ and $Q^{--} = Q^{-+} = Q^-$. More generally, we can think of the interface term as a boundary term that imposes a boundary condition on the propagator. The generic form of the propagator is that of eq. (3.36), but in order to satisfy the boundary condition $Q^{\pm\pm}$ and $Q^{\pm\mp}$ must take certain values, and so must obviously depend on κ . The general lesson is that κ controls the size of the image charges, along with g_+ and g_- .

For the SUSY interface, the interface-localized term in eq. (2.32) involves only three of the six real scalars. The three scalars that do not appear in eq. (2.32) will have propagators of the same form as the non-SUSY case, with $\kappa = 0$. For the three scalars that do appear in eq. (2.32), the interface-localized terms will modify the values of $Q^{\pm\pm}$ and $Q^{\pm\mp}$ relative to the non-SUSY, $\kappa = 0$ case. As a result, the Wilson loop expectation value will depend on the choice of the θ^I in eq. (3.26), since these determine the scalars to which the test charges couple. For a SUSY interface, we will only compute Wilson loop expectation values holographically, and we will indeed find that the results depend sensitively on the choice of θ^I .

For the non-SUSY interface where the coupling jumps, we will now show that when $\kappa = 0$ a test charge has no image charge. To do so, we will focus on a rectangular Wilson loop parallel to the interface, W_{\parallel} , depicted in fig. 1 (b). For such test charges, we will compute the expectation value $\langle W_{\parallel} \rangle$, and from that extract $V_{\parallel}(L, L_3)$ via eq. (3.25), in perturbation theory for arbitrary κ and then show that when $\kappa = 0$ the image charge vanishes thanks to a cancellation between the gauge fields and scalars. Moreover, for the special case $\kappa = 0$, we will extend the result for $V_{\parallel}(L, L_3)$ beyond perturbation theory by performing the sum of ladder diagrams, following refs. [25, 26].

For a rectangular Wilson loop parallel to the interface, we parameterize the path C as

$$\begin{aligned} x(s) &= \{s, 0, 0, L_3\}, & -T/2 \leq s \leq T/2, \\ x(s) &= \{T - s, L, 0, L_3\}, & T/2 \leq s \leq 3T/2, \end{aligned} \quad (3.37)$$

with $L > 0$, and we will neglect the segments $\{\pm T/2, s, 0, L_3\}$ with $0 \leq s \leq L$ (the short ends of the rectangle) since to obtain $V_{\parallel}(L, L_3)$ we will ultimately take the limit $T \gg L, L_3$. The contribution

to the expectation value $\langle W_{\parallel} \rangle$ from the gauge fields is

$$\begin{aligned}
& -\frac{N_c}{2} \oint_C ds \oint_C d\tilde{s} [\dot{x}^\mu(s) \dot{x}^\nu(\tilde{s}) \langle \mathcal{P} A_\mu(x(s)) A_\nu(x(\tilde{s})) \rangle] \\
& = -\frac{N_c}{2} \frac{T}{2\pi} \left[\lim_{\epsilon \rightarrow 0} \frac{g_\pm^2}{\epsilon} - \frac{g_\pm^2}{L} + \frac{g_\pm^2 Q^\pm}{2L_3} - \frac{g_\pm^2 Q^\pm}{\sqrt{L^2 + 4L_3^2}} \right] + \mathcal{O}\left(\frac{L}{T}, \frac{L_3}{T}\right), \quad (3.38)
\end{aligned}$$

where the $+$ sign is for $L_3 > 0$ and the $-$ sign is for $L_3 < 0$. We have introduced a cutoff, ϵ , to regulate the divergent contribution to the self-energy of the test charges from the gauge fields, *i.e.* the first term on the right-hand-side of eq. (3.38). Ignoring that divergent self-energy term and applying eq. (3.25), we find that $V_{\parallel}(L, L_3)$ is precisely that of electromagnetism, eq. (3.23), times a factor of N_c , as expected. The contribution to $\langle W_{\parallel} \rangle$ from the scalar fields is, for arbitrary κ ,

$$\begin{aligned}
& +\frac{N_c}{2} \oint_C ds \oint_C d\tilde{s} [|\dot{x}(s)| |\dot{x}(\tilde{s})| \theta^I \theta^J \langle \mathcal{P} \Phi^I(x(s)) \Phi^J(x(\tilde{s})) \rangle] \\
& = +\frac{N_c}{2} \frac{T}{2\pi} \left[\lim_{\epsilon \rightarrow 0} \frac{g_\pm^2}{\epsilon} + \frac{g_\pm^2}{L} + \frac{g_\pm^2 Q^{\pm\pm}}{2L_3} + \frac{g_\pm^2 Q^{\pm\pm}}{\sqrt{L^2 + 4L_3^2}} \right] + \mathcal{O}\left(\frac{L}{T}, \frac{L_3}{T}\right). \quad (3.39)
\end{aligned}$$

The scalars also produce a divergent contribution to the self-energy, but with precisely the right coefficient to cancel the divergent contribution from the gauge fields, as we expect for $\mathcal{N} = 4$ SYM without an interface, where a single test charge has vanishing self-energy. The final result for $V_{\parallel}(L, L_3)$ is finite,

$$V_{\parallel}(L, L_3) = -\frac{N_c}{4\pi} \left[\frac{2g_\pm^2}{L} + \frac{g_\pm^2 (-Q^\pm + Q^{\pm\pm})}{2L_3} + \frac{g_\pm^2 (Q^\pm + Q^{\pm\pm})}{\sqrt{L^2 + 4L_3^2}} \right]. \quad (3.40)$$

The first term on the right-hand-side of eq. (3.40) is simply the $\lambda \ll 1$ result for $\mathcal{N} = 4$ SYM in eq. (1.3), representing the interaction of the two test charges with one another. The other two terms on the right-hand-side of eq. (3.40) represent interactions with image charges. If we send $L \rightarrow \infty$, effectively sending one test charge to infinity, then we isolate the self-energy of a single test charge in the presence of the interface, the second term on the right-hand-side of eq. (3.40). That term will be non-zero if $(-Q^\pm + Q^{\pm\pm}) \neq 0$, in which case the potential diverges when $L_3 \rightarrow 0$ because the test charge sits on top of its own image charge. As explained below eq. (3.36), if $\kappa = 0$ then $Q^{\pm\pm} = Q^\pm$, in which case $(-Q^\pm + Q^{\pm\pm}) = 0$: the interaction of each test charge with its own image vanishes. We have thus proven that the cancellation of gauge field and scalar contributions to the self-energy that occurred in $\mathcal{N} = 4$ SYM without an interface, due to SUSY, persists to $\mathcal{N} = 4$ SYM with a jumping coupling that *breaks* SUSY, in the special case that $\kappa = 0$.

We can demonstrate that this effect persists beyond leading order in perturbation theory by computing the contribution from the sum of ladder diagrams to the Wilson loop expectation value, $\langle W_{\text{ladder}} \rangle \equiv \Gamma$, in the large- N_c limit. For large- N_c $\mathcal{N} = 4$ SYM without an interface, Γ obeys a recursion relation, as shown in ref. [25, 26]. The proof of that fact relies crucially on the vanishing self-energy of a single test charge in $\mathcal{N} = 4$ SYM without an interface. For $\mathcal{N} = 4$ SYM with

a non-SUSY interface where the coupling jumps, in the special case $\kappa = 0$ the self-energy again vanishes. In that case, a straightforward exercise shows that Γ again obeys a recursion relation,

$$\Gamma(T, T') = 1 + \int_0^T ds \int_0^{T'} d\tilde{s} \frac{g_+^2 N}{2\pi^2} \left[\frac{1}{(s - \tilde{s})^2 + L^2} + \frac{Q^+}{(s - \tilde{s})^2 + L^2 + 4L_3^2} \right] \Gamma(s, \tilde{s}), \quad (3.41)$$

which is of precisely the same form as in $\mathcal{N} = 4$ SYM without an interface. In particular, the term in brackets on the right-hand-side of eq. (3.41) is the sum of gauge and scalar propagators. The ladder sum $\Gamma(T, T')$ obeys the boundary conditions

$$\Gamma(T, 0) = \Gamma(0, T') = 1. \quad (3.42)$$

Taking two derivatives of eq. (3.41), we obtain

$$\frac{\partial^2 \Gamma(T, T')}{\partial T \partial T'} = \frac{g_+^2 N}{2\pi^2} \left[\frac{1}{(T - T')^2 + L^2} + \frac{Q^+}{(T - T')^2 + L^2 + 4L_3^2} \right] \Gamma(T, T'). \quad (3.43)$$

As in refs. [25, 26], at large $T = T'$ and with large $g_+^2 N_c$, the solution is of the form

$$\Gamma(T, T') \propto e^{\frac{T}{L} \sqrt{\frac{2g_+^2 N_c}{\pi^2} \left(1 + \frac{Q^+}{1 + 4(L_3/L)^2}\right)}}. \quad (3.44)$$

We thus find

$$V_{\parallel}(L, L_3) = -\frac{1}{\pi} \frac{\sqrt{2g_+^2 N_c}}{L} \sqrt{1 + \frac{Q^+}{1 + 4(L_3/L)^2}}, \quad \text{sum of ladder diagrams.} \quad (3.45)$$

When $g_+ = g_-$, so that $Q^+ = 0$, we recover the result in eq. (1.3) for $\mathcal{N} = 4$ SYM without an interface. In fig. 7 we show the $V_{\parallel}(L, L_3)$ in eq. (3.45) for the case $\lambda_- = \lambda_+/2$. Notice the striking difference from the analogous result in electromagnetism, shown in fig. 6 (a). In particular, in electromagnetism, $V_{\parallel}(L, L_3)$ diverges as $L_3/L \rightarrow 0$ because the test charges approach their image charges, whereas the result in eq. (3.45) remains finite as $L_3/L \rightarrow 0$ because the self-energy of each test charge vanishes. Moreover, fig. 7 clearly shows that the dipole of test charges is attracted to the side with *larger* coupling, again because the self-energy of each test charge vanishes, in stark contrast to the electromagnetism.

4 Wilson Loops: Holographic Calculation

To compute the expectation value of a Wilson loop in the fundamental representation holographically, we must introduce a fundamental string in the bulk with its endpoints on the boundary, tracing out the loop [22, 23]. Our Wilson loops, and hence our strings, will be static, with time extent T . We must solve the string equations of motion with the given boundary conditions and then plug that solution into the string action. Generically, the on-shell action of a string with endpoints on the boundary is divergent due to the infinite distance to the boundary. The procedure to

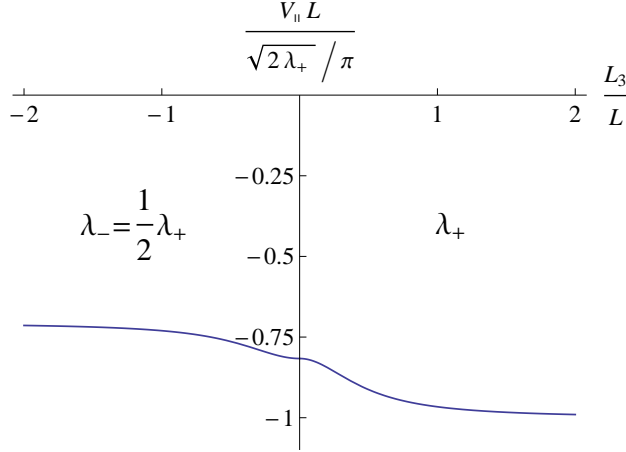


Figure 7: The contribution from the sum of ladder diagrams to the potential $V_{\parallel}(L, L_3)$, eq. (3.45), between two heavy test charges along a line parallel to a non-SUSY interface where the coupling jumps in large- N_c , strongly-coupled $\mathcal{N} = 4$ SYM, for the special value $\kappa = 0$ of the constant defined in eq. (2.23). More precisely, we chose $\lambda_- = \lambda_+/2$ and plotted $V_{\parallel}(L, L_3)L/(\sqrt{2\lambda_+}/\pi)$ as a function of L_3/L . In stark contrast to the analogous result in electromagnetism, shown in fig. 6 (a), here $V_{\parallel}(L, L_3)$ remains finite at $L_3/L = 0$, and the dipole is attracted to the side with *larger* coupling (to the right), because the self-energy of each test charge vanishes.

render the on-shell action finite is called holographic renormalization [97–100]. We will denote the renormalized on-shell string action as S_{ren} . According to the AdS/CFT dictionary, the expectation value of the Wilson loop, $\langle W \rangle$, is then given by

$$\langle W \rangle \propto e^{-S_{\text{ren}}}. \quad (4.1)$$

We can extract a potential V from either a straight timelike Wilson line or a rectangular Wilson loop via eq. (3.25)

$$V = -\lim_{T \rightarrow \infty} \frac{1}{T} \log \langle W \rangle = \lim_{T \rightarrow \infty} \frac{S_{\text{ren}}}{T}. \quad (4.2)$$

In section 4.1 we write the action for strings in Janus spacetimes and describe our Ansätze and numerical methods for solving the equations of motion. In section 4.2 we perform the holographic renormalization of the on-shell action of these strings. In sections 4.3, 4.4, and 4.5 we present our results for V for straight, perpendicular and parallel Wilson lines/loops located away from the interface (at finite x_3), respectively. In each case we discuss both a jumping coupling and a jumping θ -angle, with and without SUSY. In section 4.6 we consider the special case of Wilson loops located exactly on the interface, where we can obtain analytic (rather than numerical) results for V .

Sections 4.1 and 4.2 are technical. Readers who only want to see our results for V may skip directly to sections 4.3 through 4.6.

4.1 String Equations of Motion and Solutions

To accommodate both non-SUSY and SUSY Janus, we write both metrics in the same general form as that of SUSY Janus, eq. (2.26a),

$$ds^2 = G_{MN} dx^M dx^N = f_4^2 \left(\frac{du^2}{u^2} + u^2 (dt^2 + dx_1^2 + dx_2^2) \right) + \rho_1^2 dx^2 + \rho_2^2 dy^2 + f_1^2 ds_{S^2}^2 + f_2^2 ds_{S^2}^2, \quad (4.3)$$

with $M, N = 0, \dots, 9$, and where for SUSY Janus the warp factors f_4^2 , f_1^2 , f_2^2 , ρ_1^2 , and ρ_2^2 are functions of x and y , while for non-SUSY Janus f_4^2 and ρ_1^2 depend only on x while f_1^2 and f_2^2 depend only on y , and $\rho_2^2 = R^2$, as we can see from eqs. (2.10) and (2.24).

At leading order in α' , the string action includes two terms. The first is the Nambu-Goto term, representing the area of the string worldsheet times the string tension. The second is a term involving the pull-back of the NS two-form. The non-SUSY Janus solution has a vanishing NS two-form, but the SUSY Janus solution includes a non-trivial NS two-form. We will argue below that for our string solutions in SUSY Janus, the pull-back of the NS two-form vanishes. We thus only present the Nambu-Goto term explicitly, which in Euclidean signature and Einstein frame is

$$S = \frac{1}{2\pi\alpha'} \int d\tau d\sigma \sqrt{\det e^\phi G_{MN} \partial_m X^M \partial_n X^N}, \quad (4.4)$$

where $X^M(\tau, \sigma)$ are the worldsheet scalars, and the determinant is over the worldsheet coordinates $m, n = \tau, \sigma$. We employ static gauge, $\tau = t$ in all that follows. In that gauge, the integration over τ in eq. (4.4) always trivially produces a factor of T .

As explained in section 2.3, we will use $SL(2, \mathbb{R})$ transformations to convert jumping-dilaton Janus into jumping-axion Janus. The only way that our strings will “know” about these $SL(2, \mathbb{R})$ transformations is via their coupling to ϕ in eq. (4.4), since they do not couple directly to $C_{(0)}$ and the Einstein-frame metric G_{MN} is $SL(2, \mathbb{R})$ -invariant.

We can use the isometries of the bulk metric to simplify the string action. Using the $SO(3) \times SO(3)$ symmetry of the internal space, we may place the string at a fixed point on each S^2 . For a string in SUSY Janus, which has NS two-form flux on one S^2 , the pull-back of the NS two-form to the worldsheet then vanishes, as advertised. Using the symmetries of the (x_1, x_2) plane, we may place the string at $x_2 = 0$. After these simplifications, the most general Ansatz we can write is $u = u(\sigma)$, $x = x(\sigma)$, $y = y(\sigma)$, $x_1 = x_1(\sigma)$, in which case the Nambu-Goto action becomes

$$S = \frac{T}{2\pi\alpha'} \int d\sigma e^\phi \sqrt{f_4^4 u^4 (\partial_\sigma x_1)^2 + f_4^4 (\partial_\sigma u)^2 + f_4^2 u^2 [\rho_1^2 (\partial_\sigma x)^2 + \rho_2^2 (\partial_\sigma y)^2]}. \quad (4.5)$$

This action depends only on the derivative of $x_1(\sigma)$, hence the system has a conserved charge, C , obeying $\partial_\sigma C = 0$,

$$C \equiv - \frac{e^\phi f_4^4 u^4 \partial_\sigma x_1}{\sqrt{f_4^4 u^4 (\partial_\sigma x_1)^2 + f_4^4 (\partial_\sigma u)^2 + f_4^2 u^2 [\rho_1^2 (\partial_\sigma x)^2 + \rho_2^2 (\partial_\sigma y)^2]}}. \quad (4.6)$$

The following rescaling of the coordinates is an isometry of the bulk metric:

$$u \rightarrow \mu^{-1} u, \quad (t, x_1, x_2) \rightarrow \mu (t, x_1, x_2), \quad (x, y) \rightarrow (x, y), \quad (4.7)$$

with μ a real, positive constant. This rescaling isometry is dual to the field theory dilatation symmetry. Letting σ transform with arbitrary weight α under this rescaling, $\sigma \rightarrow \mu^\alpha \sigma$, the action transforms only by an overall constant, $S \rightarrow \mu^{-1} S$, hence this rescaling will be a symmetry of the string equations of motion. Notice that $C \rightarrow \mu^{-2} C$ under this rescaling.

The straight timelike Wilson line and the rectangular Wilson loop perpendicular to the interface are both localized in the (x_1, x_2) plane, and the corresponding strings both preserve the same subgroup of the isometries, while the rectangular Wilson loop parallel to the interface is extended in one direction in the (x_1, x_2) plane, and so the corresponding string preserves a different subgroup of the isometries. To simplify the string action and equations of motion any further we must treat these two cases separately.

For the timelike line and the perpendicular loop, depicted in fig. 1 (a), we can choose x_1 to be constant, $\partial_\sigma x_1 = 0$. In that case the conserved charge $C = 0$ trivially. To write the equations of motion in a simple form, let us define

$$F \equiv \sqrt{(\partial_\sigma u)^2 + u^2 [\rho_1^2 (\partial_\sigma x)^2 + \rho_2^2 (\partial_\sigma y)^2]} / f_4^2. \quad (4.8)$$

The equations of motion arising from the action in eq. (4.5) then take the form

$$\partial_\sigma \left(\frac{e^\phi f_4^2}{F} \partial_\sigma u \right) - \frac{e^\phi u}{F} [\rho_1^2 (\partial_\sigma x)^2 + \rho_2^2 (\partial_\sigma y)^2] = 0, \quad (4.9a)$$

$$\partial_\sigma \left[\frac{u^2 \rho_1^2 e^\phi}{F} \partial_\sigma x \right] - \partial_x (e^\phi f_4^2 F) = 0, \quad (4.9b)$$

$$\partial_\sigma \left[\frac{u^2 \rho_2^2 e^\phi}{F} \partial_\sigma y \right] - \partial_y (e^\phi f_4^2 F) = 0. \quad (4.9c)$$

We will first solve y 's equation of motion, eq. (4.9c), although not in complete generality. We will restrict to a special subset of solutions that are particularly simple: we consider constant y , meaning $\partial_\sigma y = 0$. Eq. (4.9c) then reduces to $\partial_y (e^\phi f_4^2 F) = 0$. For non-SUSY Janus, this condition is satisfied for any constant y . For SUSY Janus this condition is only satisfied for $y = 0$ or $y = \pi/2$, meaning the string sits at a point where one or the other S^2 collapses to zero size.

Strings sitting at different values of y translate into heavy test charges that couple to different subsets of the adjoint scalars, *i.e.* different values of the θ^I in eq. (3.24). In non-SUSY Janus, a choice of y breaks the $SO(6)$ isometry but does not change the solutions for the remaining fields, $u(\sigma)$ and $x(\sigma)$, or the on-shell action. The corresponding field theory statements are that a choice of the θ^I breaks $SO(6)$ but does not otherwise affect the Wilson loop expectation value. In SUSY Janus, where the $SO(6)$ is broken to $SO(3) \times SO(3)$, each of our y solutions, $y = 0$ or $y = \pi/2$, breaks one $SO(3)$ but preserves the other. Here the choice of y will affect the solutions for $u(\sigma)$

and $x(\sigma)$, since the metric and dilaton factors appearing in their equations of motion depend on the value of y . The on-shell action will also depend on the value of y . In the field theory, we divide the six adjoint scalars into two subsets of three, those that appear in the interface-localized term in eq. (2.32) and those that do not. The choice of y corresponds to a choice of the θ^I such that the test charge couples to one subset but not the other, and hence breaks one $SO(3)$ but preserves the other. Clearly the associated Wilson loop expectation value will depend on that choice.

What remains is to solve the equations of motion for $u(\sigma)$ and $x(\sigma)$. As a gauge choice we take $x(\sigma) = \sigma$, in which case a straightforward exercise shows that eqs. (4.9a) and (4.9b) are equivalent. We thus obtain a single second-order, non-linear, ordinary differential equation, eq. (4.9a), for a single function, $u(\sigma) = u(x)$.

We solve eq. (4.9a) numerically as follows. Strings describing a perpendicular loop will have a “turn-around point” at some value of x , which we call \bar{x} , where $\partial_x u(\bar{x}) = 0$. The existence of a turn-around point is intuitively obvious from fig. 1 (a): the string will emerge from the boundary at the point x_3^R and extend in the x_3 direction as it dips into the bulk, eventually turning around and rising back up to intersect the boundary at the point x_3^L . A solution of the second-order eq. (4.9a) will be completely specified by two boundary conditions, which we take to be the values of \bar{x} and $u(\bar{x})$. Thanks to the rescaling symmetry of eq. (4.7), under which u rescales but x does not, we can obtain all physically inequivalent solutions by fixing $u(\bar{x})$ and scanning through values of \bar{x} . The solutions are thus distinguished only by a single number, \bar{x} , which is consistent with the parameter counting in the field theory: as explained in the introduction, for the perpendicular loop the potential V depends only on the single dimensionless ratio L_{av}/L . For a given \bar{x} , we numerically integrate eq. (4.9a) up to some values of u and x near the boundary, and extract the x_3 values of the endpoints (in units of the asymptotic $AdS_5 \times S^5$ radius) using either eq. (2.2) or eqs. (A.5) and (A.9) in the appendix. Those x_3 values then give us L_{av}/L .

For the straight timelike Wilson line, we look for solutions with the turn-around point at the Poincaré horizon, *i.e.* $\partial_x u(\bar{x}) = 0$ occurs at $u(\bar{x}) = 0$. These describe “straight strings” that extend from a point at the boundary to the Poincaré horizon. Intuitively, such strings represent perpendicular Wilson loops with one of the test charges sent to the “point at infinity,” leaving behind a single test charge. In practice, we “shoot from the boundary”: we pick a value of $u(x)$ near the boundary, which fixes the x_3 value of the endpoint at the boundary, pick a value of $\partial_x u(x)$ at that point, integrate eq. (4.9a) up to $x = \bar{x}$ such that $\partial_x u(\bar{x}) = 0$, and then check whether $u(\bar{x}) = 0$.

Now let us consider the parallel loop, depicted in fig. 1 (b). Using $x_1(\sigma)$ ’s equation of motion, $\partial_\sigma C = 0$, and making the gauge choice $x_1(\sigma) = \sigma$, in which case C is nonzero, we can write the remaining equations of motion as

$$\partial_\sigma^2 u - 3 \frac{(\partial_\sigma u)^2}{u} - \frac{e^{2\phi} f_4^4 u^7}{C^2} - u^3 = 0, \quad (4.10a)$$

$$\partial_\sigma \left(\frac{\rho_1^2}{f_4^2} \frac{\partial_\sigma x}{u^2} \right) - \frac{u^4}{2C^2} \partial_x \left(e^{2\phi} f_4^4 \right) - \frac{1}{2u^2} \left[\left(\partial_x \frac{\rho_1^2}{f_4^2} \right) (\partial_\sigma x)^2 + \left(\partial_x \frac{\rho_2^2}{f_4^2} \right) (\partial_\sigma y)^2 \right] = 0, \quad (4.10b)$$

$$\partial_\sigma \left(\frac{\rho_2^2}{f_4^2} \frac{\partial_\sigma y}{u^2} \right) - \frac{u^4}{2C^2} \partial_y \left(e^{2\phi} f_4^4 \right) - \frac{1}{2u^2} \left[\left(\partial_y \frac{\rho_1^2}{f_4^2} \right) (\partial_\sigma x)^2 + \left(\partial_y \frac{\rho_2^2}{f_4^2} \right) (\partial_\sigma y)^2 \right] = 0. \quad (4.10c)$$

Again we will only consider y solutions with $\partial_\sigma y = 0$, in which case in eq. (4.10c) two nonzero terms remain. We will only consider solutions for which each of these terms vanishes independently, *i.e.* solutions for which

$$\partial_y \left(e^{2\phi} f_4^4 \right) = 0, \quad \partial_y \left(\frac{\rho_1^2}{f_4^2} \right) = 0. \quad (4.11)$$

For non-SUSY Janus, the conditions in eq. (4.11) are satisfied for any constant value of y . For SUSY Janus, the conditions in eq. (4.11) are only satisfied for $y = 0$ or $y = \pi/2$. All of our comments above about constant y solutions apply to these solutions as well.

We solve eqs. (4.10a) and (4.10b) for $u(\sigma) = u(x_1)$ and $x(\sigma) = x(x_1)$ numerically as follows. Strings describing a parallel loop will have a turn-around point at some x_1 , which we can take to be $x_1 = 0$. To guarantee that both ends of the string have the same position in x_3 , we impose $\partial_{x_1} u(0) = 0$ and $\partial_{x_1} x(0) = 0$. The existence of a turn-around point is intuitively obvious from fig. 1 (b.): the string will emerge from the boundary and extend in the x_1 direction as it dips into the bulk before turning around and rising up to intersect the boundary again. Notice that with our gauge choice $x_1 \in [-L/2, +L/2]$. Solutions of the second-order eqs. (4.10a) and (4.10b) are completely specified by four boundary conditions: $\partial_{x_1} u(0) = 0$ and $\partial_{x_1} x(0) = 0$ and the values of $u(0)$ and $x(0)$. Thanks to the rescaling symmetry of eq. (4.7) we can obtain all physically inequivalent solutions by fixing $u(0)$ and scanning through values of $x(0)$. The solutions are thus distinguished only by a single number, $x(0)$, which is consistent with the parameter counting in the field theory: as explained in the introduction, for the parallel loop the potential V depends only on the single dimensionless ratio L_3/L . Notice that eqs. (4.10a) and (4.10b) depend on the value of C . Once we pick a gauge, solve for y , and pick our values of $u(0)$ and $x(0)$, the value of C is fixed. For a given $x(0)$, we numerically integrate eqs. (4.10a) and (4.10b) up to values of u and x near the boundary, and then extract the x_1 and x_3 values of the endpoints (in units of the asymptotic $AdS_5 \times S^5$ radius) using either eq. (2.2) or eqs. (A.5) and (A.9) in the appendix. These x_1 and x_3 values then give us L_3/L .

4.2 Holographic Renormalization of the String Action

Having obtained solutions to the string equations of motion, we now need to plug those solutions into the string action, eq. (4.5), which will then be divergent due to the integration all the way to the AdS boundary. For a string in $AdS_5 \times S^5$, we know of three methods to obtain a finite on-shell string action. The first method is holographic renormalization, in which we add counterterms to the string action to cancel any divergences [97–100]. The second method, proposed in ref. [24], is to perform a Legendre transform of the string action. The third method is to subtract from the on-shell action the (divergent) action of a straight string extending from the boundary to the Poincaré horizon [22, 23]. In field theory terms, that means computing not the renormalized expectation value of a Wilson loop, but the difference between the expectation values of a Wilson loop and

straight timelike Wilson line(s). Although these three methods are distinct in principle, for strings in $AdS_5 \times S^5$ they all produce the same result: they all cancel the divergence of the on-shell action, and nothing more. In particular they make no finite contribution to the on-shell action.

In this subsection, for strings in Janus spacetimes we will show that for a string with endpoint(s) on the boundary away from the interface the divergence of the on-shell string action is the same as that in $AdS_5 \times S^5$, and that the first two methods again cancel the divergence of the on-shell string action, and nothing more. On the other hand, at the end of this subsection we will argue that subtracting a straight string does more than simply cancel the divergence of the on-shell action.

We begin with holographic renormalization. In principle we could work with the coordinates u and x of the last subsection, however, holographic renormalization is dramatically simpler in Fefferman-Graham coordinates, so we will now switch to those. Any asymptotically AdS_5 metric can, near the boundary, be written in Fefferman-Graham form,

$$ds^2 = \frac{R^2}{z^2} (dz^2 + g_{\mu\nu}(z, x^\rho) dx^\mu dx^\nu), \quad (4.12)$$

where z is the radial coordinate with the boundary at $z = 0$. The coordinate z is related to the radial coordinate r of the Poincaré slicing in eq. (2.1) by $z = R^2/r$. Expanding the metric near the boundary, *i.e.* in powers of z , the leading term, $g_{\mu\nu}(z = 0, x^\rho)$, corresponds to the metric of the spacetime in which the field theory “lives.” We use Euclidean-signature Poincaré slicing, in which case $g_{\mu\nu}(z = 0, x^\rho) = \delta_{\mu\nu}$.

In the appendix we present some details of the coordinate transformation that puts the Janus metrics of eq. (4.3) into the form of eq. (4.12). For simplicity, in this subsection we will completely ignore the internal spaces of the Janus spacetimes, since the strings we consider do not move at all there (all of our strings sit at constant y). In going from AdS_5 to the Janus spacetimes, translations in x_3 are broken, hence unlike AdS_5 the near-boundary Fefferman-Graham forms of the Janus metrics can depend on x_3 . The rescaling isometry of eq. (4.7) remains unbroken in Janus space times, however, so the Fefferman-Graham form of the Janus metric must depend on x_3 only in the combination z/x_3 . We can thus write the Fefferman-Graham form of the Janus metrics as

$$ds^2 = \frac{R^2}{z^2} (dz^2 + g_{11}(z/x_3)(dt^2 + dx_1^2 + dx_2^2) + g_{33}(z/x_3)dx_3^2). \quad (4.13)$$

The near-boundary, small z/x_3 expansions of the functions $g_{11}(z/x_3)$ and $g_{33}(z/x_3)$ are of the form

$$g_{11}(z/x_3) = 1 + \left(\frac{z}{x_3}\right)^n \sum_{i=0}^{\infty} \mathcal{A}_i^{(\pm)} \left(\frac{z}{x_3}\right)^i, \quad g_{33}(z/x_3) = 1 + \left(\frac{z}{x_3}\right)^n \sum_{i=0}^{\infty} \mathcal{B}_i^{(\pm)} \left(\frac{z}{x_3}\right)^i, \quad (4.14)$$

with coefficients $\mathcal{A}_i^{(\pm)}$ and $\mathcal{B}_i^{(\pm)}$ that depend on the size of the jump in the axio-dilaton, and that go to zero if the jump in the axio-dilaton goes to zero. The superscripts \pm on $\mathcal{A}_i^{(\pm)}$ and $\mathcal{B}_i^{(\pm)}$ indicate that in general these coefficients take different values in the two distinct asymptotic $AdS_5 \times S^5$ regions of a Janus spacetime, in which the dilaton approaches the values ϕ_+ and ϕ_- . Both $g_{11}(z/x_3)$ and $g_{33}(z/x_3)$ equal one when $z/x_3 = 0$, hence the metric indeed approaches the

Poincaré-sliced AdS_5 metric asymptotically. In the appendix we present some of the coefficients $\mathcal{A}_i^{(\pm)}$ and $\mathcal{B}_i^{(\pm)}$ explicitly, in eqs. (A.7) and (A.11). In particular, the first non-trivial power n of z/x_3 in the expansions is $n = 8$ for non-SUSY Janus and $n = 2$ for SUSY Janus. The near-boundary expansion of the dilaton takes the form (see eqs. (A.8) and (A.12))

$$\phi(z/x_3) = \phi_{\pm} + \left(\frac{z}{x_3}\right)^4 \sum_{i=0}^{\infty} \mathcal{C}_i^{(\pm)} \left(\frac{z}{x_3}\right)^i, \quad (4.15)$$

where again the coefficients $\mathcal{C}_i^{(\pm)}$ depend on the size of the jump in the axio-dilaton, and go to zero if the jump in the axio-dilaton goes to zero. Notice that the first non-trivial power of z/x_3 in eq. (4.15) is four for both non-SUSY and SUSY Janus.

Let us again simplify the string action of eq. (4.4) using isometries, but now using Fefferman-Graham coordinates. We use the symmetries of the (x_1, x_2) plane to set $x_2 = 0$. The most general Ansatz we can then write is $z(\sigma)$, $x_1(\sigma)$, $x_3(\sigma)$. In static gauge, $\tau = t$, the string action then reduces to

$$S = \frac{T}{2\pi\alpha'} \int d\sigma e^{\phi} \frac{R^2}{z^2} \sqrt{g_{11}} \sqrt{(\partial_{\sigma} z)^2 + g_{11}(\partial_{\sigma} x_1)^2 + g_{33}(\partial_{\sigma} x_3)^2}. \quad (4.16)$$

Notice that if the jump in the axio-dilaton is zero, in which case $g_{11}(z/x_3) = 1$ and $g_{33}(z/x_3) = 1$, then our string action reduces to that of refs. [22, 23], for a string in $AdS_5 \times S^5$. For later use, let us write the canonical momentum associated with z ,

$$\frac{\delta S}{\delta \partial_{\sigma} z} = \frac{1}{2\pi\alpha'} e^{\phi} \frac{R^2}{z^2} \sqrt{g_{11}} \frac{\partial_{\sigma} z}{\sqrt{(\partial_{\sigma} z)^2 + g_{11}(\partial_{\sigma} x_1)^2 + g_{33}(\partial_{\sigma} x_3)^2}}. \quad (4.17)$$

As a gauge choice we now take $z(\sigma) = \sigma$. The equations of motion for $x_1(\sigma) = x_1(z)$ and $x_3(\sigma) = x_3(z)$ are straightforward to obtain but unilluminating, so we will omit them. What we need for holographic renormalization are the small- z asymptotic expansions of the on-shell $x_1(z)$ and $x_3(z)$,

$$x_1(z) = x_1^{(0)} + x_1^{(1)} z^3 + \dots, \quad x_3(z) = x_3^{(0)} + x_3^{(1)} z^3 + \dots, \quad (4.18)$$

where $x_1^{(0)}$, $x_1^{(1)}$, $x_3^{(0)}$, and $x_3^{(1)}$ are independent of z . In each case, the \dots represent terms of higher order in z . In AdS_5 , for both $x_1(z)$ and $x_3(z)$ the first sub-leading term is order z^7 . In non-SUSY Janus, for $x_1(z)$ the first sub-leading term is again order z^7 , but for $x_3(z)$ the first sub-leading term is order z^6 , with a coefficient proportional to the coefficient \mathcal{C}_0^{\pm} from eq. (4.15). In SUSY Janus, for $x_1(z)$ the first sub-leading term is order z^5 and for $x_3(z)$ the first sub-leading term is order z^4 , both with coefficients proportional to the coefficient \mathcal{A}_0^{\pm} from eq. (4.14).

In holographic renormalization, we proceed as follows [97–100]. First, in the action we introduce a cutoff on the z integration to regulate any divergences: we integrate not to $z = 0$ but to some small but finite $z = \varepsilon$. The result is a regulated on-shell action, which we will denote S_{reg} . Next, we insert the solutions for $x_1(z)$ and $x_3(z)$ into the action, expand the integrand in powers of z , perform the integration in z , and then isolate all terms that diverge in the $\varepsilon \rightarrow 0$ limit. Finally, we add a counterterm action, S_{CT} , consisting of terms localized at $z = \varepsilon$, built from the induced metric

on the $z = \varepsilon$ surface and designed to cancel all divergences in the $\varepsilon \rightarrow 0$ limit. The renormalized action is then

$$S_{\text{ren}} = \lim_{\varepsilon \rightarrow 0} (S_{\text{reg}} + S_{CT}). \quad (4.19)$$

Plugging eq. (4.18) into eq. (4.16) and expanding in z , we find

$$S_{\text{reg}} = \frac{T}{2\pi\alpha'} \int_{\varepsilon} dz \left[e^{\phi_{\pm}} \frac{R^2}{z^2} + \dots \right] = + \frac{T}{2\pi\alpha'} e^{\phi_{\pm}} \frac{R^2}{\varepsilon} + \dots, \quad (4.20)$$

where the \dots represents all non-divergent terms. After the z integration (*i.e.* in the second equality), that includes terms that remain finite or that vanish as $\varepsilon \rightarrow 0$. For both $AdS_5 \times S^5$ and non-SUSY Janus, among the terms that vanish as $\varepsilon \rightarrow 0$, the leading term is $\mathcal{O}(\varepsilon^3)$, while for SUSY Janus, the leading term is $\mathcal{O}(\varepsilon)$, with a coefficient proportional to the coefficient \mathcal{A}_0^{\pm} from eq. (4.14).

Now we need counterterms. In our case, these are built from the induced metric on the $z = \varepsilon$ surface, which we denote γ_{tt} ,

$$\gamma_{tt} dt^2 = + \frac{R^2}{\varepsilon^2} g_{11}(\varepsilon/x_3(\varepsilon)) dt^2 = + \frac{R^2}{\varepsilon^2} dt^2 + \mathcal{O}(\varepsilon^{n-2}), \quad (4.21)$$

where n was defined in eq. (4.14). The counterterm we need is then

$$S_{CT} = - \frac{R}{2\pi\alpha'} e^{\phi(\varepsilon/x_3)} \int dt \sqrt{\gamma_{tt}} = - \frac{T}{2\pi\alpha'} e^{\phi_{\pm}} \frac{R^2}{\varepsilon} + \dots \quad (4.22)$$

We introduced an overall factor of R to make S_{CT} dimensionless, like S_{reg} . In our case S_{CT} involves an integral over dt , but more generally the integral will be over the worldline of the endpoint of the string. In $AdS_5 \times S^5$, the $1/\varepsilon$ divergent term is the only contribution to S_{CT} . In the Janus spacetimes, additional terms appear, but these vanish as $\varepsilon \rightarrow 0$. These terms are represented by the \dots in eq. (4.22). For non-SUSY Janus, the first sub-leading term is $\mathcal{O}(\varepsilon^3)$, with coefficient proportional to the coefficient \mathcal{C}_0^{\pm} from eq. (4.15). For SUSY Janus, the first sub-leading term is $\mathcal{O}(\varepsilon)$, with coefficient proportional to the coefficient \mathcal{A}_0^{\pm} from eq. (4.14). With our counterterm, the S_{ren} defined in eq. (4.19) will be finite.

Crucially, notice that the divergence in S_{reg} and the counterterm are not only independent of the solutions $x_1(z)$ and $x_3(z)$, but are also independent of the size of the jump in the axio-dilaton: the divergence or counterterm in each asymptotically $AdS_5 \times S^5$ region depends on the value of the dilaton ϕ_{\pm} in that region, and not on the difference $\phi_+ - \phi_-$. The holographic renormalization of the string action in Janus spacetimes is identical to that in $AdS_5 \times S^5$, up to terms that vanish as $\varepsilon \rightarrow 0$. *A priori* that is intuitively obvious, if we recall that the AdS_5 radial direction corresponds to the field theory energy scale, with the boundary corresponding to the UV [43, 44]: deforming $\mathcal{N} = 4$ SYM by a conformal interface should not affect any field theory physics in the extreme UV, including in particular UV divergences of Wilson loop expectation values. Translating that statement into the bulk, we expect the divergences of the on-shell string action, and hence its holographic renormalization, to be identical in the Janus and $AdS_5 \times S^5$ spacetimes.

Additionally, no finite counterterms are possible in our cases. Finite counterterms can produce ambiguities in the value of the on-shell action, since we cannot fix their coefficients by demanding cancellation of divergences. If we think of $x_1(z)$ and $x_3(z)$ as scalar fields in AdS, then in our cases the only candidates for finite counterterms that are allowed by covariance are of the form

$$e^{\phi(\varepsilon/x_3)} \int dt \sqrt{\gamma_{tt}} x_1(\varepsilon)^p x_3(\varepsilon)^q = T e^{\phi_{\pm}} \frac{R}{\varepsilon} (x_1^{(0)})^p (x_3^{(0)})^q + \mathcal{O}(\varepsilon^2), \quad (4.23)$$

where p and q are non-negative integers, and never both zero. Clearly, in cases where $x_1^{(0)}$ and/or $x_3^{(0)}$ are nonzero, which includes all the cases we consider in sections 4.1 to 4.6, such counterterms will introduce divergences beyond those in S_{reg} , and hence the coefficients of these counterterms must be set to zero. The upshot is that in our cases covariance forbids any finite counterterms.

Now let us consider the Legendre transform of the string action, proposed in ref. [24] as a method to obtain a finite on-shell string action. To motivate a Legendre transform, the authors of ref. [24] presented the following intuitive argument. Consider N_c D9-branes in type IIB string theory. The D9-brane worldvolume theory is maximally SUSY (9+1)-dimensional $U(N_c)$ Yang-Mills. Suppose we want to compute a Wilson loop expectation value in that theory. In string theory the Wilson loop will be described by an open string with worldsheet bounded by the loop. Crucially, notice that we must impose the *opposite* of the standard open string boundary conditions, *i.e.* we must impose Dirichlet rather than Neumann boundary conditions, because we specify the loop that the string endpoints traverse. We must therefore perform a Legendre transform of the string action. We next T-dualize six times to obtain D3-branes. T-duality exchanges Dirichlet and Neumann boundary conditions, so at this stage the string obeys Dirichlet boundary conditions in directions along the D3-branes and Neumann boundary conditions in the transverse directions. Finally, upon taking the Maldacena limits we find a string in $AdS_5 \times S^5$ with a Legendre-transformed action guaranteeing that the string obeys Dirichlet boundary conditions in the field theory directions, where the Wilson loop is, and Neumann boundary conditions in the transverse directions, including the radial and S^5 directions. For the S^5 directions, local SUSY along the loop implies that Neumann and Dirichlet boundary conditions are in fact equivalent, so we only need to Legendre transform in the radial direction [24].¹⁴ The claim of ref. [24] is thus that the actual quantity to use as the renormalized action S_{ren} in eq. (4.1) is this Legendre-transformed on-shell string action.

We will denote the Legendre-transformed string action as \hat{S} , which in our cases takes the form

$$\hat{S} = S - \left[\int d\tau \frac{\delta S}{\delta \partial_\sigma z} z \right]_{z=\varepsilon}. \quad (4.24)$$

Choosing $z(\sigma) = \sigma$ gauge and plugging the asymptotic expansions in eqs. (4.14), (4.15) and (4.18)

¹⁴As a side comment, to obtain a genuine Wilson loop, rather than a Maldacena loop, we can simply perform a Legendre transform in the S^5 directions, so that the string obeys a Neumann boundary condition only in the radial direction [101]. Notice that the holographic results for the expectation values of the Wilson and Maldacena loops will then be the same. Differences will appear in the spectra of fluctuations about these loops and at sub-leading orders in the large- N_c and large- λ expansions [101].

into $z(\sigma)$'s canonical momentum, eq. (4.17), we find

$$-\left[\int d\tau \frac{\delta S}{\delta \partial_\sigma z} z\right]_{z=\varepsilon} = -\frac{T}{2\pi\alpha'} e^{\phi_\pm} \frac{R^2}{\varepsilon} + \dots, \quad (4.25)$$

where on the right-hand-side the \dots represent terms that vanish in the $\varepsilon \rightarrow 0$ limit. The first sub-leading terms in the \dots in eq. (4.25) are in fact exactly identical (up to the sign), both in the powers of ε and their coefficients, to the sub-leading terms in S_{reg} that vanish as $\varepsilon \rightarrow 0$, described below eq. (4.20).

The contributions to the string action from S_{CT} , eq. (4.22), or from the Legendre transform, eq. (4.25), differ only in terms that vanish as $\varepsilon \rightarrow 0$. We have thus demonstrated two things. First, we have shown that the divergence of S_{reg} is exactly the same in $AdS_5 \times S^5$ and in Janus spacetimes. Second, we have proven that in $AdS_5 \times S^5$ and in Janus spacetimes either holographic renormalization or the Legendre transform has the same net effect: each cancels the divergence of S_{reg} , and nothing more.

We will denote the *un-renormalized* on-shell action for the strings dual to the straight timelike Wilson line and the perpendicular loop as S^\perp and for the string dual to the parallel Wilson loop as S^\parallel . Starting from eq. (4.5), we simplify S^\perp as follows:

$$S^\perp = \frac{T}{2\pi\alpha'} \int_{x_{(1)}}^{x_{(2)}} dx e^\phi f_4^2 F = \frac{T}{2\pi\alpha'} \int_{x_{(1)}}^{x_{(2)}} dx \partial_x \left[\frac{e^\phi f_4^2}{F} u \partial_x u \right] = \frac{T}{2\pi\alpha'} \frac{e^\phi f_4^2}{F} u \partial_x u \Big|_{x_{(1)}}^{x_{(2)}}, \quad (4.26)$$

where in the first equality we used our definition of F in eq. (4.8) and our gauge choice $x(\sigma) = \sigma$, while in the second equality we used our constant solutions for y and the equation of motion for $u(x)$, eq. (4.9a). We choose conventions such that the endpoint of integration $x_{(1)}$ corresponds to $x_3^{(0)} < 0$ while $x_{(2)}$ corresponds to $x_3^{(0)} > 0$. Returning to eq. (4.5), we simplify S^\parallel as follows:

$$\begin{aligned} S^\parallel &= \frac{T}{2\pi\alpha'} \int_{-L/2}^{+L/2} dx_1 \left[-\frac{1}{C} e^{2\phi} f_4^4 u^4 \right] = \frac{T(-C)}{2\pi\alpha'} \int_{-L/2}^{+L/2} dx_1 \left[\partial_{x_1} \left(\frac{\partial_{x_1} u}{u^3} \right) - 1 \right] \\ &= \frac{T(-C)}{2\pi\alpha'} \left[\frac{\partial_{x_1} u}{u^3} \Big|_{-L/2}^{+L/2} - L \right], \end{aligned} \quad (4.27)$$

where in the first equality we used the definition of C in eq. (4.6) and our gauge choice $x_1(\sigma) = \sigma$, while in the second equality we used the equation of motion for $u(x_1)$, eq. (4.10a). Eqs. (4.26) and (4.27) demonstrate that in our cases the on-shell action depends only on data near the asymptotic boundary. Using the general asymptotic solution in eq. (4.18), we can easily show that these *un-renormalized* on-shell actions are indeed divergent due to the integration to the AdS boundary. First, we use the coordinate transformations given by eqs. (A.5) and (A.9) in the appendix to write the asymptotic solutions in terms of $x_1(z)$ and $x_3(z)$. Plugging the resulting expressions into eq. (4.26), and introducing a cutoff at $z = \varepsilon$, we obtain the regulated actions

$$S_{\text{reg}}^\perp = \frac{T}{2\pi\alpha'} \left[e^{\phi_-} \left(\frac{R^2}{\varepsilon} + 3R^2 x_3^{(0)} x_3^{(1)} + \dots \right) \Big|_{x_{(1)}} + e^{\phi_+} \left(\frac{R^2}{\varepsilon} + 3R^2 x_3^{(0)} x_3^{(1)} + \dots \right) \Big|_{x_{(2)}} \right], \quad (4.28a)$$

$$S_{\text{reg}}^{\parallel} = 2 \frac{T}{2\pi\alpha'} e^{\phi_{\pm}} \left(\frac{R^2}{\varepsilon} + 3R^2(x_1^{(0)}x_1^{(1)} + x_3^{(0)}x_3^{(1)}) + \dots \right) \Big|_{+L/2}, \quad (4.28b)$$

where ϕ takes one of the values ϕ_{\pm} , depending on the side of the interface that the parallel loop is, and the \dots represent terms that vanish as $\varepsilon \rightarrow 0$, as described below eq. (4.20). In eq. (4.28b) we used the fact that the string profile is symmetric around $x_1 = 0$ to write the contribution from the $x_1 = -L/2$ endpoint as a contribution from $x_1 = +L/2$. After adding the counterterm in eq. (4.22), or Legendre transforming, and then taking $\varepsilon \rightarrow 0$, we obtain the renormalized actions,

$$S_{\text{ren}}^{\perp} = \frac{T}{2\pi\alpha'} 3R^2 \left(e^{\phi_-} x_3^{(0)} x_3^{(1)} \Big|_{x_{(1)}} + e^{\phi_+} x_3^{(0)} x_3^{(1)} \Big|_{x_{(2)}} \right), \quad (4.29a)$$

$$S_{\text{ren}}^{\parallel} = 2 \frac{T}{2\pi\alpha'} e^{\phi_{\pm}} 3R^2 (x_1^{(0)}x_1^{(1)} + x_3^{(0)}x_3^{(1)}) \Big|_{+L/2}. \quad (4.29b)$$

Our procedure to calculate S_{ren}^{\perp} and $S_{\text{ren}}^{\parallel}$ numerically is the following. We find string solutions as explained in the previous subsection, using $u(\sigma)$ and $x(\sigma)$, up to some finite cutoff near the asymptotic AdS_5 boundary. We then convert those solutions for $u(\sigma)$ and $x(\sigma)$ into solutions for $x_1(z)$ and $x_3(z)$ using eqs. (A.5) and (A.9) in the appendix. In these Fefferman-Graham coordinates, the cutoff is simply $z = \varepsilon$. We then fit the numerical solutions for $x_1(z)$ and $x_3(z)$ to the asymptotic solution given in eq. (4.18).¹⁵ From these fits we obtain the values of $x_1^{(0)}$, $x_1^{(1)}$, $x_3^{(0)}$ and $x_3^{(1)}$ for each endpoint of the string. We then extract from these constants the values of L , L_{av} , and S_{ren}^{\perp} for the perpendicular string, and L , L_3 , and $S_{\text{ren}}^{\parallel}$ for the parallel string.

For the straight string dual to the timelike Wilson line, one subtlety arises: in this case, only one endpoint of the string reaches the boundary, while the other endpoint lies on the Poincaré horizon, $u = 0$. From the form of the un-renormalized action S^{\perp} in eq. (4.26), and in particular the factor of u there, we have reason to expect that the contribution from the Poincaré horizon will vanish. We have indeed confirmed that, using our numerical solutions. The holographic renormalization of the action then proceeds as above, with the renormalized action given by S_{ren}^{\perp} in eq. (4.29a), with $x_{(1)}$ corresponding to the boundary endpoint and the contribution from $x_{(2)}$ set to zero.

Finally, let us consider the third method to obtain a finite on-shell action: subtracting straight strings. We consider first $AdS_5 \times S^5$, where a static straight string sits at fixed constant values of x_1 , x_2 , and x_3 , and is spatially extended only in z . For such a string, the non-renormalized on-shell action reduces to two boundary terms, one from the Poincaré horizon $z \rightarrow \infty$ and one from the cutoff surface $z = \varepsilon$, as can be easily verified from eq. (4.16) or eq. (4.26). The contribution from $z \rightarrow \infty$ vanishes, so the on-shell action reduces to a single term, namely the divergent term in eq. (4.20). In particular, no finite terms appear. As a result, in $AdS_5 \times S^5$, subtracting a straight string, holographic renormalization, and the Legendre transform are all equivalent: they all subtract the divergent term, and nothing more.

The divergence of the straight string's non-renormalized on-shell action has a simple physical interpretation in the field theory. The on-shell action of the straight string corresponds to the

¹⁵In fact, in our numerics we work to higher order in z than in eq. (4.18), to improve the the quality of the fits.

potential of a single test charge. In $\mathcal{N} = 4$ SYM, this test charge experiences no external force, so the only contribution to the potential is the test charge's self-energy. That self-energy is naïvely divergent, hence the on-shell action of the straight string is divergent. Upon (holographic) renormalization, the divergence is exactly cancelled, indicating that the physical self-energy is zero, as guaranteed by SUSY: the straight Wilson line is BPS and commutes with half of the sixteen SUSY generators of $\mathcal{N} = 4$ SYM, which prevents its expectation value from receiving quantum corrections [24,25]. In $AdS_5 \times S^5$, subtracting the straight string, holographic renormalization, and the Legendre transform thus all have the same field theory interpretation: they all correspond to subtracting the naïvely divergent self-energy of a single test charge.

In $\mathcal{N} = 4$ SYM deformed by a conformal interface, in general the potential of a single test charge will include a contribution not only from a divergent self-energy but also from the interaction with the interface, *i.e.* from the interaction with an image charge. In that case, in the bulk we expect that, generically, for a straight string in a Janus spacetime the non-renormalized on-shell action will include not only the divergent term but also a finite term. Specifically, in eq. (4.28a), the non-renormalized on-shell action will include the contribution from the single endpoint $x_{(1)}$, generically with non-zero $x_3^{(0)} x_3^{(1)}$. As a result, in a Janus spacetime, generically holographic renormalization or the Legendre transform will *not* be equivalent to subtracting a straight string: the former still subtract the divergent term, and nothing more, while the latter subtracts both the divergent term and a finite term. In field theory language, holographic renormalization or the Legendre transform both correspond to subtracting the infinite self-energy of a test charge, while subtracting a straight string corresponds to subtracting not only the infinite self-energy of a test charge but also the finite interaction energy of the test charge with its image. Notice that special cases are possible. For example, we will see that for a straight string in SUSY Janus with $y = 0$ the finite term vanishes, indicating that the corresponding test charge has no image.

In all of our holographic calculations of Wilson loop expectation values from strings in Janus spacetimes, we used holographic renormalization or equivalently the Legendre transform to obtain a finite on-shell action. In the next three subsections we present our (mostly numerical) results for these Wilson loop expectation values.

4.3 Straight Wilson Lines

In this subsection we present our results for the expectation values of straight timelike Wilson lines in $\mathcal{N} = 4$ SYM with a jumping coupling or θ -angle, with and without SUSY, as obtained from holographic calculations using straight strings in Janus spacetimes. More precisely, we will present our results for the self-energy V , obtained from the Wilson line expectation value via eqs. (4.29a) and (4.2). In subsection 4.3.1 we present our numerical results, and in subsection 4.3.2 we present some exact results for the SUSY case at leading order in a small jump in the coupling or θ -angle.

4.3.1 Numerical Results

In fig. 8 we present our numerical results for the renormalized self-energy V of a single heavy test charge in $\mathcal{N} = 4$ SYM with a jumping coupling. In the non-SUSY case, shown in fig. 8 (a), for any non-zero jump in the coupling we always find a non-zero result for V , indicating that a non-zero image charge is present. Recalling our discussions from sections 2.1 and 3.2, that provides very suggestive evidence that the field theory dual to non-SUSY Janus has $\kappa \neq 0$. Moreover, we find that the qualitative behavior is the same as in electromagnetism with a jumping coupling: $VL_3 < 0$ in all cases, indicating that the test charge is always attracted to the side with smaller coupling. In fact, for a test charge on the side of the interface with smaller coupling (the blue dots in fig. 8 (a)) we find that to a very good approximation our numerical results obey $V \propto \frac{\lambda_+ - \lambda_-}{\lambda_+ + \lambda_-} = \frac{g_+^2 - g_-^2}{g_+^2 + g_-^2}$, which is the same behavior as in electromagnetism: in eqs. (3.19) and (3.20) simply set $\theta_+ = \theta_-$. This linear dependence on the jump in the coupling-squared is a non-trivial and surprising outcome, given that $\mathcal{N} = 4$ SYM is a non-linear (*i.e.* interacting) theory. Indeed, in $\mathcal{N} = 4$ SYM with a constant coupling, when $\lambda \gg 1$, the non-linearities produce the $\sqrt{\lambda}$ factor in the potential between test charges, instead of the λ that appears when $\lambda \ll 1$, as we discussed below eq. (1.3).

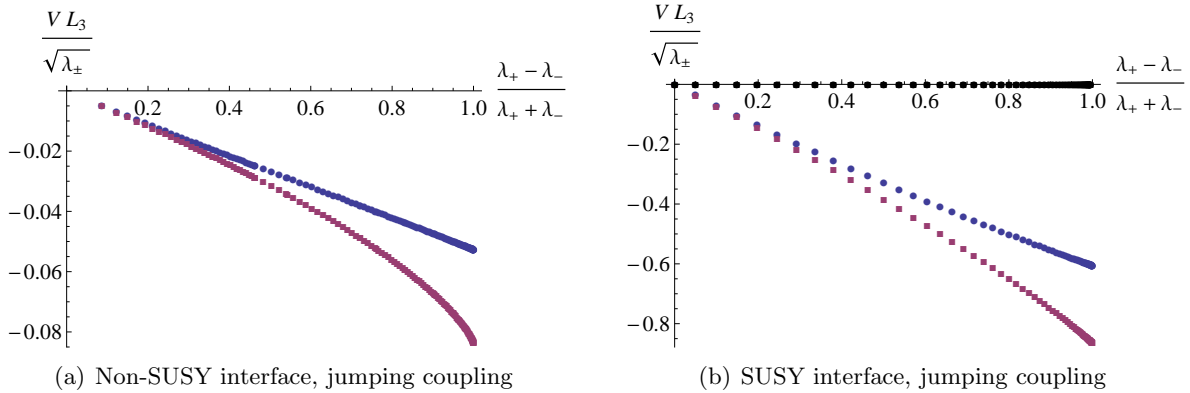


Figure 8: The self-energy V , expressed as $VL_3/\sqrt{\lambda_{\pm}}$, as a function of $\frac{\lambda_+ - \lambda_-}{\lambda_+ + \lambda_-} = \frac{g_+^2 - g_-^2}{g_+^2 + g_-^2}$ for a single heavy test charge in large- N_c , strongly-coupled $\mathcal{N} = 4$ SYM with a jumping coupling, computed from straight strings in Janus spacetimes. (a) Our results for the non-SUSY interface, dual to non-SUSY Janus. The blue dots are our numerical results for a test charge to the left of the interface, $L_3 < 0$, which has smaller coupling, $\lambda_- < \lambda_+$, and for which we plot $VL_3/\sqrt{\lambda_-}$. The purple squares are our numerical results for a test charge with $L_3 > 0$, where we plot $VL_3/\sqrt{\lambda_+}$. The blue circles form a line: for a test charge on the side with smaller coupling, V is linear in $\frac{\lambda_+ - \lambda_-}{\lambda_+ + \lambda_-}$, the same as in electromagnetism with a jumping coupling (see eqs. (3.19) and (3.20)). (b) Our results for the SUSY interface, dual to SUSY Janus. The blue dots and purple squares have the same meaning as in (a), and come from a straight string at $y = \pi/2$. The black dots are for a straight string at $y = 0$ on either side of the interface. In that case $V = 0$.

We show our results for the SUSY case in fig. 8 (b). Here we find that the result for V depends

sensitively on y , the location of the straight string in the internal space, dual to the couplings θ^I in the definition of the Wilson loop in eq. (3.24). For $y = \pi/2$, the results are similar to those in the non-SUSY case: for non-zero jump in the coupling we find non-zero V , indicating the presence of a non-zero image charge, and $VL_3 < 0$ in all cases, indicating that a test charge is always attracted to the side with smaller coupling. Now, however, for a test charge on either side of the interface V 's dependence on $\frac{g_+^2 - g_-^2}{g_+^2 + g_-^2}$ is not linear (although for a test charge on the side with smaller coupling, depicted by the blue dots in fig. 8 (b), V is close to linear in $\frac{g_+^2 - g_-^2}{g_+^2 + g_-^2}$).

Our most surprising result in the SUSY case comes from the string at $y = 0$, represented by the black dots in fig. 8 (b), where apparently $V = 0$ exactly! To dispel any fear that this result may be a numerical artifact, in the next subsection we consider a small jump in the coupling and, working to leading order in that small jump, we show that $V = 0$ analytically (*i.e.* without numerics). Additionally, the numerical results for the expectation value of a Wilson loop perpendicular to the interface that we will present in section 4.4 will provide another, independent, consistency check. Apparently in this case the test charge has no image charge!

As we discussed in the introduction, the fact that we find $V = 0$ from the straight string with $y = 0$ in SUSY Janus has a number of potential implications. One implication is for the rectangular Wilson loop: as we saw in section 3.2, in a case such as this, where the self-energy vanishes, the sum of ladder diagrams may be relatively easy to do for the expectation value of the rectangular Wilson loop. Another implication is for a circular Wilson loop. In field theory terms, we have a system with conformal symmetry and a straight Wilson line with trivial expectation value. We may perform a conformal transformation to map the straight line to a circle. A non-zero expectation value of that circular Wilson loop may imply the existence of a matrix model, as in $\mathcal{N} = 4$ SYM with constant coupling [25, 29, 30]. A natural question is whether such a matrix model could be obtained from a calculation using SUSY localization in Euclidean $\mathcal{N} = 4$ SYM on S^4 with an interface. Indeed, in ref. [27] a matrix model was derived for a circular Wilson loop sitting exactly on the interface in Euclidean $\mathcal{N} = 4$ SYM on S^4 . Our results suggest that something similar may be possible for a circular Wilson loop away from the interface. A crucial question is thus how much SUSY the straight timelike Wilson line dual to the straight string at $y = 0$ preserves. Regrettably, we will leave that question for future research.

In fig. 9 we present our numerical results for the renormalized self-energy V of a single heavy test charge in $\mathcal{N} = 4$ SYM with a jumping θ -angle. Specifically, we plot $VL_3/\sqrt{\lambda}$ as a function of $\frac{g^4(\Delta\theta)^2}{64\pi^4 + g^4(\Delta\theta)^2}$, which is the natural quantity to consider from the point of view of electromagnetism with a jumping θ -angle: the image charge in eq. (3.19) depends linearly on this quantity. To produce fig. 9 we chose a vanishing θ -angle to the left ($x_3 < 0$) of the interface, $\theta_- = 0$, such that $\Delta\theta = \theta_+ - \theta_- = \theta_+$. In the 't Hooft limit $g^2 = \mathcal{O}(1/N_c)$, so implicitly we take $\theta_+ = \mathcal{O}(N_c)$, so that $g^4(\Delta\theta)^2 = \mathcal{O}(1)$, as shown in fig. 9.

In the non-SUSY case, shown in fig. 9 (a), for any non-zero $\Delta\theta$ we always find a non-zero V , indicating that a non-zero image charge is present. The qualitative behavior is the same as in

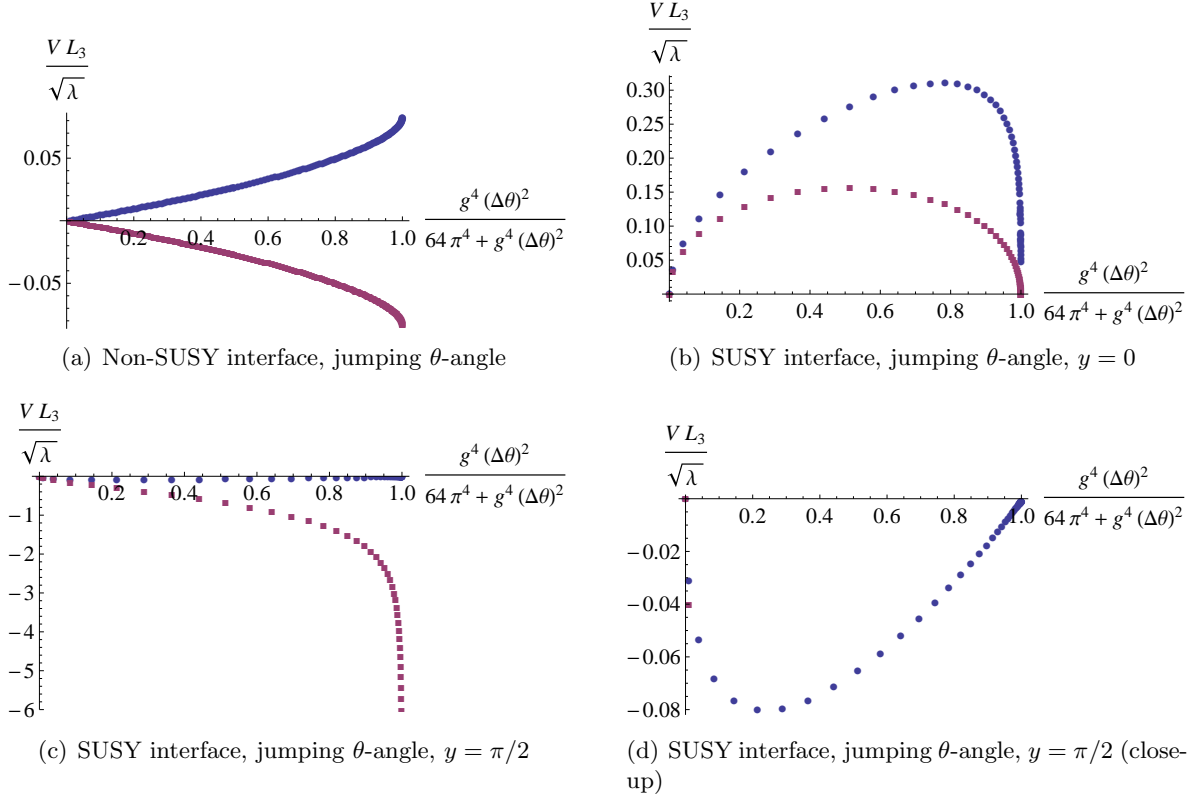


Figure 9: The self-energy V , expressed as $VL_3/\sqrt{\lambda}$, for a single heavy test charge in large- N_c , strongly-coupled $\mathcal{N} = 4$ SYM with a jumping θ -angle, computed from a straight string in Janus spacetime. We plot $VL_3/\sqrt{\lambda}$ as a function of $\frac{g^4(\Delta\theta)^2}{64\pi^4 + g^4(\Delta\theta)^2}$, the quantity that appears in the image charge in electromagnetism with a jumping θ -angle, *i.e.* eq. (3.19) with $g_+ = g_-$. (a) Our results for the non-SUSY interface, dual to non-SUSY Janus. The blue dots are our numerical results for a test charge to the left of the interface, $L_3 < 0$, while the purple squares are our numerical results for a test charge with $L_3 > 0$. (b) Our results for a SUSY interface, computed using a string with $y = 0$ in SUSY Janus. The blue dots and purple squares have the same meaning as in (a). (c) Our results for a SUSY interface, computed using a string with $y = \pi/2$ in SUSY Janus. The blue dots and purple squares have the same meaning as in (a). (d) Close-up of (c).

electromagnetism with a jumping θ -angle: $VL_3 < 0$ to the right of the interface (the purple squares in fig. 9 (a)) while $VL_3 > 0$ to the left (the blue dots in fig. 9 (a)), indicating that the test charge is always attracted towards the interface. The fact that VL_3 is not linear in $\frac{g^4(\Delta\theta)^2}{64\pi^4 + g^4(\Delta\theta)^2}$ is distinctly different from electromagnetism with a jumping θ -angle, however.

For a SUSY interface, we find that the result for V depends sensitively on y . For the $y = 0$ case, shown in fig. 9 (b), we find that V is non-zero for any finite $\Delta\theta$. Two curious features also appear, compared to the non-SUSY interface. First, $VL_3 \geq 0$ for a test charge on either side of the interface, indicating that a test charge is always attracted to the side with *larger* θ . In other words, when

the test charge is on the side with larger θ -angle (to the right of the interface, the purple squares in fig. 9 (b)), the image charge has the *opposite* sign from what we expect based on our intuition from electromagnetism, so that the test charge is *repelled* from the interface. Second, for a test charge on either side of the interface, we find that as $\Delta\theta$ increases, VL_3 increases, reaches a maximum, and then eventually goes to zero as $\Delta\theta \rightarrow \infty$, which suggests that the image charge vanishes in that limit. Such behavior is dramatically different from electromagnetism with a jumping θ -angle: the image charge in eq. (3.19) goes to a non-zero constant when $g_+ = g_-$ and $|\theta_+ - \theta_-| \rightarrow \infty$.

For the $y = \pi/2$ case, shown in figs. 9 (c) and (d), we find that V is non-zero for any finite $\Delta\theta$, but now $VL_3 \leq 0$, indicating that a test charge is always attracted to the side with *smaller* θ . In other words, when the test charge is on the side with smaller θ -angle (to the left of the interface, the blue dots in fig. 9 (c) and (d)), the image charge has the opposite sign from what we expect based on our intuition from electromagnetism, and the test charge is repelled from the interface. Moreover, for such a test charge, as $\Delta\theta$ increases, VL_3 decreases, reaches a minimum, and then increases and goes to zero as $\Delta\theta \rightarrow \infty$, as depicted in fig. 9 (d). For a test charge to the right of the interface (the purple squares in fig. 9 (c)), however, as $\Delta\theta$ increases, VL_3 monotonically decreases, and indeed diverges to $-\infty$ as $\Delta\theta \rightarrow \infty$, which suggests that the image charge actually *diverges* in that limit. Apparently, in that limit the force on the test charge, which pushes towards the side with smaller θ , will be infinite.

As shown in ref. [27], for Euclidean $\mathcal{N} = 4$ SYM on S^4 with a SUSY interface where the coupling jumps, the matrix model that determines the expectation value of a circular Wilson loop on the interface is of exactly the same form as that in the absence of the interface. One claim of ref. [27] was that the same is not true for an interface where the θ -angle jumps. We can compare these results to our results for the expectation value of the straight timelike Wilson line in $\mathcal{N} = 4$ SYM with a SUSY interface in \mathbb{R}^4 . In particular, the fact that we find vanishing self-energy in the case with a jumping coupling and $y = 0$, while we find a non-zero self-energy in the case with a jumping θ -angle and $y = 0$, is nicely consistent with the results of ref. [27].

4.3.2 Exact Results for Straight Strings in SUSY Janus

In fig. 8 (b) we presented numerical evidence that a straight string with $y = 0$ in jumping-dilaton SUSY Janus gives rise to a trivial expectation value for a straight, timelike Wilson line, indicating that the associated test charge has no image charge. In this subsection we will demonstrate that to be the case without numerics. Moreover, we will show that the same does not happen for a string with $y = \pi/2$ in jumping-dilaton SUSY Janus or for a string with either $y = 0$ or $y = \pi/2$ in jumping-axion SUSY Janus. Our strategy is to consider a small jump in the coupling or θ -angle, meaning $\delta\phi \ll 1$, and to work to leading order in perturbation theory in that small parameter.

To proceed for the jumping-dilaton case, we return to the equation of motion for the perpendicular case, eq. (4.9b), only now we choose the gauge $\sigma = u$, so that we need to solve for $x(u)$ instead of $u(x)$. When the jump in the dilaton vanishes, $\delta\phi = 0$, the background solution is $AdS_5 \times S^5$, in which case a straight string sits at constant (x_1, x_2, x_3) , and is spatially extended in z , as we

discussed in section 4.2. Placing the string at $(x_1, x_2, x_3) = (0, 0, L_3)$, and using eq. (2.2), the solution for the straight string is

$$x(u) = \tanh^{-1}(L_3 u). \quad (4.30)$$

Now introducing a small jump in the dilaton, $\delta\phi \ll 1$, we expand the equation of motion in $\delta\phi$. The solution for the straight string is then straightforward to obtain to order $\delta\phi$,

$$\begin{aligned} x(u) &= \tanh^{-1}(L_3 u) - \delta\phi \left(\frac{c_1 u}{1 - L_3^2 u^2} + \frac{c_2 \sqrt{1 - L_3^2 u^2}}{3u^2} + \frac{1 + L_3^2 u^2}{2(1 - L_3^2 u^2)} \right) + \mathcal{O}(\delta\phi^2), & y = 0, \\ x(u) &= \tanh^{-1}(L_3 u) - \delta\phi \left(\frac{d_1 u}{1 - L_3^2 u^2} + \frac{d_2 \sqrt{1 - L_3^2 u^2}}{3u^2} - \frac{1 - 3L_3^2 u^2}{6L_3^2 u^2 (1 - L_3^2 u^2)} \right) + \mathcal{O}(\delta\phi^2), & y = \frac{\pi}{2}, \end{aligned} \quad (4.31)$$

where c_1, c_2, d_1 , and d_2 are integration constants, which we fix as follows. At the Poincaré horizon, $u = 0$, we find a quadratic pole in u . If the coefficient of that pole is non-zero, then the solution will describe a string that bends and returns to the boundary, rather than a straight string. We thus set the coefficient of that pole to zero by choosing $c_2 = 0$ in the case $y = 0$ and $d_2 = 1/(2L_3^2)$ in the case $y = \pi/2$. To fix c_1 and d_1 , we require the string to intersect the boundary at $x_3 = L_3$, which means $c_1 = -|L_3|$ and $d_1 = -L_3/3$. We next insert these solutions into eq. (4.29a) to obtain the renormalized on-shell action:

$$\begin{aligned} S_{\text{ren}}^{\text{straight}} &= \mathcal{O}(\delta\phi^2), & y = 0, \\ S_{\text{ren}}^{\text{straight}} &= -\frac{T}{2\pi\alpha'} R^2 e^{\phi_{\pm}} \frac{\delta\phi}{2L_3} + \mathcal{O}(\delta\phi^2), & y = \pi/2, \end{aligned} \quad (4.32)$$

where in the $y = \pi/2$ case we take ϕ_+ when $L_3 > 0$ and ϕ_- when $L_3 < 0$. We have confirmed that our numerical results, presented in fig. 8 (b), agree with eq. (4.32) in the $\delta\phi \ll 1$ regime. We have thus demonstrated that for a SUSY interface with a small jump in the coupling, $V = 0$ when $y = 0$, while V is non-zero when $y = \pi/2$.

To proceed for the jumping-axion case, we begin with a jumping-dilaton SUSY Janus solution, with some $\delta\hat{\phi} \ll 1$, and then perform an $SL(2, \mathbb{R})$ transformation with

$$a = \frac{1}{1 + e^{2\delta\hat{\phi}}}, \quad b = e^{-(\hat{\phi}_+ + \hat{\phi}_-)} \frac{e^{2\delta\hat{\phi}}}{1 + e^{2\delta\hat{\phi}}}, \quad c = -e^{\hat{\phi}_+ + \hat{\phi}_-}, \quad d = 1. \quad (4.33)$$

The resulting solution has zero jump in the dilaton, but a non-zero jump in the axion:

$$e^{2\phi_+} = e^{2\phi_-} = e^{2\hat{\phi}_+} + e^{2\hat{\phi}_-}, \quad C_{(0)-} = 0, \quad C_{(0)+} = e^{-(\hat{\phi}_+ + \hat{\phi}_-)} \tanh(\delta\hat{\phi}). \quad (4.34)$$

We next expand the equation of motion in $\delta\hat{\phi} \ll 1$, which is equivalent to expanding in $\delta C_{(0)} =$

$C_{(0)+} - C_{(0)-} \ll 1$. The solution for $x(u)$, to order $\delta\hat{\phi}$, is

$$\begin{aligned} x(u) &= \tanh^{-1}(L_3 u) - \delta\hat{\phi} \left(\frac{c_1 u}{1 - L_3^2 u^2} + \frac{c_2 \sqrt{1 - L_3^2 u^2}}{3u^2} + \frac{1 + 3L_3^4 u^4}{12L_3^2 u^2 (1 - L_3^2 u^2)} \right) + \mathcal{O}(\delta\hat{\phi}^2), \quad y = 0, \\ x(u) &= \tanh^{-1}(L_3 u) - \delta\hat{\phi} \left(\frac{d_1 u}{1 - L_3^2 u^2} + \frac{d_2 \sqrt{1 - L_3^2 u^2}}{3u^2} - \frac{1 + 3L_3^4 u^4}{12L_3^2 u^2 (1 - L_3^2 u^2)} \right) + \mathcal{O}(\delta\hat{\phi}^2), \quad y = \frac{\pi}{2}, \end{aligned} \quad (4.35)$$

where c_1 , c_2 , d_1 , and d_2 are integration constants. To avoid a quadratic pole in the solutions at $u = 0$, we choose $c_2 = -1/(2L_3^2)$ for the $y = 0$ case and $d_2 = 1/(2L_3^2)$ for the $y = \pi/2$ case. Requiring that the string intersect the boundary at $x_3 = L_3$ fixes $c_1 = -|L_3|/3$ for the $y = 0$ case and $d_1 = |L_3|/3$ for the $y = \pi/2$ case. Inserting these solutions into eq. (4.29a), we find

$$\begin{aligned} S_{\text{ren}}^{\text{straight}} &= \frac{T}{2\pi\alpha'} R^2 e^{\phi} \frac{\delta\hat{\phi}}{4L_3} + \mathcal{O}(\delta\hat{\phi}^2) = \frac{T}{2\pi\alpha'} R^2 e^{3\phi} \frac{\delta C_{(0)}}{8|L_3|} + \mathcal{O}(\delta C_{(0)}^2), \quad y = 0, \\ S_{\text{ren}}^{\text{straight}} &= -\frac{T}{2\pi\alpha'} R^2 e^{\phi} \frac{\delta\hat{\phi}}{4L_3} + \mathcal{O}(\delta\hat{\phi}^2) = -\frac{T}{2\pi\alpha'} R^2 e^{3\phi} \frac{\delta C_{(0)}}{8|L_3|} + \mathcal{O}(\delta C_{(0)}^2), \quad y = \pi/2. \end{aligned} \quad (4.36)$$

We have confirmed that our numerical results, presented in figs. 9 (b), (c), and (d), agree with eq. (4.36) in the $\delta C_{(0)} \ll 1$ regime. We have thus demonstrated that for a SUSY interface with a small jump in the θ -angle, V is non-zero for both $y = 0$ and $y = \pi/2$.

In summary, we have shown that for a SUSY interface with either a small jump in the coupling or a small jump in the θ -angle, in all cases the renormalized self-energy V is non-zero, with one exception: a small jump in the coupling and $y = 0$. Our numerical results in figs. 8 and 9 suggest that the same is also true for *all* finite values of the jump in the coupling or θ -angle.

4.4 Perpendicular Wilson Loops

In this subsection we present our numerical results for the expectation values of Wilson loops perpendicular to the interface, depicted in fig. 1 (a), representing two test charges along a line perpendicular to the interface, on opposite sides of the interface. In particular, we present our results for the interaction potential $V_{\perp}(L, L_{\text{av}})$ as determined from strings in Janus spacetimes via eqs. (4.29a) and (4.2).

In electromagnetism with an interface, the $V_{\perp}(L, L_{\text{av}})$ in eq. (3.22) is linear, *i.e.* is simply a sum of the interaction energy between the two test charges and the interaction energies with the image charges. In a non-Abelian gauge theory such as $SU(N_c)$ $\mathcal{N} = 4$ SYM, however, generically $V_{\perp}(L, L_{\text{av}})$ will not be linear. To provide some measure of the deviation from linearity, we will compare our numerical results for $V_{\perp}(L, L_{\text{av}})$ to an *ad hoc* linear potential of the form

$$V_{\perp}^{\text{lin}}(L, L_{\text{av}}) \equiv V_{\perp}^{\text{int}}(L) + V_{\text{self}}(L, L_{\text{av}}), \quad (4.37)$$

where for the “interaction potential” $V_{\perp}^{\text{int}}(L)$ we use the holographic result for $V(L)$ in $\mathcal{N} = 4$ SYM with constant coupling, eq. (1.2), but replacing λ with an “effective ’t Hooft coupling,”

$$V_{\perp}^{\text{int}}(L) = -\frac{4\pi^2}{\Gamma(1/4)^4} \frac{\sqrt{2\lambda_+}}{L} \sqrt{1 + \tilde{Q}^e/Q^e}, \quad (4.38)$$

where \tilde{Q}^e is defined in eq. (3.19). Notice that our effective ’t Hooft coupling, $\lambda_+(1 + \tilde{Q}^e/Q^e)$, is invariant under $g_+ \leftrightarrow g_-$ and $\theta_+ \leftrightarrow \theta_-$. The self-energy $V_{\text{self}}(L, L_{\text{av}})$ is a sum of two terms, representing the interaction of each test charge with its own image charge, which we obtain from our numerical results in section 4.3. Our $V_{\perp}^{\text{lin}}(L, L_{\text{av}})$ is designed to mimic the analogous potential $V_{\perp}(L, L_{\text{av}})$ in electromagnetism, eq. (3.22), but with modifications for the $\lambda \gg 1$ regime, in which $V(L) \propto \sqrt{\lambda}/L$ rather than $V(L) \propto \lambda/L$ as in the $\lambda \ll 1$ regime. Specifically, $V_{\perp}^{\text{int}}(L)$ is designed to mimic the first two terms on the right-hand-side of eq. (3.22), while $V_{\text{self}}(L, L_{\text{av}})$ is designed to mimic the last two terms.

In figs. 10 (a) and (b) we present our numerical results for a non-SUSY interface with jumping coupling or θ -angle, respectively. In each case, notice first and foremost the striking similarity to the analogous results in electromagnetism shown in fig. 5. We can thus infer that for a jumping coupling a test charge is always attracted to the side with smaller coupling, and for a jumping θ -angle, a test charge is always attracted to the interface, which is consistent with our analysis of image charges in section 4.3. We also see that in most cases our *ad hoc* linear potential V_{\perp}^{lin} provides a surprisingly good approximation to the holographic results. That approximation grows worse as the jump in the coupling or θ -angle grows: in the case of jumping θ -angle, depicted in fig. 10 (b), compare the results for $g^2\Delta\theta = 2\pi^2$ (the blue circles) with those for $g^2\Delta\theta = 40\pi^2$ (the golden crosses).

In fig. 11 we present our numerical results for SUSY interfaces with a jumping coupling. Here again we find that the results depend sensitively on y . For the case with $y = 0$, we presented evidence in section 4.3 that the test charge has no image charge, so we have good reason to expect something qualitatively different from electromagnetism. Indeed, in that case, our holographic result for $V_{\perp}L$, depicted in fig. 11 (a), remains finite at $L_{\text{av}}/L = \pm 1/2$, in stark contrast to electromagnetism, where $V_{\perp}L$ diverges at those points because a test charge coincides with its own image. The fact that the holographic result for $V_{\perp}L$ remain finite at $L_{\text{av}}/L = \pm 1/2$ provides another, independent, piece of evidence that for a SUSY interface with a jumping coupling, a test charge with $y = 0$ does not have an image charge. For the case with $y = \pi/2$, our results for the self-energy of a single test charge with $y = \pi/2$ in fig. 8 (b) suggested that we should see behavior qualitatively similar to that in electromagnetism. Indeed, our results in fig. 11 (b) are similar to the result in electromagnetism, fig. 5 (a). In particular, $V_{\perp}(L, L_{\text{av}}) \rightarrow \pm\infty$ and $L_{\text{av}}/L \rightarrow \pm 1/2$ because in each limit a test charge approaches its own image charge.

In fig. 12 we present our numerical results for a SUSY interface with a jumping θ -angle. Once again the results are dramatically different for different values of y . Recall that in electromagnetism with a jumping θ -angle, $V_{\perp}(L, L_{\text{av}}) \rightarrow -\infty$ as $L_{\text{av}}/L \rightarrow \pm 1/2$, as depicted in fig. 5 (b). For $\mathcal{N} = 4$

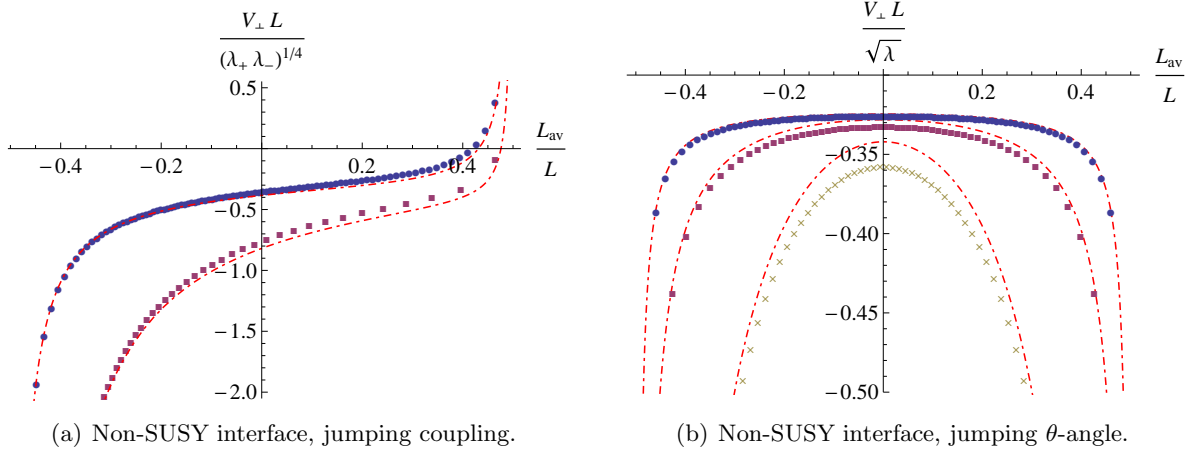


Figure 10: The potential $V_{\perp}(L, L_{\text{av}})$ between two test charges along a line perpendicular to a non-SUSY interface in large- N_c , strongly-coupled $\mathcal{N} = 4$ SYM, depicted in fig. 1 (a), as computed from strings in non-SUSY Janus spacetimes. (a) $V_{\perp}L/(\lambda_+\lambda_-)^{1/4}$ as a function of $L_{\text{av}}/L \in [-1/2, 1/2]$ for a non-SUSY interface with jumping coupling. The blue dots are our numerical results for $\log(\lambda_+/\lambda_-) = 1$ (equivalently, $\lambda_+ = e\lambda_- > \lambda_-$) while the purple squares are our numerical results for $\log(\lambda_+/\lambda_-) = 3$. (b) $V_{\perp}L/\sqrt{\lambda}$ as a function of L_{av}/L for a non-SUSY interface with jumping θ -angle. Here again we take $\theta_- = 0$ so that $\Delta\theta = \theta_+ - \theta_- = \theta_+$. The blue dots, purple squares, and golden crosses are our numerical results for $g^2\Delta\theta = 2\pi^2, 4\pi^2$, and $40\pi^2$, respectively. In both (a) and (b) the red dot-dashed lines are our results for the *ad hoc* linear potential V_{\perp}^{lin} defined in eq. (4.37). For both (a) and (b), our results are qualitatively similar to the analogous results in electromagnetism shown in fig. 5.

SYM with a SUSY interface where the θ -angle jumps, when $y = 0$ our holographic result is that $V_{\perp} \rightarrow -\infty$ only when $L_{\text{av}}/L \rightarrow +1/2$, whereas when $L_{\text{av}}/L \rightarrow -1/2$ we find $V_{\perp} \rightarrow +\infty$, as depicted in fig. 12 (a). Such behavior is consistent with our results for a single test charge in fig. 9 (b), which indicated that a test charge on the side with larger θ -angle (to the right of the interface, the purple squares in fig. 9 (b)) has an image charge with a sign opposite to what we expect based on our intuition from electromagnetism. In fig. 12 (a) we thus see that as $L_{\text{av}}/L \rightarrow -1/2$, the test charge on the right approaches its “wrong-sign” image charge, and so the potential diverges the “wrong” way, to $+\infty$ instead of $-\infty$. Similarly, in the case with $y = \pi/2$, depicted in fig. 12 (b), we see that $V_{\perp}(L, L_{\text{av}}) \rightarrow -\infty$ as $L_{\text{av}}/L \rightarrow -1/2$ but when $L_{\text{av}}/L \rightarrow +1/2$ we find that the potential diverges the “wrong” way, $V_{\perp}(L, L_{\text{av}}) \rightarrow +\infty$. Here again the culprit is a “wrong sign” image charge: as our results for a single test charge with $y = \pi/2$ in figs. 9 (c) and (d) showed, the test charge on the side with smaller θ -angle (to the left of the interface, the blue dots in figs. 9) has an image charge with a sign opposite to what we expect based on our intuition from electromagnetism.

We also see from figs. 11 and 12 that in all cases with a SUSY interface V_{\perp}^{lin} (the red dot-dashed lines in the figures) again provides a surprisingly good approximation to the holographic results, with one exception: an interface with a jumping coupling and a test charge with $y = 0$. In that

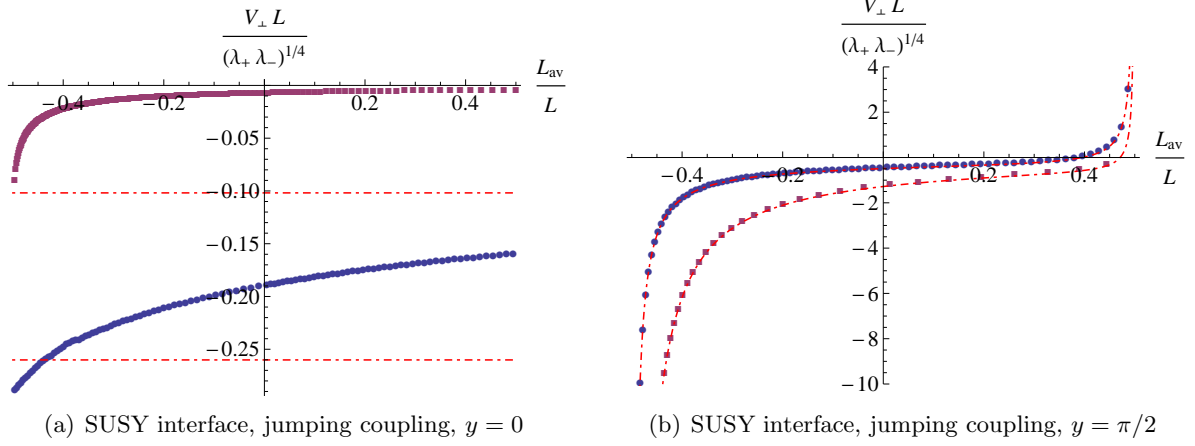


Figure 11: The potential $V_{\perp}(L, L_{\text{av}})$ between two test charges along a line perpendicular to a SUSY interface where the coupling jumps in large- N_c , strongly-coupled $\mathcal{N} = 4$ SYM, depicted in fig. 1 (a), as computed from strings in SUSY Janus spacetimes with a jumping dilaton. More precisely, we plot $V_{\perp}L/(\lambda_+\lambda_-)^{1/4}$ versus L_{av}/L , as computed from a string at (a) $y = 0$ and (b) $y = \pi/2$. In both (a) and (b), the blue dots and purple squares are our numerical results for $\log(\lambda_+/\lambda_-) = 1, 3$, respectively, while the red dot-dashed lines are our numerical results for the *ad hoc* linear potential V_{\perp}^{lin} defined in eq. (4.37).

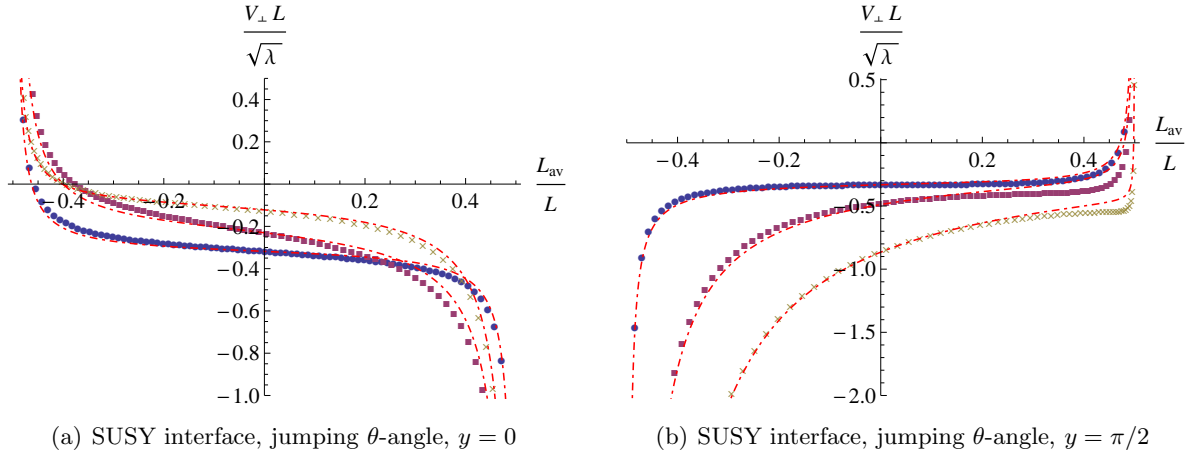


Figure 12: The potential $V_{\perp}(L, L_{\text{av}})$ between two test charges along a line perpendicular to a SUSY interface where the θ -angle jumps in large- N_c , strongly-coupled $\mathcal{N} = 4$ SYM, depicted in fig. 1 (a), as computed from strings in SUSY Janus spacetimes with a jumping axion. More precisely we plot $V_{\perp}L/\sqrt{\lambda}$ versus L_{av}/L as computed from a string at (a) $y = 0$ or (b) $y = \pi/2$. In both (a) and (b), The blue dots, purple squares, and golden crosses are our numerical results for $g^2\Delta\theta = 2\pi^2, 12\pi^2$, and $40\pi^2$, respectively, while the red dot-dashed lines are our results for the *ad hoc* linear potential V_{\perp}^{lin} defined in eq. (4.37).

case, the fact that $V_{\text{self}} = 0$ means $V_{\perp}^{\text{lin}} = V_{\perp}^{\text{int}}$, which is constant in L_{av}/L . The holographic results are clearly not constant in L_{av}/L .

4.5 Parallel Wilson Loops

In this subsection we present our numerical results for the expectation values of Wilson loops parallel to the interface, depicted in fig. 1 (b), representing two test charges along a line parallel to the interface. In particular, we present our results for the interaction potential $V_{\parallel}(L, L_3)$ as determined from strings in Janus spacetimes via eqs. (4.29b) and (4.2).

As in the previous subsection, we will compare our holographic results to an *ad hoc* linear potential, $V_{\parallel}^{\text{linear}}(L, L_3)$, defined similarly to $V_{\perp}^{\text{lin}}(L, L_{\text{av}})$,

$$V_{\parallel}^{\text{lin}}(L, L_3) \equiv V_{\parallel}^{\text{int}}(L, L_3) + V_{\text{self}}(L_3), \quad (4.39)$$

where, for $L_3 > 0$,

$$V_{\parallel}^{\text{int}}(L, L_3) \equiv -\frac{4\pi^2}{\Gamma(1/4)^4} \frac{\sqrt{2\lambda_+}}{L} \sqrt{1 + \frac{\tilde{Q}^e/Q^e}{\sqrt{1 + 4L_3^2/L^2}}}, \quad (4.40)$$

and the same for $L_3 < 0$ but with $g_+ \leftrightarrow g_-$ and $\theta_+ \leftrightarrow \theta_-$. The self-energy $V_{\text{self}}(L_3)$ is a sum of two terms, representing the interaction of each test charge with its own image charge, which we obtain from our numerical results in section 4.3. As in the previous subsection, our *ad hoc* linear potential is designed to mimic the analogous potential $V_{\parallel}(L, L_3)$ in electromagnetism, eq. (3.23). Specifically, $V_{\parallel}^{\text{int}}(L, L_3)$ is designed to mimic the first and fourth terms on the right-hand-side of eq. (3.23), while $V_{\text{self}}(L_3)$ is designed to mimic the second and third terms.

In fig. 13 we present our results for a non-SUSY interface with a jumping coupling. As in the previous cases with non-SUSY interfaces, we find a striking similarity to the analogous results in electromagnetism, as shown in fig. 6 (a). In particular, we see that the dipole is attracted to the side with smaller coupling. Moreover, the fact that the results in fig. 13 are qualitatively different from the potential obtained from the sum of ladder diagrams when $\kappa = 0$, shown in fig. 7, provides additional circumstantial evidence that the field theory dual to non-SUSY, jumping-dilaton Janus has non-zero κ . Of course, we must bear in mind that even in $\mathcal{N} = 4$ SYM without an interface, other diagrams besides the ladders contribute to $V_{\parallel}(L, L_3)$ [25, 26], so the comparison between figs. 7 and 13, though suggestive, is not conclusive.

Here we can also do something that was not possible for two test charges on opposite sides of the interface: we can move both test charges infinitely far away from the interface, on one side: $L_3/L \rightarrow \pm\infty$. In each limit, we should recover the result for $\mathcal{N} = 4$ SYM without an interface, eq. (1.2), with the appropriate value of λ for that side of the interface, λ_{\pm} . In fig. 13 we depict the result of eq. (1.2) for the two sides of the interface as horizontal green dashed lines. Our holographic results for $V_{\parallel}(L, L_3)$ indeed approach these limiting values as $L_3/L \rightarrow \pm\infty$.

In fig. 14 we present our results for a non-SUSY interface with a jumping θ -angle. Once again we find a striking similarity to the analogous results in electromagnetism, as shown in fig. 6 (b). In

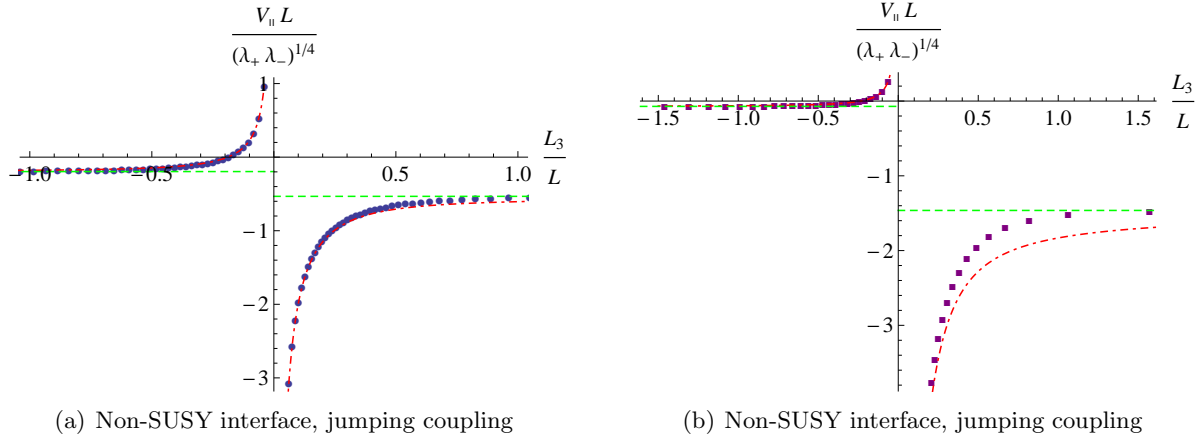


Figure 13: The potential $V_{\parallel}(L, L_3)$ between two test charges along a line parallel to a non-SUSY interface where the coupling jumps in large- N_c , strongly-coupled $\mathcal{N} = 4$ SYM, depicted in fig. 1 (b), as computed from a string in non-SUSY Janus spacetime with a jumping dilaton. More precisely, we plot $V_{\parallel}L/(\lambda_+\lambda_-)^{1/4}$ as a function of L_3/L . (a) The blue dots are our numerical results for $\log(\lambda_+/\lambda_-) = 1$. (b) The purple squares are our numerical results for $\log(\lambda_+/\lambda_-) = 3$. In both (a) and (b), the horizontal green dashed lines are the result for $\mathcal{N} = 4$ SYM without an interface, eq. (1.2), for the values of the 't Hooft coupling on the two sides of the interface, λ_{\pm} . Clearly as the two test charges move infinitely far from the interface, $L_3/L \rightarrow \pm\infty$, the potential approaches that of $\mathcal{N} = 4$ SYM with constant coupling. Additionally, in both (a) and (b) the red dot-dashed lines are our results for the *ad hoc* linear potential $V_{\parallel}^{\text{lin}}$ defined in eq. (4.39). For both (a) and (b) our results are qualitatively similar to the analogous results in electromagnetism shown in fig. 6 (a).

particular, we see that the dipole is attracted to the interface. Again we see that our holographic results approach the result in eq. (1.2), depicted as the horizontal green dashed line in fig. 14, in the limits $L_3/L \rightarrow \pm\infty$.

From figs. 13 and 14 we see that $V_{\parallel}^{\text{lin}}(L, L_3)$ again provides a surprisingly good approximation to the holographic results, and that, as also occurred for $V_{\perp}(L, L_{\text{av}})$ for non-SUSY interfaces, that approximation grows worse as the jump in the coupling or θ -angle increases: in both figs. 13 and 14, the red dot-dashed lines fit the blue dots (smaller jump) better than the purple squares (larger jump).

We will not present results for $V_{\parallel}(L, L_3)$ for SUSY interfaces. In contrast to all previous cases, here we found the matching between our numerical string solutions in SUSY Janus and the near-boundary asymptotics in eq. (4.18) prohibitively difficult.

4.6 Wilson Loops on the Interface

In this subsection, we consider rectangular Wilson loops located precisely on the interface, at $x_3 = 0$. We can obtain these by taking the $L_3 \rightarrow 0$ limit of the parallel Wilson loops we considered in the

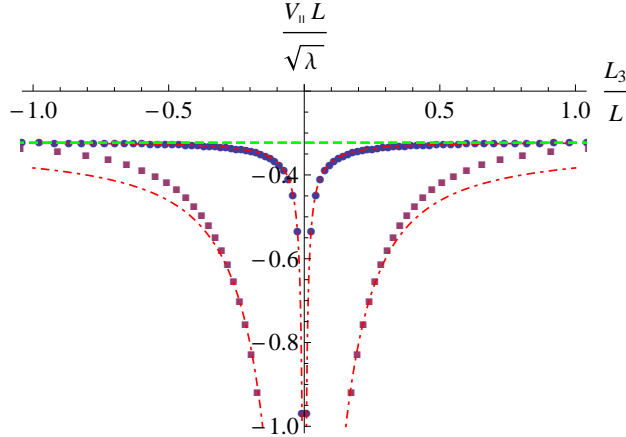


Figure 14: The potential $V_{\parallel}(L, L_3)$ between two test charges along a line parallel to a non-SUSY interface where the θ -angle jumps in large- N_c , strongly-coupled $\mathcal{N} = 4$ SYM, depicted in fig. 1 (b), as computed from a string in non-SUSY Janus spacetime with a jumping axion. More precisely, we plot $V_{\parallel}L/\sqrt{\lambda}$ as a function of L_3/L . The blue dots and purple squares are our numerical results for $g^2\Delta\theta = 2\pi^2$ and $40\pi^2$, respectively. The horizontal green dashed line is the result for $\mathcal{N} = 4$ SYM without an interface, eq. (1.2). The red dot-dashed lines are our results for the *ad hoc* linear potential $V_{\parallel}^{\text{lin}}$ defined in eq. (4.39). In both cases our results are qualitatively similar to the analogous results in electromagnetism shown in fig. 6 (b).

previous subsection. In electromagnetism, in such a limit the potential between two test charges diverges because the test charges approach the interface and eventually coincide with their image charges: recall fig. 6. In other words, in that limit the self-energy of each test charge diverges. Our results of the previous subsections for the self-energy of a single test charge, figs. 8 and 9, show that the same divergence occurs for either a non-SUSY or SUSY interface in $\mathcal{N} = 4$ SYM at large N_c and large coupling, with one exception, a SUSY interface and a test charge with $y = 0$.

The divergence of the self-energy at the interface has a simple, intuitive explanation from the gravity point of view. As mentioned in section 2.3, the boundary of the Janus solutions is not globally flat, but rather has an angular excess at the point where the axio-dilaton jumps. As a result, the Janus metrics do not admit a globally well-defined Fefferman-Graham expansion, so holographic renormalization must be performed separately in each of the two asymptotically $AdS_5 \times S^5$ regions. In each region, the Fefferman-Graham expansion is an expansion in z/x_3 , as explained in section 4.2 and in the appendix (specifically eqs. (A.7) and (A.11)), which clearly must break down in the limit $x_3 \rightarrow 0$.¹⁶ Consequently, the entire holographic renormalization procedure breaks down, and hence we can obtain a divergent result for the self-energy.

To obtain a finite result for the expectation values of rectangular Wilson loops precisely on the interface, we need a prescription to subtract the divergent self-energies of the test charges. The dual

¹⁶For a detailed analysis of the breakdown of the Fefferman-Graham expansion in non-SUSY Janus in the $x_3 \rightarrow 0$ limit, see appendix B of ref. [102].

gravity description suggests a natural prescription. The strings describing the rectangular Wilson loops will sit at fixed x , and so will effectively behave as strings in AdS_4 . We can thus perform holographic renormalization directly in that AdS_4 . Moreover, for strings in AdS_4 , holographic renormalization, the Legendre transform, and subtracting straight strings are all equivalent, much like strings in AdS_5 , as we reviewed in section 4.2.

We are considering conformal interfaces in $\mathcal{N} = 4$ SYM, so after renormalization the expectation value of a rectangular Wilson loop sitting on the interface will depend on only one scale, the separation L between the test charges. As a result, the potential $V(L) \propto 1/L$, with a proportionality constant that will depend on the values of the coupling or θ -angle on the two sides of the interface, λ_{\pm} and θ_{\pm} . Indeed, the holographic result will provide us with a value of the “effective coupling” precisely on the interface, as defined within our renormalization prescription.

To compute $V(L)$ holographically, we need solutions of the string equations of motion, eqs. (4.10a), (4.10b), and (4.10c), describing strings with both endpoints on the boundary at $x_3 = 0$. From eq. (2.2) and fig. 2, we see that the simplest such string will sit at fixed x and y and hence will move only in x_1 and u , or in other words will move only along an AdS_4 slice. The endpoints of such a string will thus end at the AdS_4 boundary, which is $x_3 = 0$. The equations of motion for such a string require

$$\partial_x(e^{\phi} f_4^2) = 0, \quad \partial_y(e^{\phi} f_4^2) = 0. \quad (4.41)$$

If we can solve eq. (4.41), then we obtain a string that moves only in AdS_4 , hence we can compute $S_{\text{ren}}^{\parallel}$ following the procedure of refs. [22, 23]. Assuming that x and y are constants, and choosing the gauge $\sigma = x_1$, the expression for the conserved charge C in eq. (4.6) simplifies to

$$C = -\frac{e^{\phi} f_4^2 u^4}{\sqrt{u^4 + (\partial_{x_1} u)^2}}. \quad (4.42)$$

We expect the string to emerge from the boundary, move in x_1 as it dips into the bulk, and then turn around and rise back up to the boundary. Denoting the minimum value of $u(x_1)$ by u_0 , which we take to occur at $x_1 = 0$, we can write the conserved charge as $C = -e^{\phi} f_4^2 u_0^2$. Eq. (4.42) then gives us, after an integration,

$$u_0 \frac{L}{2} = \mathcal{I} \quad \text{where} \quad \mathcal{I} \equiv \int_1^{\infty} \frac{d(u/u_0)}{(u/u_0)^2 \sqrt{(u/u_0)^4 - 1}} = \frac{\sqrt{2} \pi^{3/2}}{\Gamma(1/4)^2}. \quad (4.43)$$

Introducing a cutoff for the AdS_4 radial coordinate, $u = 1/\varepsilon$, we can then evaluate the regulated on-shell action, eq. (4.27),

$$S_{\text{reg}}^{\text{int}} = \frac{T(-C)}{2\pi\alpha'} \left[\frac{\partial_{x_1} u}{u^3} \Big|_{-L/2}^{+L/2} - L \right] = \frac{T}{2\pi\alpha'} f_4^2 e^{\phi} \left[\frac{2}{\varepsilon} - \frac{4\mathcal{I}^2}{L} + \mathcal{O}(\varepsilon^3) \right], \quad (4.44)$$

where $f_4^2 e^{\phi}$ is evaluated at the constant x and y solutions of eq. (4.41). Holographic renormalization, a Legendre transform, or subtracting straight strings are all equivalent: they all cancel the $1/\varepsilon$ term

in eq. (4.44), and nothing more. We thus obtain the renormalized on-shell string action,

$$S_{\text{ren}}^{\text{int}} = -\frac{T}{2\pi\alpha'} \frac{4 \mathcal{I}^2 e^\phi f_4^2}{L}. \quad (4.45)$$

Using eq. (4.2), we then find the potential $V(L)$, which is almost identical in form to that of $\mathcal{N} = 4$ SYM without an interface, eq. (1.2), except for the value of the “effective ’t Hooft coupling” on the interface, λ_{eff} ,

$$V(L) = -\frac{4\pi^2}{\Gamma(1/4)^4} \frac{\sqrt{2\lambda_{\text{eff}}}}{L}, \quad \lambda_{\text{eff}} \equiv 2\pi e^{2\phi} N_c \frac{f_4^4}{R^4}. \quad (4.46)$$

To determine λ_{eff} requires solving eq. (4.41), which we do numerically. Our results appear in fig. 15. We compare our numerical results against the effective ’t Hooft coupling $\lambda_+(1 + \tilde{Q}^e/Q^e)$ that we used in eq. (4.38), and whose form is motivated by the result for the potential in electromagnetism, eq. (3.23), ignoring the self-energy contributions and setting $L_3 = 0$.

For either a non-SUSY or SUSY interface where the coupling jumps, shown in figs. 15 (a) and (b), we find that our numerical results for λ_{eff} agree remarkably well with $\lambda_+(1 + \tilde{Q}^e/Q^e)$. Indeed, for the SUSY interface and a test charge with $y = 0$, the agreement appears to be exact. For either non-SUSY or SUSY interfaces where the θ -angle jumps, however, the holographic results only approach $\lambda_+(1 + \tilde{Q}^e/Q^e)$ in the limits $\Delta\theta \rightarrow 0$ or $\rightarrow \infty$. For any finite $\Delta\theta$, the holographic result is larger than $\lambda_+(1 + \tilde{Q}^e/Q^e)$.

Acknowledgements

We thank C. Hoyos, E. Kiritsis, M. Lippert, H. Osborn, I. Papadimitriou, V. Pestun, A. Petkou, G. Semenoff, K. Sfetsos, K. Skenderis, D. Tong, E. Witten and J. Zaanen for useful conversations and correspondence. We especially thank A. Karch for reading and commenting on a preliminary draft of the manuscript. J. E. was supported by the FWO - Vlaanderen, Project No. G.0651.11, the “Federal Office for Scientific, Technical and Cultural Affairs through the Inter-University Attraction Poles Programme,” Belgian Science Policy P6/11-P, as well as the European Science Foundation Holograv Network, and is currently supported in part by STFC grant ST/J0003533/1. The work of A.O’B. was supported in part by the European Union grant FP7-REGPOT-2008-1-CreteHEPCosmo-228644. The research leading to these results has received funding from the European Research Council under the European Community’s Seventh Framework Programme (FP7/2007-2013) / ERC grant agreement no. 247252. The work of T.W. is supported by a Research Fellowship (Grant number WR 166/1-1) of the German Research Foundation (DFG).

Appendix: On Holographic Renormalization in Janus Spacetimes

The AdS/CFT dictionary equates the on-shell bulk action with the generating functional of field theory correlation functions [2, 3]. Generically, both of these quantities are divergent: the former

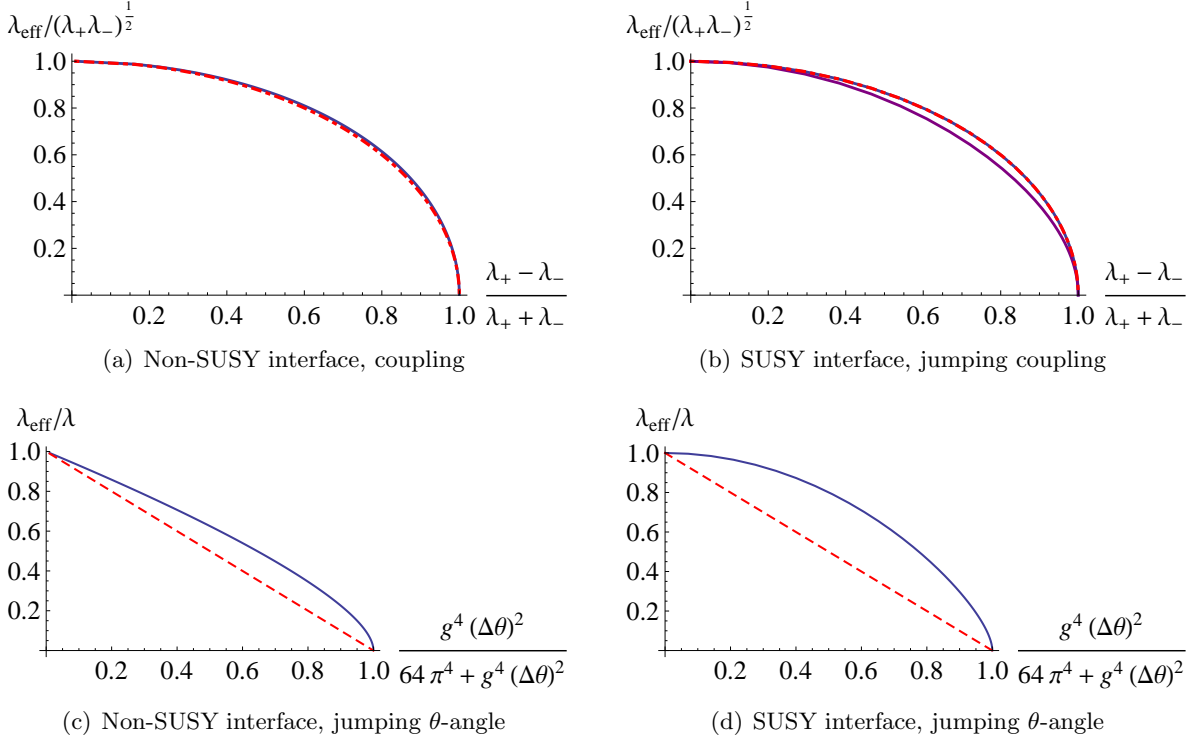


Figure 15: The effective 't Hooft coupling λ_{eff} , defined in eq. (4.46) from the potential between two test charges on an interface in large- N_c , strongly-coupled $\mathcal{N} = 4$ SYM, as computed from strings in Janus spacetimes. (a) $\lambda_{\text{eff}}/\sqrt{\lambda_+\lambda_-}$ versus $\frac{\lambda_+ - \lambda_-}{\lambda_+ + \lambda_-}$ for a non-SUSY interface where the coupling jumps. The purple solid line is our numerical result, while the red dashed line is $\lambda_+(1 + \tilde{Q}^e/Q^e)/\sqrt{\lambda_+\lambda_-}$ with \tilde{Q}^e defined in eq. (3.19). The two lines are nearly coincident. (b) The same as (a), but for a SUSY interface where the coupling jumps. Here the upper blue solid line is our numerical result for $y = 0$ while the lower purple solid line is our numerical result for $y = \pi/2$. The upper blue line is coincident with the red dashed line. (c) $\lambda_{\text{eff}}/\lambda$ versus $\frac{g^4(\Delta\theta)^2}{64\pi^4 + g^4(\Delta\theta)^2}$ for a non-SUSY interface where the θ -angle jumps. The blue solid and red dashed lines have the same meaning as in (a). (d) The same as (c), but for a SUSY interface where the θ -angle jumps. Our numerical results for $y = 0$ and $y = \pi/2$, the blue solid lines, are identical.

due to the infinite volume of any (asymptotically) AdS space and the latter due to UV divergences. The precise procedure to obtain finite, renormalized correlators from the on-shell bulk action is called holographic renormalization [97–100].

Holographic renormalization is simplest in Fefferman-Graham coordinates. Any asymptotically AdS_5 metric can, near the boundary, be written in Fefferman-Graham form,

$$ds^2 = \frac{R^2}{z^2} (dz^2 + g_{\mu\nu}(z, x^\rho) dx^\mu dx^\nu), \quad (\text{A.1})$$

where z is the radial coordinate and the boundary is at $z = 0$. Expanding the metric near the

boundary, *i.e.* in powers of z , the leading term, $g_{\mu\nu}(z = 0, x^\rho)$, corresponds to the source for the dual operator, the stress-energy tensor. In most cases, holographic renormalization reveals that the coefficient of the order z^4 term is proportional to the expectation value of the stress-energy tensor [97–100]. Similarly, the leading term in the near-boundary expansion of the dilaton corresponds to the source for the Lagrangian, $1/g^2$, while the coefficient of the order z^4 term corresponds to the expectation value of the Lagrangian [100].

Crucially, the above statements assume that the AdS_5 solution arises in a consistent Kaluza-Klein truncation of a ten-dimensional solution. As emphasized in ref. [103], extracting field theory expectation values directly from a ten-dimensional solution is often subtle, and may require more than just the lowest Kaluza-Klein modes retained in a consistent truncation. In particular, given the solution for the metric and dilaton in a ten-dimensional gravity theory, the field theory expectation values may not be given simply by the coefficients of their order z^4 terms in a near-boundary expansion [103].

The holographic renormalization of non-SUSY Janus was performed in ref. [102]. We will not attempt the holographic renormalization of SUSY Janus here. Instead, we will just present the change of coordinates from those of the Janus metrics in eq. (4.3) to Fefferman-Graham coordinates. Along the way, we will make some comments about holographic renormalization of the expectation values of the stress-energy tensor and Lagrangian for these cases.

We use Fefferman-Graham coordinates in the holographic renormalization of Wilson loop expectation values, calculated holographically from strings in Janus spacetimes, in section 4. In the coordinates of the metric in eq. (4.3), all the string solutions we study in section 4 have constant $y = 0, \pi/2$. In our conversion to Fefferman-Graham coordinates, we will thus restrict to the cases $y = 0, \pi/2$ for simplicity. In those cases, we can write the metric of eq. (4.3) in the form

$$ds^2 = f_4(x)^2 \left(\frac{du^2}{u^2} + u^2(-dt^2 + dx_1^2 + dx_2^2) \right) + \rho^2(x)dx^2. \quad (\text{A.2})$$

The change of coordinates

$$z \equiv \frac{k_1(x)}{u}, \quad x_3 \equiv \frac{k_2(x)}{u}, \quad (\text{A.3a})$$

$$k_1(x) \equiv \exp \left[\mp \int dx \frac{\rho(x)}{f_4(x)} \sqrt{\frac{f_4(x)^2}{R^2} - 1} \right], \quad k_2(x) \equiv \exp \left[\pm \int dx \frac{\rho(x)}{f_4(x)} \frac{1}{\sqrt{\frac{f_4(x)^2}{R^2} - 1}} \right], \quad (\text{A.3b})$$

puts the metric in Fefferman-Graham form,

$$ds^2 = \frac{R^2}{z^2} (dz^2 + g_{11}(z/x_3)(-dt^2 + dx_1^2 + dx_2^2) + g_{33}(z/x_3)dx_3^2), \quad (\text{A.4a})$$

$$g_{11}(z/x_3) = \frac{f_4(x)^2}{R^2} k_1(x)^2, \quad g_{33}(z/x_3) = \left(\frac{f_4(x)^2}{R^2} - 1 \right) \frac{k_1(x)^2}{k_2(x)^2}. \quad (\text{A.4b})$$

Notice that we may choose either of the \pm signs in eq. (A.3b). Both $f_4(x)$ and $\rho(x)$ are even functions of x , so changing these signs is equivalent to changing the sign of x . The metric in

eq. (A.2) is invariant under $x \rightarrow -x$, so the choice of sign of x is merely a convention, with no physical consequences. Notice also that the isometries require that g_{11} and g_{33} depend only on z/x_3 , as explained in section 4.2. To recover a Minkowski boundary metric, we must impose $g_{11}(0) = g_{33}(0) = 1$. What remains now is to express x in terms of z/x_3 .

For the non-SUSY Janus metric in eq. (2.10), near the boundaries $x \rightarrow \pm x_0$ the expansions of the z and x_3 in eq. (A.3a) are

$$z = \frac{1}{u} \left(\frac{1}{\sqrt{h(x)}} + \sqrt{2}(\gamma - 1)\gamma^{\frac{3}{4}}(x_0 \mp x)^{\frac{9}{2}} + \mathcal{O}\left((x_0 \mp x)^{\frac{11}{2}}\right) \right), \quad (\text{A.5a})$$

$$x_3 = \pm \frac{1}{u} \left(1 - \frac{1}{\sqrt{\gamma}}(x_0 \mp x) + \frac{4}{15}(\gamma - 1)(x_0 \mp x)^6 + \mathcal{O}\left((x_0 \mp x)^7\right) \right). \quad (\text{A.5b})$$

Inverting these, we find u and x in terms of z/x_3 ,

$$u = \pm \frac{1}{x_3} \left[1 - \frac{1}{2} \left(\frac{z}{x_3} \right)^2 + \frac{3}{8} \left(\frac{z}{x_3} \right)^4 - \frac{5}{16} \left(\frac{z}{x_3} \right)^6 + \frac{35}{128} \left(\frac{z}{x_3} \right)^8 - \frac{315 + 16\gamma^3 - 16\gamma^4}{1280} \left(\frac{z}{x_3} \right)^{10} + \mathcal{O}\left((z/x_3)^{12}\right) \right], \quad (\text{A.6a})$$

$$x = \pm \left[x_0 - \frac{\sqrt{\gamma}}{2} \left(\frac{z}{x_3} \right)^2 + \frac{3\sqrt{\gamma}}{8} \left(\frac{z}{x_3} \right)^4 - \frac{5\sqrt{\gamma}}{16} \left(\frac{z}{x_3} \right)^6 + \frac{35\sqrt{\gamma}}{128} \left(\frac{z}{x_3} \right)^8 + \frac{\sqrt{\gamma}(16\gamma^4 - 16\gamma^3 - 315)}{1280} \left(\frac{z}{x_3} \right)^{10} + \mathcal{O}\left((z/x_3)^{12}\right) \right]. \quad (\text{A.6b})$$

and hence the expansions of the metric factors in eq. (A.4b) are

$$g_{11}(z/x_3) = 1 + \frac{(\gamma - 1)\gamma^3}{8} \left(\frac{z}{x_3} \right)^8 + \mathcal{O}\left((z/x_3)^{10}\right), \quad (\text{A.7a})$$

$$g_{33}(z/x_3) = 1 + \frac{(\gamma - 1)\gamma^3}{8} \left(\frac{z}{x_3} \right)^8 + \mathcal{O}\left((z/x_3)^{10}\right). \quad (\text{A.7b})$$

The Fefferman-Graham expansion of the non-SUSY Janus dilaton in eq. (2.14) is

$$\phi(z/x_3) = \phi_{\pm} \mp \sqrt{\frac{3}{2}} \frac{\gamma^{\frac{3}{2}} \sqrt{1 - \gamma}}{2} \left(\frac{z}{x_3} \right)^4 + \mathcal{O}\left((z/x_3)^6\right). \quad (\text{A.8})$$

In the field theory, $SO(3, 2)$ conformal symmetry forbids the field theory stress-energy tensor from acquiring an expectation value, but allows a scalar field of conformal dimension Δ to acquire an expectation value proportional to $1/|x_3|^\Delta$ [104]. Notice that the expansions of $g_{11}(z/x_3)$ and $g_{33}(z/x_3)$ in eq. (A.7) have no z^4 term, indicating that the one-point function of the stress-energy tensor is indeed zero [5, 102]. In the expansion of the dilaton in eq. (A.8), the z^4 term has a nonzero coefficient, indicating that the Lagrangian acquires a nonzero expectation value that goes as $1/|x_3|^4$ [5, 102]. Such a straightforward identification of the coefficients of the order z^4 terms

with field theory one-point functions is possible because the non-SUSY Janus metric and dilaton are solutions of a consistent truncation of type IIB supergravity on S^5 [4, 105].

For the SUSY Janus metric in eq. (2.26a), near the boundaries $x \rightarrow \pm\infty$ the expansions of the z and x_3 in eq. (A.3a) are

$$z = \frac{1}{u} \left[\frac{1}{\cosh(x \mp \frac{1}{2} \ln \cosh \delta\varphi)} \pm \sqrt{\cosh \delta\varphi} \left(\frac{\cos 2y \sinh \delta\varphi}{2} e^{\mp 3x} - \frac{8 \cos 2y \sinh 2\delta\varphi \pm (\cos 4y - 3) \sin^2 \delta\varphi}{16} e^{\mp 5x} + \mathcal{O}(e^{\mp 7x}) \right) \right], \quad (\text{A.9a})$$

$$x_3 = \frac{1}{u} \left[\tanh(x \mp \frac{1}{2} \ln \cosh \delta\varphi) + \left(\frac{\cos 2y \sinh 2\delta\varphi}{4} e^{\mp 4x} - \frac{\cosh \delta\varphi \sinh \delta\varphi [24 \cos 2y \cosh \delta\varphi \pm (13 + 5 \cos 4y) \sinh \delta\varphi]}{24} e^{\mp 6x} + \mathcal{O}(e^{\mp 8x}) \right) \right]. \quad (\text{A.9b})$$

Inverting these, we find u and x in terms of z/x_3 ,

$$u = \pm \frac{1}{x_3} \left[1 - \frac{1}{2} \left(\frac{z}{x_3} \right)^2 + \frac{3(4 \pm \cos 2y \tanh \delta\varphi)}{32} \left(\frac{z}{x_3} \right)^4 - \frac{919 + 1001 \cosh 2\delta\varphi + 98 \cos 4y \sinh^2 \delta\varphi \pm 672 \cos 2y \sinh 2\delta\varphi}{6144 \cosh^2 \delta\varphi} \left(\frac{z}{x_3} \right)^6 + \mathcal{O}((z/x_3)^8) \right], \quad (\text{A.10a})$$

$$x = \pm \frac{1}{2} \ln \left(4 \cosh \delta\varphi \left(\frac{x_3}{z} \right)^2 \right) \pm \frac{4 \pm \cos 2y \tanh \delta\varphi}{16} \left(\frac{z}{x_3} \right)^2 \mp \frac{96 + \tanh \delta\varphi (7 \cos 4y \tanh \delta\varphi \pm 112 \cos 2y - \tanh \delta\varphi)}{1024} \left(\frac{z}{x_3} \right)^4 + \mathcal{O}((z/x_3)^6), \quad (\text{A.10b})$$

and hence the expansions of the metric factors in eq. (A.4b) are

$$g_{11}(z/x_3) = 1 \pm \frac{3 \cos 2y \tanh \delta\varphi}{8} \left(\frac{z}{x_3} \right)^2 \mp \frac{\tanh \delta\varphi [240 \cos 2y \pm (5 + 13 \cos 4y) \tanh \delta\varphi]}{512} \left(\frac{z}{x_3} \right)^4 + \mathcal{O}((z/x_3)^6), \quad (\text{A.11a})$$

$$g_{33}(z/x_3) = 1 \pm \frac{3 \cos 2y \tanh \delta\varphi}{8} \left(\frac{z}{x_3} \right)^2 \mp \frac{\tanh \delta\varphi [144 \cos 2y \pm (5 + 13 \cos 4y) \tanh \delta\varphi]}{512} \left(\frac{z}{x_3} \right)^4 + \mathcal{O}((z/x_3)^6). \quad (\text{A.11b})$$

The expansion of the SUSY Janus dilaton in eq. (2.26b) is

$$\phi = \phi_{\pm} \mp \frac{3 \tanh \delta\varphi}{16} \left(\frac{z}{x_3} \right)^4 \pm \frac{\tanh \delta\varphi (20 \pm 11 \cos 2y \tanh \delta\varphi)}{64} \left(\frac{z}{x_3} \right)^6 + \mathcal{O}((z/x_3)^8). \quad (\text{A.12})$$

In eqs. (A.9), (A.6), (A.11), and (A.12), y only takes the values $y = 0, \pi/2$ to which we restricted.

The expansions of $g_{11}(z/x_3)$ and $g_{33}(z/x_3)$ in eq. (A.11) include nonzero coefficients for the z^4 terms. Naïvely, that suggests the field theory stress-energy tensor has a nonzero expectation value. Notice, however, that the coefficients of the order z^4 terms depend explicitly on y : they are different when $y = 0$ or $y = \pi/2$. In the field theory that suggests the expectation value of the stress-energy tensor has some R-charge, which is clearly unphysical: the stress-energy tensor is invariant under all global symmetries. Clearly, we cannot simply identify the coefficient of the order z^4 term in the metric with the stress-energy tensor one-point function. Indeed, the SUSY Janus metric is genuinely ten-dimensional, *i.e.* is not obtained as the consistent truncation of a ten-dimensional solution, so extracting the one-point function of the stress-energy tensor may take more work, as emphasized in ref. [103]. Similar statements apply for the expansion of the dilaton in eq. (A.12).

References

- [1] J. M. Maldacena, *The Large N limit of Superconformal Field Theories and Supergravity*, *Adv.Theor.Math.Phys.* **2** (1998) 231–252, [[hep-th/9711200](#)].
- [2] E. Witten, *Anti-de Sitter Space and Holography*, *Adv.Theor.Math.Phys.* **2** (1998) 253–291, [[hep-th/9802150](#)].
- [3] S. Gubser, I. R. Klebanov, and A. M. Polyakov, *Gauge Theory Correlators from Noncritical String Theory*, *Phys.Lett.* **B428** (1998) 105–114, [[hep-th/9802109](#)].
- [4] D. Bak, M. Gutperle, and S. Hirano, *A Dilatonic Deformation of $AdS(5)$ and its Field Theory Dual*, *JHEP* **0305** (2003) 072, [[hep-th/0304129](#)].
- [5] A. Clark, D. Freedman, A. Karch, and M. Schnabl, *The Dual of Janus: an Interface CFT*, *Phys.Rev.* **D71** (2005) 066003, [[hep-th/0407073](#)].
- [6] E. D’Hoker, J. Estes, and M. Gutperle, *Interface Yang-Mills, Supersymmetry, and Janus*, *Nucl.Phys.* **B753** (2006) 16–41, [[hep-th/0603013](#)].
- [7] T. Azeyanagi, A. Karch, T. Takayanagi, and E. Thompson, *Holographic Calculation of Boundary Entropy*, *JHEP* **0803** (2008) 054–054, [[arXiv:0712.1850](#)].
- [8] D. Gaiotto and E. Witten, *Janus Configurations, Chern-Simons Couplings, and the θ -Angle in $N=4$ Super Yang-Mills Theory*, *JHEP* **1006** (2010) 097, [[arXiv:0804.2907](#)].
- [9] A. Karch and L. Randall, *Open and Closed String Interpretation of SUSY CFT’s on Branes with Boundaries*, *JHEP* **0106** (2001) 063, [[hep-th/0105132](#)].
- [10] O. DeWolfe, D. Freedman, and H. Ooguri, *Holography and Defect Conformal Field Theories*, *Phys.Rev.* **D66** (2002) 025009, [[hep-th/0111135](#)].

- [11] J. Erdmenger, Z. Guralnik, and I. Kirsch, *Four-dimensional Superconformal Theories with Interacting Boundaries or Defects*, *Phys.Rev.* **D66** (2002) 025020, [[hep-th/0203020](#)].
- [12] E. D'Hoker, J. Estes, and M. Gutperle, *Exact Half-BPS Type IIB Interface Solutions. II. Flux Solutions and Multi-Janus*, *JHEP* **0706** (2007) 022, [[arXiv:0705.0024](#)].
- [13] C. Kim, E. Koh, and K.-M. Lee, *Janus and Multifaced Supersymmetric Theories*, *JHEP* **0806** (2008) 040, [[arXiv:0802.2143](#)].
- [14] C. Kim, E. Koh, and K.-M. Lee, *Janus and Multifaced Supersymmetric Theories II*, *Phys.Rev.* **D79** (2009) 126013, [[arXiv:0901.0506](#)].
- [15] A. Clark and A. Karch, *Super Janus*, *JHEP* **0510** (2005) 094, [[hep-th/0506265](#)].
- [16] E. D'Hoker, J. Estes, and M. Gutperle, *Ten-dimensional Supersymmetric Janus Solutions*, *Nucl.Phys.* **B757** (2006) 79–116, [[hep-th/0603012](#)].
- [17] J. Gomis and C. Romelsberger, *Bubbling Defect CFT's*, *JHEP* **0608** (2006) 050, [[hep-th/0604155](#)].
- [18] E. D'Hoker, J. Estes, and M. Gutperle, *Exact Half-BPS Type IIB Interface Solutions. I. Local Solution and Supersymmetric Janus*, *JHEP* **0706** (2007) 021, [[arXiv:0705.0022](#)].
- [19] O. Aharony, L. Berdichevsky, M. Berkooz, and I. Shamir, *Near-horizon Solutions for D3-branes Ending on 5-branes*, *Phys.Rev.* **D84** (2011) 126003, [[arXiv:1106.1870](#)].
- [20] B. Assel, C. Bachas, J. Estes, and J. Gomis, *Holographic Duals of $D=3$ $N=4$ Superconformal Field Theories*, *JHEP* **1108** (2011) 087, [[arXiv:1106.4253](#)].
- [21] M.-W. Suh, *Supersymmetric Janus Solutions in Five and Ten Dimensions*, *JHEP* **1109** (2011) 064, [[arXiv:1107.2796](#)].
- [22] S.-J. Rey and J.-T. Yee, *Macroscopic Strings as Heavy Quarks in Large N Gauge Theory and Anti-de Sitter Supergravity*, *Eur.Phys.J.* **C22** (2001) 379–394, [[hep-th/9803001](#)].
- [23] J. Maldacena, *Wilson loops in Large N Field Theories*, *Phys.Rev.Lett.* **80** (1998) 4859–4862, [[hep-th/9803002](#)].
- [24] N. Drukker, D. Gross, and H. Ooguri, *Wilson Loops and Minimal Surfaces*, *Phys.Rev.* **D60** (1999) 125006, [[hep-th/9904191](#)].
- [25] J. Erickson, G. Semenoff, and K. Zarembo, *Wilson Loops in $N=4$ Supersymmetric Yang-Mills Theory*, *Nucl.Phys.* **B582** (2000) 155–175, [[hep-th/0003055](#)].
- [26] J. Erickson, G. Semenoff, R. Szabo, and K. Zarembo, *Static Potential in $N=4$ Supersymmetric Yang-Mills Theory*, *Phys.Rev.* **D61** (2000) 105006, [[hep-th/9911088](#)].

- [27] N. Drukker, D. Gaiotto, and J. Gomis, *The Virtue of Defects in 4D Gauge Theories and 2D CFTs*, *JHEP* **1106** (2011) 025, [[arXiv:1003.1112](#)].
- [28] K. Nagasaki, H. Tanida, and S. Yamaguchi, *Holographic Interface-Particle Potential*, *JHEP* **1201** (2012) 139, [[arXiv:1109.1927](#)].
- [29] N. Drukker and D. Gross, *An Exact Prediction of $N=4$ SUSYM Theory for String Theory*, *J.Math.Phys.* **42** (2001) 2896–2914, [[hep-th/0010274](#)].
- [30] V. Pestun, *Localization of Gauge Theory on a Four-sphere and Supersymmetric Wilson Loops*, *Commun.Math.Phys.* **313** (2012) 71–129, [[arXiv:0712.2824](#)].
- [31] D. Berenstein, R. Corrado, W. Fischler, and J. Maldacena, *The Operator Product Expansion for Wilson Loops and Surfaces in the Large N limit*, *Phys.Rev.* **D59** (1999) 105023, [[hep-th/9809188](#)].
- [32] M. Hasan and C. Kane, *Topological Insulators*, *Rev.Mod.Phys.* **82** (2010) 3045, [[arXiv:1002.3895](#)].
- [33] J. E. Moore, *The Birth of Topological Insulators*, *Nature* **464** (Mar, 2010) 194.
- [34] X.-L. Qi and S.-C. Zhang, *Topological Insulators and Superconductors*, *Rev.Mod.Phys.* **83** (Oct., 2011) 1057–1110, [[arXiv:1008.2026](#)].
- [35] M. Z. Hasan and J. E. Moore, *Three-Dimensional Topological Insulators*, *Ann.Rev.Cond.Matt.Phys.* **2** (Mar., 2011) 55–78, [[arXiv:1011.5462](#)].
- [36] S. C. Zhang, *The Chern-Simons Landau-Ginzburg Theory of the Fractional Quantum Hall Effect*, *Int.Jour.Mod.Phys.* **B06** (1992), no. 01 25–58.
- [37] X.-L. Qi, T. L. Hughes, and S.-C. Zhang, *Topological Field Theory of Time-reversal Invariant Insulators*, *Phys.Rev.* **B78** (Nov., 2008) 195424, [[arXiv:0802.3537](#)].
- [38] A. M. Essin, J. E. Moore, and D. Vanderbilt, *Magnetoelectric Polarizability and Axion Electrodynamics in Crystalline Insulators*, *Phys.Rev.Lett.* **102** (Oct., 2008) 146805, [[arXiv:0810.2998](#)].
- [39] J. Maciejko, X.-L. Qi, A. Karch, and S.-C. Zhang, *Fractional Topological Insulators in Three Dimensions*, *Phys.Rev.Lett.* **105** (2010) 246809, [[arXiv:1004.3628](#)].
- [40] B. Swingle, M. Barkeshli, J. McGreevy, and T. Senthil, *Correlated Topological Insulators and the Fractional Magnetoelectric Effect*, *Phys.Rev.* **B83** (2011) 195139, [[arXiv:1005.1076](#)].
- [41] J. Maciejko, X.-L. Qi, A. Karch, and S.-C. Zhang, *Models of Three-Dimensional Fractional Topological Insulators*, *ArXiv e-prints* (Nov., 2011) [[arXiv:1111.6816](#)].

- [42] A. Karch, *Electric-Magnetic Duality and Topological Insulators*, *Phys.Rev.Lett.* **103** (2009) 171601, [[arXiv:0907.1528](#)].
- [43] A. Peet and J. Polchinski, *UV / IR Relations in AdS Dynamics*, *Phys.Rev.* **D59** (1999) 065011, [[hep-th/9809022](#)].
- [44] L. Susskind and E. Witten, *The Holographic Bound in Anti-de Sitter Space*, [hep-th/9805114](#).
- [45] O. Aharony, O. DeWolfe, D. Z. Freedman, and A. Karch, *Defect Conformal Field Theory and Locally Localized Gravity*, *JHEP* **0307** (2003) 030, [[hep-th/0303249](#)].
- [46] D. Thouless, M. Kohmoto, M. Nightingale, and M. den Nijs, *Quantized Hall Conductance in a Two-Dimensional Periodic Potential*, *Phys.Rev.Lett.* **49** (1982) 405–408.
- [47] J. E. Moore and L. Balents, *Topological Invariants of Time-reversal-invariant Band Structures*, *Phys.Rev.* **B75** (Mar., 2007) 121306, [[cond-mat/0607314](#)].
- [48] R. Roy, *Topological Phases and the Quantum Spin Hall Effect in Three Dimensions*, *Phys.Rev.* **B79** (May, 2009) 195322, [[cond-mat/0607531](#)].
- [49] L. Fu, C. L. Kane, and E. J. Mele, *Topological Insulators in Three Dimensions*, *Phys.Rev.Lett.* **98** (Mar., 2007) 106803, [[cond-mat/0607699](#)].
- [50] A. J. Niemi and G. W. Semenoff, *Axial-Anomaly-Induced Fermion Fractionization and Effective Gauge-Theory Actions in Odd-Dimensional Space-Times*, *Phys.Rev.Lett.* **51** (Dec, 1983) 2077–2080.
- [51] A. N. Redlich, *Gauge Noninvariance and Parity Nonconservation of Three-Dimensional Fermions*, *Phys.Rev.Lett.* **52** (Jan, 1984) 18–21.
- [52] S. Ryu, J. E. Moore, and A. W. Ludwig, *Electromagnetic and Gravitational Responses and Anomalies in Topological Insulators and Superconductors*, *Phys.Rev.* **B85** (2012) 045104, [[arXiv:1010.0936](#)].
- [53] K. Nomura, M. Koshino, and S. Ryu, *Topological Delocalization of Two-Dimensional Massless Dirac Fermions*, *Phys. Rev. Lett.* **99** (Oct, 2007) 146806.
- [54] R. B. Laughlin, *Quantized Hall Conductivity in Two Dimensions*, *Phys. Rev.* **B23** (May, 1981) 5632–5633.
- [55] B. I. Halperin, *Quantized Hall Conductance, Current-carrying Edge States, and the Existence of Extended States in a Two-dimensional Disordered Potential*, *Phys. Rev.* **B25** (Feb, 1982) 2185–2190.

- [56] L. Fu and C. L. Kane, *Topological Insulators with Inversion Symmetry*, *Phys.Rev.* **B76** (July, 2007) 045302, [[cond-mat/0611341](#)].
- [57] A. P. Schnyder, S. Ryu, A. Furusaki, and A. W. W. Ludwig, *Classification of Topological Insulators and Superconductors in Three Spatial Dimensions*, *Phys. Rev.* **B78** (Nov, 2008) 195125.
- [58] A. P. Schnyder, S. Ryu, A. Furusaki, and A. W. W. Ludwig, *Classification of Topological Insulators and Superconductors*, *AIP Conf.Proc.* **1134** (2009) 10–22.
- [59] A. Kitaev, *Periodic Table for Topological Insulators and Superconductors*, *AIP Conf.Proc.* **1134** (2009) 22–30, [[arXiv:0901.2686](#)].
- [60] S. Ryu, A. P. Schnyder, A. Furusaki, and A. Ludwig, *Topological Insulators and Superconductors: Ten-fold Way and Dimensional Hierarchy*, *New J.Phys.* **12** (2010) 065010.
- [61] A. LeClair and D. Bernard, *Holographic Classification of Topological Insulators and its 8-fold Periodicity*, [arXiv:1205.3810](#).
- [62] S. A. Hartnoll and D. Radicevic, *Holographic Order Parameter for Charge Fractionalization*, [arXiv:1205.5291](#).
- [63] J. Voit, *One-dimensional Fermi Liquids*, *Rep.Prog.Phys.* **58** (Sept., 1995) 977–1116, [[cond-mat/9510014](#)].
- [64] R. B. Laughlin, *Anomalous Quantum Hall Effect - An Incompressible Quantum Fluid with Fractionally Charged Excitations*, *Phys.Rev.Lett.* **50** (May, 1983) 1395–1398.
- [65] J. K. Jain, *Incompressible Quantum Hall States*, *Phys. Rev.* **B40** (Oct, 1989) 8079–8082.
- [66] X.-G. Wen, *Edge Excitations in the Fractional Quantum Hall States at General Filling Fractions*, *Mod.Phys.Lett.* **B05** (1991), no. 01 39–46.
- [67] X.-G. Wen, *Non-Abelian Statistics in the Fractional Quantum Hall States*, *Phys.Rev.Lett.* **66** (Feb, 1991) 802–805.
- [68] B. Blok and X.-G. Wen, *Many-body Systems with Non-Abelian Statistics*, *Nucl.Phys.* **B374** (1992), no. 3 615 – 646.
- [69] X.-G. Wen, *Theory of the Edge States in Fractional Quantum Hall Effects*, *Int.J.Mod.Phys.* **B06** (1992), no. 10 1711–1762.
- [70] X.-G. Wen, *Projective Construction of Non-Abelian Quantum Hall Liquids*, *Phys. Rev.* **B60** (Sep, 1999) 8827–8838.

- [71] M. Barkeshli and X.-G. Wen, *Effective Field Theory and Projective Construction for Z_k Parafermion Fractional Quantum Hall States*, *Phys.Rev.* **B81** (Apr., 2010) 155302, [[arXiv:0910.2483](#)].
- [72] C. Hoyos-Badajoz, K. Jensen, and A. Karch, *A Holographic Fractional Topological Insulator*, *Phys.Rev.* **D82** (2010) 086001, [[arXiv:1007.3253](#)].
- [73] M. Ammon and M. Gutperle, *A Supersymmetric Holographic Dual of a Fractional topological insulator*, *Phys.Rev.* **D86** (2012) 025018, [[arXiv:1204.2217](#)].
- [74] A. Karch and E. Katz, *Adding Flavor to AdS / CFT*, *JHEP* **0206** (2002) 043, [[hep-th/0205236](#)].
- [75] S. Nakamura, Y. Seo, S.-J. Sin, and K. Yogendran, *A New Phase at Finite Quark Density from AdS/CFT*, *J.Korean Phys.Soc.* **52** (2008) 1734–1739, [[hep-th/0611021](#)].
- [76] S. Kobayashi, D. Mateos, S. Matsuura, R. Myers, and R. Thomson, *Holographic Phase Transitions at Finite Baryon Density*, *JHEP* **0702** (2007) 016, [[hep-th/0611099](#)].
- [77] M. Kruczenski, D. Mateos, R. Myers, and D. Winters, *Meson Spectroscopy in AdS / CFT with Flavor*, *JHEP* **0307** (2003) 049, [[hep-th/0304032](#)].
- [78] J. Davis, P. Kraus, and A. Shah, *Gravity Dual of a Quantum Hall Plateau Transition*, *JHEP* **0811** (2008) 020, [[arXiv:0809.1876](#)].
- [79] R. Myers and M. Wapler, *Transport Properties of Holographic Defects*, *JHEP* **0812** (2008) 115, [[arXiv:0811.0480](#)].
- [80] S.-J. Rey, *String Theory on Thin Semiconductors*, *Prog.Theor.Phys.Supp.* **177** (2009) 128–142.
- [81] M. Wapler, *Holographic Experiments on Defects*, *Int.J.Mod.Phys.* **A25** (2010) 4397–4473, [[arXiv:0909.1698](#)].
- [82] M. Wapler, *Thermodynamics of Holographic Defects*, *JHEP* **1001** (2010) 056, [[arXiv:0911.2943](#)].
- [83] D. Kutasov, J. Lin, and A. Parnachev, *Conformal Phase Transitions at Weak and Strong Coupling*, *Nucl.Phys.* **B858** (2012) 155–195, [[arXiv:1107.2324](#)].
- [84] O. Bergman, N. Jokela, G. Lifschytz, and M. Lippert, *Quantum Hall Effect in a Holographic Model*, *JHEP* **1010** (2010) 063, [[arXiv:1003.4965](#)].
- [85] N. Jokela, G. Lifschytz, and M. Lippert, *Magneto-roton Excitation in a Holographic Quantum Hall Fluid*, *JHEP* **1102** (2011) 104, [[arXiv:1012.1230](#)].

- [86] N. Jokela, G. Lifschytz, and M. Lippert, *Magnetic Effects in a Holographic Fermi-like Liquid*, *JHEP* **1205** (2012) 105, [[arXiv:1204.3914](#)].
- [87] J. Davis, H. Omid, and G. Semenoff, *Holographic Fermionic Fixed Points in $d=3$* , *JHEP* **1109** (2011) 124, [[arXiv:1107.4397](#)].
- [88] J. Davis and N. Kim, *Flavor-symmetry Breaking with Charged Probes*, *JHEP* **1206** (2012) 064, [[arXiv:1109.4952](#)].
- [89] G. Grignani, N. Kim, and G. Semenoff, *D7-anti-D7 Bilayer: Holographic Dynamical Symmetry Breaking*, [arXiv:1208.0867](#).
- [90] H. Omid and G. Semenoff, *D3-D7 Holographic Dual of a Perturbed 3D CFT*, [arXiv:1208.5176](#).
- [91] O. Bergman, N. Jokela, G. Lifschytz, and M. Lippert, *Striped Instability of a Holographic Fermi-like Liquid*, *JHEP* **1110** (2011) 034, [[arXiv:1106.3883](#)].
- [92] T. Azeyanagi, W. Li, and T. Takayanagi, *On String Theory Duals of Lifshitz-like Fixed Points*, *JHEP* **0906** (2009) 084, [[arXiv:0905.0688](#)].
- [93] D. Mateos and D. Trancanelli, *The Anisotropic $N=4$ Super Yang-Mills Plasma and Its Instabilities*, *Phys.Rev.Lett.* **107** (2011) 101601, [[arXiv:1105.3472](#)].
- [94] D. Mateos and D. Trancanelli, *Thermodynamics and Instabilities of a Strongly Coupled Anisotropic Plasma*, *JHEP* **1107** (2011) 054, [[arXiv:1106.1637](#)].
- [95] A. Rebhan and D. Steineder, *Violation of the Holographic Viscosity Bound in a Strongly Coupled Anisotropic Plasma*, *Phys.Rev.Lett.* **108** (2012) 021601, [[arXiv:1110.6825](#)].
- [96] O. Aharony, S. Gubser, J. Maldacena, H. Ooguri, and Y. Oz, *Large N Field Theories, String Theory and Gravity*, *Phys.Rept.* **323** (2000) 183–386, [[hep-th/9905111](#)].
- [97] M. Henningson and K. Skenderis, *The Holographic Weyl Anomaly*, *JHEP* **9807** (1998) 023, [[hep-th/9806087](#)].
- [98] V. Balasubramanian and P. Kraus, *A Stress Tensor for Anti-de Sitter Gravity*, *Commun.Math.Phys.* **208** (1999) 413–428, [[hep-th/9902121](#)].
- [99] S. de Haro, S. Solodukhin, and K. Skenderis, *Holographic Reconstruction of Space-time and Renormalization in the AdS / CFT Correspondence*, *Commun.Math.Phys.* **217** (2001) 595–622, [[hep-th/0002230](#)].
- [100] K. Skenderis, *Lecture Notes on Holographic Renormalization*, *Class.Quant.Grav.* **19** (2002) 5849–5876, [[hep-th/0209067](#)].

- [101] L. Alday and J. Maldacena, *Comments on Gluon Scattering Amplitudes via AdS/CFT*, *JHEP* **0711** (2007) 068, [[arXiv:0710.1060](#)].
- [102] I. Papadimitriou and K. Skenderis, *Correlation Functions in Holographic RG Flows*, *JHEP* **0410** (2004) 075, [[hep-th/0407071](#)].
- [103] K. Skenderis and M. Taylor, *Kaluza-Klein Holography*, *JHEP* **0605** (2006) 057, [[hep-th/0603016](#)].
- [104] D. M. McAvity and H. Osborn, *Conformal Field Theories Near a Boundary in General Dimensions*, *Nucl.Phys.* **B455** (Feb., 1995) 522–576, [[cond-mat/9505127](#)].
- [105] D. Freedman, C. Nunez, M. Schnabl, and K. Skenderis, *Fake Supergravity and Domain Wall Stability*, *Phys.Rev.* **D69** (2004) 104027, [[hep-th/0312055](#)].